Dr Essaieb Hamdi
Université de Tunis El Manar
Ecole Nationale d'Ingénieurs de Tunis
LR14ES03-Ingénierie Géotechnique

Civil Engineering Department
BP 37 Le Belvédère, 1002 Tunis. Tunisia
Phone: (216) 20 32 32 89
Email : essaieb.hamdi@enit.rnu.tn

FULBRIGHT VISITING REPORT

RESEARCH ACTIVITIES

Analysis of Urban Structures Response to Ultra-High Frequency Excitation from Close-in Blasting

Department of Civil and Environmental Engineering
Northwestern University – Evanston – Illinois (USA)

August 11, 2014 – February 10, 2015

Acknowledgments

This report has been written during my Fulbright Visiting Research Stay at the Department of Civil and Environmental Engineering of Northwestern University (IL, USA). Special thanks go to the Fulbright Visiting Program selection committee at the US Embassy in Tunisia and in Washington DC and namely Mr. Sami Saaied from the US Embassy in Tunisia and Ms Ashley Gempp and Mr from the Council for International Exchange of Scholars (USA).

I would like to thank Professor Charles H. Dowding for inviting me to this research stay at Northwestern University, for his guidance, motivation, expertise, and foresight without which this work would certainly not have been possible. A lot of expertise has been acquired by me during this stay on construction and quarrying blasting operations and on how to measure and interpretate crack displacements and temperature measured by wireless and wired systems.

I am very grateful to Professor Catherine Aimone, Professor at New Mexico Institute of Mining and Technology and manager of Aimone-Martin Associates LLC. She gave me the opportunity to work on the New York City project which provided field experience for the analysis of blast induced vibrations from construction blasting.

Pr Karen Chou is very thanked for her kindness towards me and for her very helpful assistance in the early steps of my stay.

Special thanks go as well to Graig, Jennie, and George from the Infrastructure Technology Institute at Northwestern University for technical and administrative assistance provided during my stay.

All colleagues that I met at the Nothwestern University, Yida, Montacer, Ferdinando, Constance, Ze Pei, Mehmet, Jo are very thanked for their friendship and the good atmosphere during my stay at Evanston.

I cannot end without a thought to my wife Jihene, my children Mohamed Salah and Adem, my sisters Amira, Salma and Yosra and all my family and my wife's family for the support and encouragement they have continued to give me.

I dedicate this report to the souls of my parents as a sign of reconnaissance of all education and principles they have given me.

Essaieb HAMDI

Abstract

This report summarizes a case study that provides the multiple position, time correlated measurements of structure response needed to advance the understanding of the response of larger urban structures to ultra-high frequency blast induced excitation. While the first part of the report provides information to determine the type of response, the second part provides the information concerning calculation of strains and the distortion. The response is divided into three main chapters: Site & Instrumentation, Time Histories, and Response. Site and Instrumentation is divided into three sections: site and geology, transducers, and blasting practice. Time history is divided into three sections: attenuation, dominant frequencies, and propagation. Structure Response is divided into two sections: amplification-deamplification and response spectrum. The case study allowed the following conclusions: Urban structures respond predominantly in a wave transmission mode where there is noticeable difference in time, frequency, phase, and amplitude of motions measured at the extreme top corners of the structure. Excitation motions along the base are not the same; they differ significantly in time, frequency, and amplitude. Excitation frequencies are so much larger than the natural frequencies of the structures and components that the excitation motions were deamplified for all events.

Content

Acknowledgments ..... **ii**
Abstract ..... **iii**
Content ..... **iv**
List of figures ..... **vi**
List of tables ..... **vii**
Introduction **8**
1 Close-in blasting 8
2 Present study summary 9
Chapter 1. Site environment and building monitoring **11**
1 Site and Geology 11
2 Transducer description and installation 12
2.1 Building 1 transducers 12
2.2 Building 2 transducers 13
3 Blasting practice 14
Chapter 2. Time histories analysis **16**
1 Analysis methodology 16
2 Blast-induced vibrations time histories 16
2.1 Attenuation of peak particle velocity 18
2.2 Ground vibration and frequency 19
3 Propagation velocity in rock and structure 20
3.1 Rock wave velocity 20
3.2 Wave velocity within the structure 20
4 Structure response to ultra high frequency excitation from close-in blasting 21
4.1 Comparison of ground motion and structure response 21
4.2 Natural frequency and damping ratio 22
4.3 Amplification-deamplification 23
4.1 Mid-wall versus upper structure amplification 23
4.1 Comparison with wall and superstructure response measured by USBM 23
5 Pseudo velocity response spectra demonstrate the expectaion of low distortion 25
5.1 Filtering and SDOF Calculation 25

5.2 Comparison with MS Excel 200-central moving average filtering 27
5.3 Comparison with tunnel and quarrying blasts 28
6 Comparison of time correlated time histories illustrates wave transmission 29
7 Conclusion 30
Chapter 3. Close-in blast induced strains 32
1 Ground Motion Environment 32
1.1 Integration of velocity time history 32
1.2 Differential displacement calculation 33
2 Strain calculations 34
2.1 Procedure for calculating strains 34
2.3 Basement Wall response at building 2 36
2.4 Comparison with ACM surveillance 37
2.5 Comparison with previous studies of tall structure response in urban close-in blasting 38
3 Strains versus Peak Particle Velocities 39
4 Single-Degree-Of-Freedom response spectra 41
4.1 Displacement estimated from SDOF response spectrum 42
4.2 SDOF displacement versus PPV/freq and PPV 46
4.1 Use of SDOF as Control Index 48
4.2 Absolute displacement calculations 51
5 Conclusions 53
References 55
Appendix A 57
Appendix B 60

List of figures

Figure 1. Blast locations with regards to the buildings. 11
Figure 2. Locations of the sensors at the upper and lower parts of the monitored walls at the two buildings. 13
Figure 3. Simplified Sketch of the two buildings and a current blast 14
Figure 4. Flowchart of the general methodology adopted for the buildings response analysis. 17
Figure 5. Transmission of the ground motion to the lower transducer during blast 06/02. 17
Figure 6. Transmission of the ground motion to the lower transducer during blast 06/02. 18
Figure 7. Comparison of measured square root scaled distance attenuation and Oriard's (1972) 19
Figure 8. Transit time estimation 21
Figure 9. Upper North transverse velocity time history recorded at Building 1 22
Figure 10. Peak velocities for radial ground motion and north lower radial component 24
Figure 11. Instrumentation for USBM 1-story, 2-story residential structures and the taller urban structures of this study. 25
Figure 12. Comparison of ratios of response to excitation observed by Siskind et al. (1980) 25
Figure 13. Drift correction and response spectrum calculation (case of NBT, blast 06/02/2014) 26
Figure 14. Radial rock motion time history (case of NG, blast 06/02/2014) 26
Figure 15. Raw NBT velocity time history as recorded during 06/02 blast event and 200-central moving average. 27
Figure 16. Drift correction using 200-central moving average in MS Excel 27
Figure 17. Drift correction using 200-central moving average in Matlab 27
Figure 18. Comparison of response spectra of ground motions from close-in blast event 06/02 28
Figure 19. Wave transmission theory in the structure ..... **Error! Bookmark not defined.**
Figure 20. Displacements calculation by drift correction and 200 point central-moving-average filtering 33
Figure 21. Differential transverse displacements between the top and bottom north corners of building 1 34
Figure 22. Displacement in the bottom southern part of the wall in Building 2 36
Figure 23. Differential displacements calculation 37
Figure 24. Strains at the top and bottom of buildings versus peak ground displacement. 39
Figure 25. Variation of Maximum Differential Displacement versus the PPV of ground/street level motion. 40
Figure 26. Variation of Shear strains versus the PPV of ground/street level motion. 40
Figure 27. Variation of Maximum Differential Displacement versus the PPV/f of ground/street level motion. 41
Figure 28. Variation of Shear strains versus the PPV/f of ground/street level motion. 41
Figure 29. SDOF displacement calculation for NBR time history recorded during 08/05 event in building 1. 43
Figure 30. SDOF displacement calculation for NBT time history recorded during 08/05 event in building 1. 44
Figure 31. SDOF displacement calculation for NBR time history recorded during 06/02 event in building 1. 45
Figure 32. SDOF displacement calculation for NBT time history recorded during 06/02 event in building 1. 46
Figure 33. Variation of SDOF displacement versus the PPV/f from lower street level velocity time histories. 47
Figure 34. Variation of SDOF displacement versus the PPV from lower street level velocity time histories. 47
Figure 35. SDOF displacement/maximum differential displacement versus the principal peak frequency 48
Figure 36. SDOF displacement/maximum differential displacement versus the PPV/f ratio 48
Figure 37. SDOF based prediction of absolute displacements at 2.5Hz and 16Hz 52
Figure 38. SDOF based prediction of absolute displacements at 2.5Hz and 16Hz 52
Figure 39. Frequency and Maximum Peak Velocity compared to the safety USBM and DIN 4150 criteria 53

List of tables

Table 1. Different prediction models used in literature 9
Table 2. Used Explosive characteristics. 15
Table 3. Charges per delay and distances from monitored buildings for the different investigated blasts. 19
Table 4. Principal peak frequencies for rock motion time histories recorded in the two buildings 20
Table 5. Wave velocity in rock 21
Table 6. Time amplification factors. 24
Table 7. Amplitudes and time arrival at northern upper and southern upper part for the transverse component. 29
Table 8. Differential displacements and strain levels in previous ACM and non ACM studies 38

Introduction

1 CLOSE-IN BLASTING

The vibration environment associated with urban blasting works has become of increasing interest, especially in cities where construction activities become increasingly significant. In this special case of blasting operations, a lot of attention is required in order to design more efficiently the blast to produce vibrations not exceeding the thresholds in terms of amplitudes and dominant frequencies.

This concern leads naturally to the instrumentation of surrounding buildings and to analyze thoroughly the recorded results in terms of time histories and frequency content. Since the works of Siskind et al. (1980) and Dowding (1980) on the frequency bounds and their relationship with the maximum allowable particle velocity, a lot of research work has been undertaken around the world in order to adapt the regulations to ground and constructions types. In all these studies, several techniques have been used, among them Fourier frequency spectrum, Single Degree of Freedom response spectrum (Dowding, 2000; Snider, 2003; Dowding et McKenna, 2005). The ratio of the natural frequency of the system (building) divided by the frequency of excitation (blast loading) is often used in construction vibration analysis as ground motions generally have frequencies that are 2 to 10 times the fundamental frequencies of most common structures (Dowding, 2000).

Several methods and approaches have been suggested in previous research works to predict amplitude and frequency levels such as the hybrid modeling method proposed by Hinzen (1988) which uses both field measurement of one single blasthole shot vibrations and computer simulation to linearly superpose these recorder vibrations and thus calculating vibration theoretical seismograms. More recently, Blair (2008) used a non-linear superposition modeling procedure considered to be more appropriate especially for near-field distances. He showed that non-linear superposition modeling gives lower vibration levels than those predicted by linear superposition (Blair, 1987).

Besides these first type approaches, based on analytical and field measurements, one can find other prediction methods based on empirical field experience such as the conventional predictors of USBM (Duvall and Petkof, 1959), of Langefors–Kihlstrom (1963), of Ambraseys–Hendron (1968), of the Bureau of Indian Standard (1973) and of Ghosh–Daemen (1983).
Table 1 shows the different attenuation laws proposed by these researchers.

Table 1. Different prediction models used in literature
(Qmax: maximum charge per delay (kg), R: distance blast-transducer (m) and PPV: peak particle velocity (mm/s).

Reference	Equation
USBM (1959)	$PPV = K(R/\sqrt{Q_{\max}})^{-B}$
Langefors–Kihlstrom (1963)	$PPV = K(\sqrt{Q_{\max}/R^{2/3}})^{B}$
Ambraseys–Hendron (1968)	$PPV = K[R/(Q_{\max})^{1/3}]^{-B}$
Bureau of Indian Standard (1973)	$PPV = K[Q_{\max}/R^{2/3}]^{B}$
Ghosh–Daemen predictor (1983)	$PPV = K(R/\sqrt{Q_{\max}})^{-B}\, e^{-\alpha R}$

Finally, a third predication method set is based on the mathematical and artificial intelligence techniques such statistical multivariate methods (Hudaverdi, 2012; Singh et al. 2008) and Artificial Neural Networks techniques (Khandelwal and Singh, 2006; 2007 and 2009; Mohamed, 2009). These methods are based on the previous acquainted vibrations records and have the disadvantage to require a large number of data in order to be efficient in predicting future blast vibration results.

2 PRESENT STUDY SUMMARY

The case study summarized by this study provides the multiple positions, time-correlated velocity time histories needed to advance understanding of response of urban structures to ultra-high frequency excitation. Much of the current regulation and understanding are based upon measurements of the response of residential, 1 to 2 story structures (Siskind et al., 1980; Dowding, 2000). Extension of these observations by response spectrum analysis to taller structures when excited by high frequency excitation needs to be validated (Abeel, 2012).

Most often standard response spectrum analysis assumes that excitation wave lengths are long enough that buildings are excited homogenously and respond synchronously. In other words excitation motions along the base of the structure are the same and response at the top occurs synchronously. As will be shown, for close-in rock blasting this is not valid. With high excitation frequencies (> 100 Hz for rock to rock transmission) the amplitudes and phase are likely to change along the bottom. For instance, with a propagation velocity of 3000 m/s, 150 Hz frequency and a distance along the bottom of the structure of 60 m, the excitation pulse would have traveled (60/(3000/150)=) 3 wave lengths and might have attenuated significantly (Woods and Jedele, 1985). In addition the time of arrival would not be equal at the ends of the building if the blast were detonated at one end. The peak would arrive some 60/3000 = 20 milliseconds later the other end. If the building was 5 stories high and had a fundamental response frequency of 0.5 sec., its response at the other end would be (0.020/0.5)2π or 0.080π out of phase from the end where the blast was initiated.

This study provides needed additional multiple position, time-correlated information not provided by required compliance monitoring. Current regulations often only require that the excitation motions be measured at one location. Building response is then most likely to be considered as synchronous and similar to that measured by the Siskind et al (1980). There is no requirement to measure building response, and as a result compliance measurements provide no new information about the nature of larger building response to ultra-high frequency excitation.

While this study provides this needed information to determine the type of response, the second part provides the information concerning calculation of strains and the distortion. Additional interpretation and information in the second part will help initiate development of strain- and displacement-based methods and guidelines and criteria for the evaluation and protection of structures,

Regulatory guidance that will result from these measurements can reduce the confusion in specifications, help define the most appropriate locations of measurement of response, and provide more appropriate construction controls and thus reduce costs of urban construction in rock founded cities around the world

The present study is divided into three main parts: Site and Instrumentation, Time Histories, Response. Site and Instrumentation is divided into three sections: Site and geology, Transducers, Blasting Practice. The Time History section is divided into three sections: attenuation, dominant frequencies, and propagation. The concluding section on Structure Response is divided into two sections: amplification-deamplification and response spectrum.

Chapter 1. Site environment and building monitoring

1 SITE AND GEOLOGY

This study was conducted in a dense urban location where blasting was required not just adjacent to buildings but contiguous to them as shown by the photograph in Figure 1. Blast excavation was carried out at the two sites simultaneously which led to instrumentation of the two buildings and allowed response from a blast at one to be measured at both. Contiguous blasting produced excitation ground motions that were unusually high in amplitude and with ultra-high dominant frequencies.

Both of the buildings are over 100 years old and are landmarked structures. They are 4- to 6-story unreinforced brick masonry buildings, built from the late1800s, and are typical of those structures built in this city at that time. They both have basements, details of which are shown by the photographs of the excavation for building 1 shown in Figure 2.

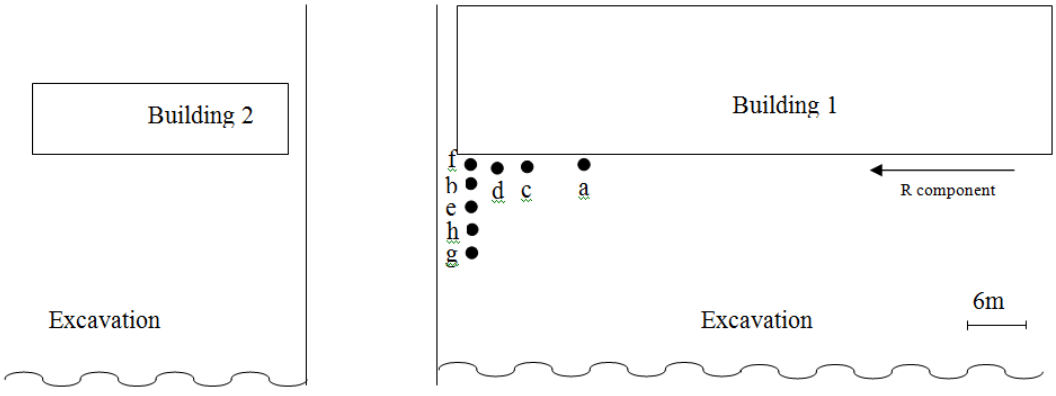

Figure 1. Blast locations with regards to the buildings.
The close proximity and simultaneous construction allows blast response from ground motions with high amplitudes and ultra-high frequency to be measured at both buildings. (a: blast 06/02/2014; b: blast 06/05/2014; c: blast 06/06/2014; d: blast 06/09/2014; e: blast 06/27/2014; f: blast 06/30/2014; g: blast 07/07/2014; h: blast 08/05/2014).

The rock supporting these structures is a mica schist whose foliation dips into the excavation from beneath the structures. It is a dark-gray to silvery, rusty-weathering, generally coarse grained, foliated but poorly layered to massive gneiss or schistose gneiss, composed of quartz, oligoclase, microcline, biotite, and muscovite, and generally sillimanite and garnet (Panish, 1992). Vertical rock faces are supported by rock bolts that are 3m long. As will be described later in the data section, propagation velocities confirm the relative stiffness of the rock mass.

2 TRANSDUCER DESCRIPTION AND INSTALLATION

Buildings and rock were instrumented with geophone transducers that meet International Society of Explosive Engineers (ISEE) standards. They measure velocity and have flat responses between 2 and 250 Hz. These transducers were monitored with LARCOR Mini Seis seismographs. Transducer output is digitized at 2048 samples per second (sps). Seismographs begin recording (6 seconds duration with 0.25 seconds of pre-trigger) when the particle velocity exceeds a threshold. The threshold had to be variably set because of the background noise produced by mechanical, rock excavation through hoe ramming. Where possible the seismographs were connected in series with one channel that provided a common time stamp that was accurate within one sample interval of 0.0005 sec. This time stamp allows measurements to be time-correlated. When the closest seismograph detects ground motion that exceeds the threshold value, it starts recording and triggers the other sensors.

2.1 *Building 1 transducers*

Four transducers were placed at the north and south corners of the west wall nearest the excavation as shown in Figure 2 (a). Two sensors were bolted at the building street level (denoted in the following as B (bottom) sensor) and two to the top of the wall (denoted hereafter sensors A). Vertical distance between the sensors B and A differs at the south and north locations because of the differing building geometry. The lower (B) transducers are bolted on brackets which in turn are bolted into the mortar between bricks on the building about 1 m (3-4ft) above street level. The upper (A) transducers are epoxied to the inside of the parapet wall just above roof mastic.

At each location, there were two transducers; one in the radial direction, parallel to the west wall and the other in the transverse direction, perpendicular to the west wall. Each set of transducers was monitored with a mini Seis. Each Mini Seis was connected vertically to provide a common time stamp. In addition, where and when possible, south and north sets of transducers were connected to provide a common time stamp.

In addition one set of rock transducers was installed in the rock beneath the north corner. These transducers were also oriented in the radial (parallel) and transverse west wall directions. Typical construction interference and hoe ramming reduced the number of blast events wherein rock transducers were in place and operating so as to trigger off the blast events. Construction interaction prevented installation of rock transducers altogether at the south end.

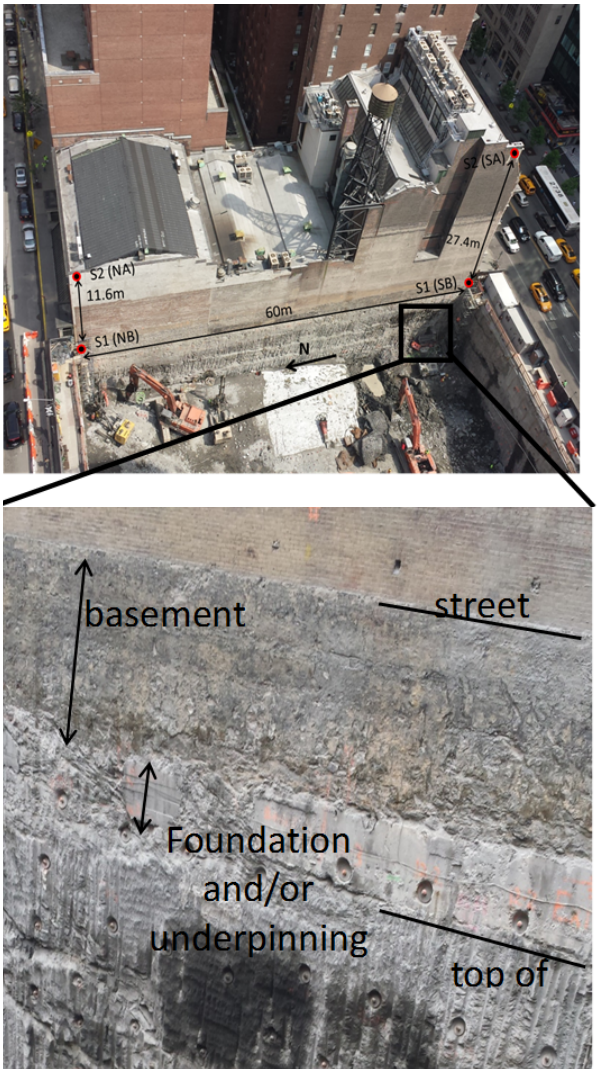

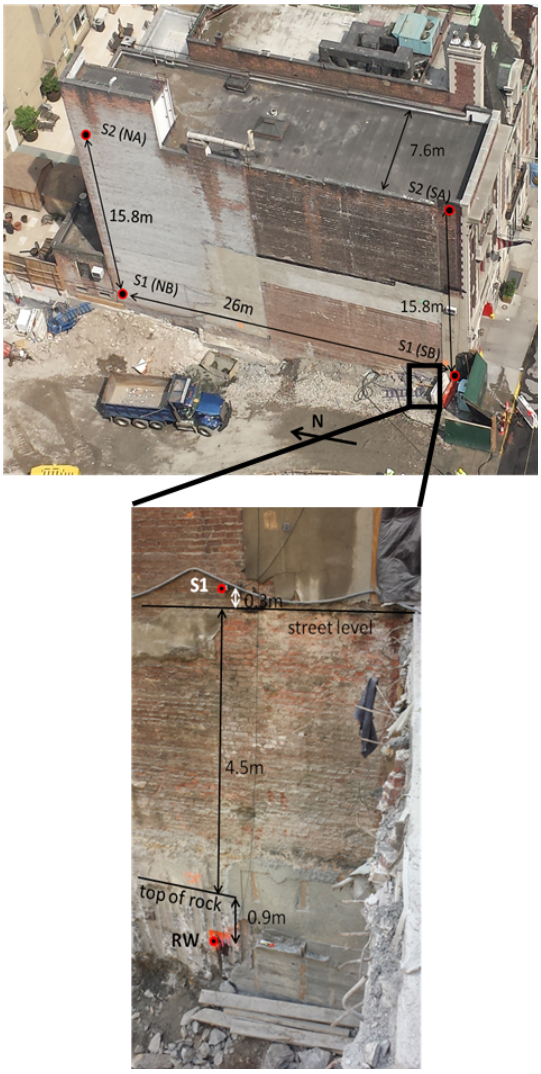

Foundation details of Building 1 *Foundation details of south end of Building 2*

Figure 2. Locations of the sensors at the upper and lower parts of the monitored walls at the two buildings.

2.2 *Building 2 transducers*

Building 2 was instrumented in a manner similar to that of building 1 as shown in Figure 2 (b). As with building 1, transducers were placed at the lower and upper parts of the wall in the radial and transverse directions. North A transducers with bolted to the inside of the upper tower portion instead of the parapet location. As with building 1, the north and south sets of transducers were time correlated. In addition, the north and south pairs of transducers sets were wired to produce time correlated response time histories.

Two other transducers were also bolted to building 2. One transversely sensitive transducer was bolted to the inside of the basement wall at mid height, 10 m (33 ft) north of the south wall as shown in Figure 2. A second, vertically sensitive transducer was mounted to the underside to the basement ceiling (first floor) also 10 m north of the south wall.

Two sets of rock transducers were installed beneath building 2; one set beneath each the north and south wall. As with the building motion transducers, rock transducers were oriented both radially (parallel) and transversely to the west wall. As shown in Figure 2, they were installed 5.5m (18ft) below the basement floor level.

Time correlation connections and timing of transducer installation were difficult to coordinate with construction and blasting. As is true for instrumentation of any construction project, many opportunities are lost because of either timing. There was no provision for time correlation between the two buildings, as the distance was too large and the cable rout too complex. While much of the data obtained for bottom (B) and top (A) responses is time correlated, correlation between corners was difficult to obtain because of connection challenges. Because of late installation, rock response is missing for several of the blasts.

3 BLASTING PRACTICE

Rock fragmentation and excavation was accomplished with close-in blasting technique shown in Figure 3. Blasts are initiated by a Nonel initiation system. Holes are delayed with 25 and 17 ms surface delays with 500 ms in-hole delays. A blast typically contains 20-50 holes with 2 to 10 rows. The holes are arranged in a spacing and burden pattern of less than 60cm x 60cm (2ft x 2ft). There was usually at least one free vertical face, and often two.

Blastholes are charged with either of two explosives types described in Table 1. Because of limitations in blast-induced vibrations, the number of holes is often high, hole diameter is small and in-hole delays are used. A typical blast hole contains capped Emulex cartridges at the bottom of the hole as it is a detonator sensitive emulsion explosive. Then, a couple Emulex chubs above and few sticks of Red-D Lite-E, followed by one capped Emulex chub are incorporated at the top of the hole before stemming.

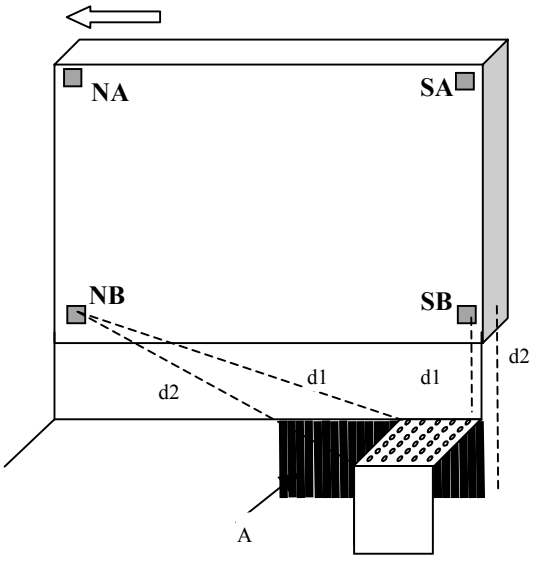

Figure 3. Simplified Sketch of the two buildings and a current blast (A: half casts of continuous line-drilling to produce a slot).

Table 2. Used Explosive characteristics.

Explosive	Type	Cartridge size (mm)	Cartridge weight (kg)	Density (g/cm3)	Water resistance	VOD (m/s)
Emulex 927	Emulsion	38 x 300	0.4	1.17	Excellent	5413
Red-D Lite-E	Emulsion	22 x 600	0.43	1.06	Excellent	4570

Chapter 2. Time histories analysis

1 ANALYSIS METHODOLOGY

Several Matlab® routines have been developed during this work in order to derive the main time and frequency characteristics of the recorded velocity time histories and to calculate the displacements and to finally estimate the strains level within the west walls of the two buildings. The following sections present the different results. This includes Peak Particle Velocity (PPV), Wave velocity within the structure, Principal Peak frequency, Fast Fourier Transform Analysis and Transfer Function calculations between the upper and the lower records, Single-Degree-Of-Freedom response spectra, displacement histories and strain levels.

The general methodology followed in the present work is summarized in the flowchart of Figure 4 and described in the following subsections.

2 BLAST-INDUCED VIBRATIONS TIME HISTORIES

Events for which response velocity time histories were time correlated can be grouped into four clusters on the basis of the number of active transducers whose responses were time correlated.

- Set 1: four transducers at the N (upper and lower) and S corners of the west wall of building 1: 06/27/2014; 06/30/2014; 07/07/2014; 08/05/2014
- Set 2: three transducers at Ground level (rock) and the N (upper and lower) corner of building 1: 06/09/2014 and 06/05/2014.

- Set 3: five transducers at Ground level (rock) and the N (lower and upper) and S corners of building 1: 06/06/2014 and 06/02/2014.
- Set 4: five transducers at Ground level (rock) and the N (upper) and S corners of building 2: 08/05/2014. Building 1 response to this blast was also recorded.

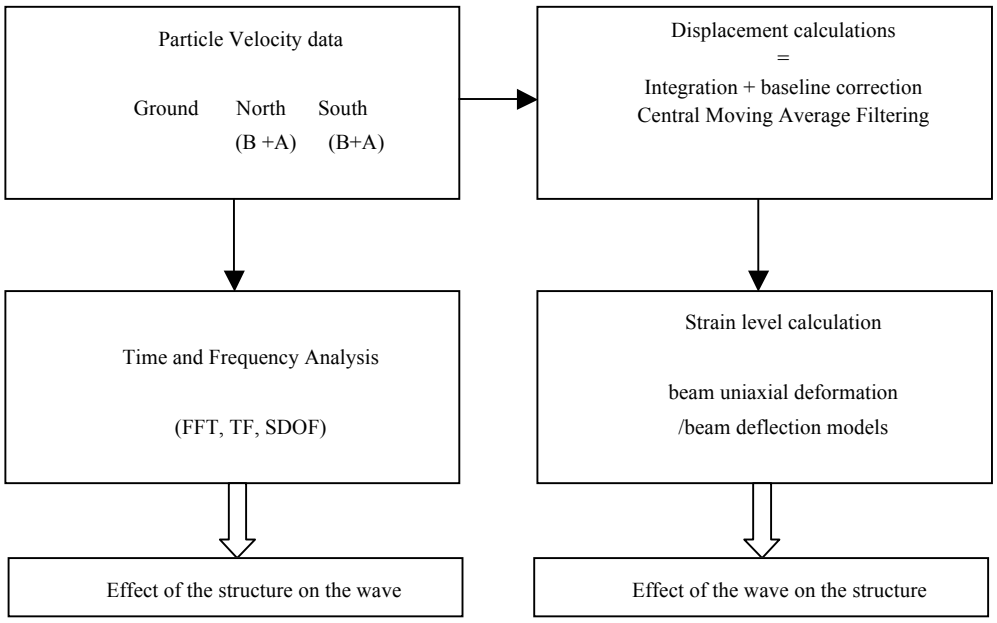

Figure 4. Flowchart of the general methodology adopted for the buildings response analysis.

Description of the transducers types and installation having been presented previously, the same methodology as for the Building 1 was adopted. Appendix A presents the time correlated channels along with maximum peak particle velocities (PPV) and dominant frequencies. Locations of these events are presented in Figure 1and are labeled by letter, a-g. Figure 5 and Figure 6 present velocity time histories of responses to event 06/02 (a). Rock excitation motions (GR) are shown with top of basement motions (NB) in Figure 5. Attenuation is so large that the south (SB & SA) and top north (NB &NA) motions had to be plotted on a separate figure, (Figure 6) to be visible. Rock motion PPV is attenuated when it arrives at the bottom part of the building 1 and continues attenuating up and across the structure.

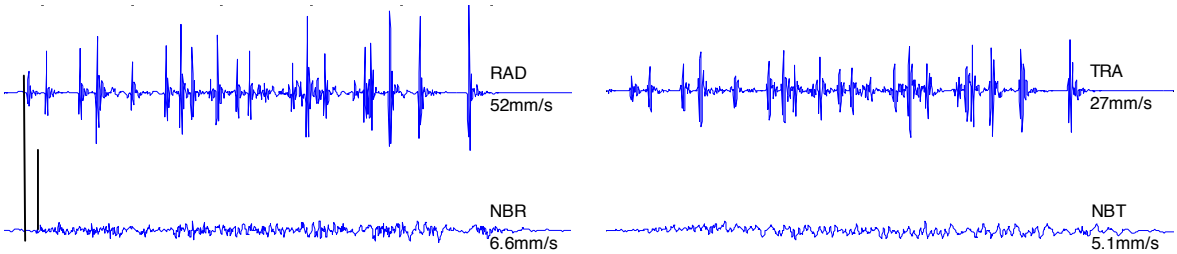

Figure 5. Transmission of the ground motion to the lower transducer during blast 06/02.

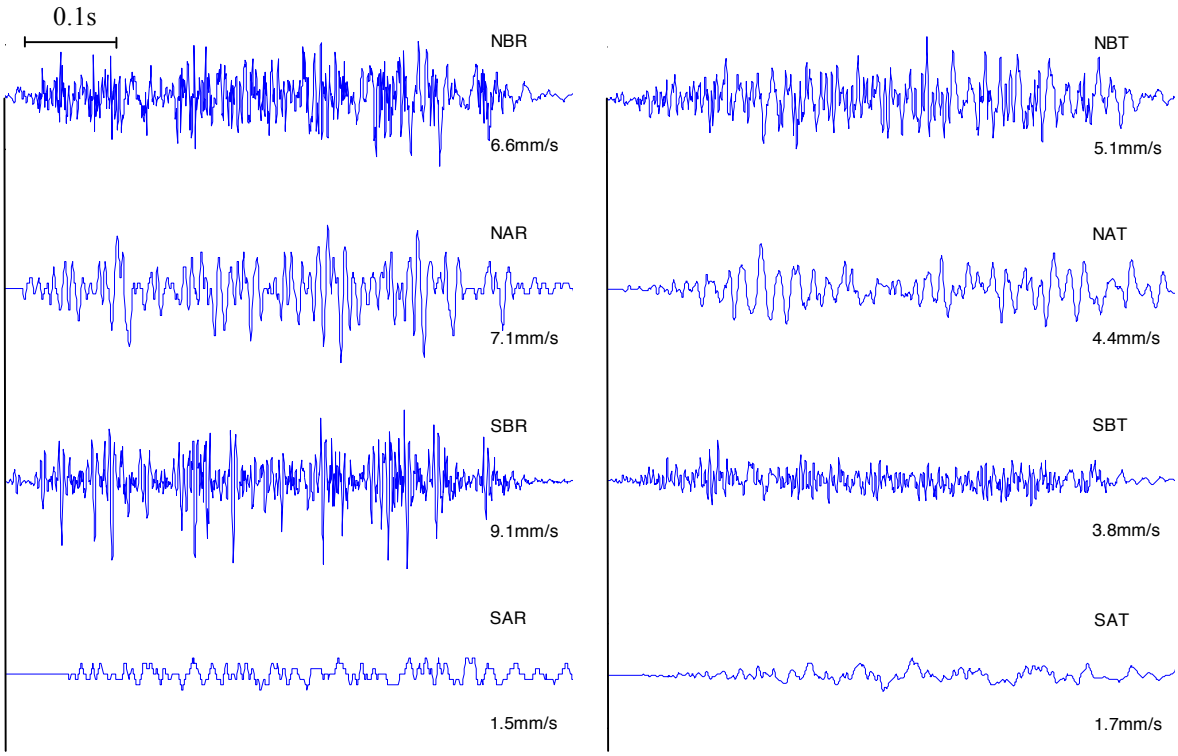

Figure 6. Transmission of the ground motion to the lower transducer during blast 06/02.

2.1 *Attenuation of peak particle velocity*

Ground motions monitored in this study produced peak particle velocities (PPV's) that attenuate at expected rates when plotted against square root scaled distance .Table 2 gives the charge per delay and the distances from the two buildings for the eight blasts.

Peak particle velocity (PPV) and their scaled distances are compared to Oriard's expected values in Figure 7 (Oriard, 1972). Building PPV's fall between the upper and lower bounds of typical blasts and are well below the upper bound for confined blasts. Rock PPVs occur along Oriard's upper bound. The higher rock motions are likely a result of the unusually small transmission distances and complete rock to rock transmission. As will be shown later, these rock to rock motions occur at unusually high frequencies and produce unusually low building response. They are rarely measured because most urban geometries only allow measurement at the street level, the lower or B level in this study.

The lower, typical PPV's at the street level in such proximate and challenging conditions result from the high drill factor (large number of holes per fractured volume) and the line drilling illustrated in Figure 3. The over lapping line drilling produces a slot that in most instances prevents immediate rock to rock transmission above the bottom of the slot. Typical practice advances the slot below the elevation of the bottom of the present blast holes.

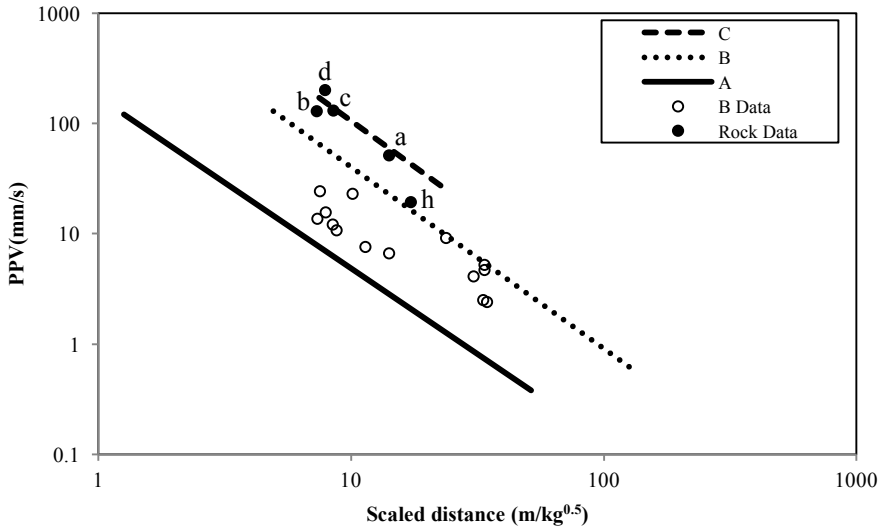

Figure 7. Comparison of measured square root scaled distance attenuation and Oriard's (1972) expected values for typical practice showing the difference between rock to rock motions and those from rock to street motions.

Table 3. Charges per delay and distances from monitored buildings for the different investigated blasts.

Blast	Sym-bol	Charge/del ay(kg)	Vertical distance (m)	(Scaled) Distance from Building 1 (m/kg$^{0.5}$) (m)		(Scaled) Distance from Building 2 (m/kg$^{0.5}$) (m)	
				North	South	North	South
06/02/2014	a	2.41	9.4	(14.1) 19.8	(23.7) 35.6	(42.6) 65.5	(26.8) 40.5
06/05/2014	b	2.29	9.4	(7.3) 5.8	(35.6) 53.0	(33.1) 49.1	(17.1) 24.1
06/06/2014	c	2.41	9.4	(8.5) 9.1	(30.4) 46.3	(35.8) 54.9	(20.0) 29.6
06/09/2014	d	2.41	10.4	(7.9) 6.7	(32.1) 48.7	(34.6) 52.7	(18.9) 27.4
06/27/2014	e	2.81	13.4	(8.8) 6.0	(33.2) 54.0	(29.4) 47.4	(16.1) 23.5
06/30/2014	f	2.81	12.5	(7.5) 1.9	(33.7) 55.1	(28.2) 45.7	(14.5) 20.9
07/07/2014	g	2.81	11.0	(10.1) 12.9	(34.5) 56.7	(29.1) 47.9	(16.1) 24.7
08/05/2014	h	2.96	16.2	(11.4) 11.0	(33.6) 55.5	(29.7) 48.5	(17.2) 24.7

2.2 *Ground vibration and frequency*

Measurement of particle velocity time histories of rock to rock motions reveals ultra-high excitation frequencies. The principal peak frequency of ground motion was calculated directly from the time history because of the singular pulse excitation. Fourier frequency calculations of transient motions can be misleading unless windowed tightly around the principal pulses, which is likely to return the same frequency as that calculated directly from the time history as shown below. First, the principal pulse is detected. Then, a zero-crossing half-period of that pulse is determined and the dominant frequency is calculated as 1/(2x (½ T)) as shown in Figure 8.

Principal pulse frequencies for the radial and transverse components of all ground motion time histories recorded during the survey are compared in Table 3. These range from 250Hz to 465 Hz for the building 1 and 68 to 128 for the more distant building 2. These high principal peak frequencies are one of the important unique features of this study. Implication of this ultra-high frequency motions will be discussed in the following sections.

Table 4. Principal peak frequencies for rock motion time histories recorded in the two buildings

Blast	Symbol	Building	Radial	Transverse
06/02/14	a	1	435	385
06/05/14	b	1	465	341
06/06/14	c	1	333	250
06/09/14	d	1	286	266
08/05/14	h	2	68	128

3 PROPAGATION VELOCITY IN ROCK AND STRUCTURE

Propagation velocities in the rock and structure can be calculated from the differences in time correlated arrival times. Complexity of the time histories produced by close-in multi-hole blasts only allows calculation of the first arriving compressive waves. Arrival times at the N & S, lower, B, locations were employed to estimate rock propagation velocities. Arrival times at the A & B locations at the either the N or S locations were employed to calculate building propagation velocities. Figure 3 shows a simplified sketch of the geometry for a hypothetical position of the blast.

3.1 *Rock wave velocity*

Assume that the blast is initiated at time t_0 and that the ground motion arrives at the northern lower point at t_1 and the southern lower receiver at time t_2. If the distances between the blast and these two sensor positions are respectively d_1 and d_2 then, the compressive wave propagation velocity within the rock is given by:

$$V = \frac{d_1}{t_1 - t_0} = \frac{d_2}{t_2 - t_0} \quad so \quad V = \frac{d_2 - d_1}{t_2 - t_1}$$

Based on the blast and lower N and S sensor positions, as well as on the arrival time difference between the S and N records, the wave velocity could be estimated with either the R or T component records. Table 4 shows the computed values and the mean value using the three blast records. Distances account for both plan locations of the nearest boreholes and shot induced travel path shown in Figure 3.

3.2 *Wave velocity within the structure*

The compressive wave propagation velocity within the structure was derived from the transit time differences between A and B transducers and the distance between them. The transit time was computed as the difference between the wave arrival times to the lower (B) and upper (A) sensors at Northern and Southern parts of the structure. Figure 8illustrates the time differences in arrival times with full wave forms at northern positions of the structure. Table 5 gives the propagation velocity values when traveling within the structure at the N and S corners.

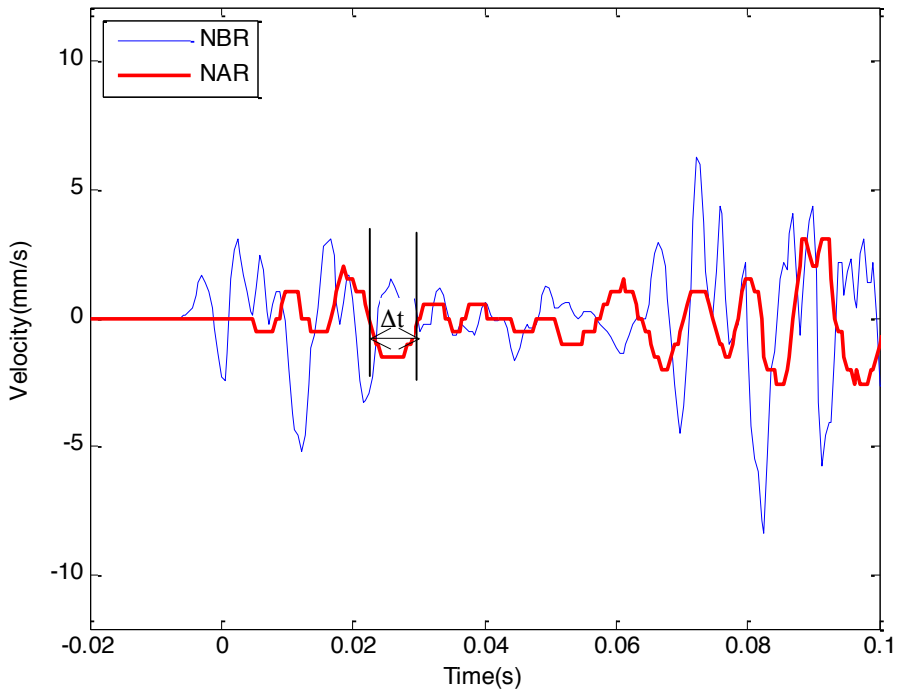

Figure 8. Transit time estimation
Case of north radial velocity wave recorded at lower and upper transducers in building 1 during 06/06/2014 event.

Table 5. Wave velocity in rock

Blast #	Blast date	Distance to blast (m)		(t_S-t_N) (s)		Wave velocity in rock (m/s)	
		N	S	R	T	R	T
1	6/30/2014	13.3	62.4	0.006347	0.007812	7729	6280
2	6/27/2014	10.3	66.7	0.006348	0.008301	8871	6784
3	7/7/2014	21.9	72.6	0.011718	0.0078123	4328	6492
				Mean value		6976	6518

4 STRUCTURE RESPONSE TO ULTRA HIGH FREQUENCY EXCITATION FROM CLOSE-IN BLASTING

4.1 *Comparison of ground motion and structure response*

Rock ground motion wave arrives with high amplitudes (up to 200 mm/s) and ultra-high frequency (250~500Hz). It is quickly attenuated in the structure (down to 24 mm/s in the lower, B, transducers and 21 mm/s in the upper, A, transducers) and filtered (down to 50Hz). Dominant frequencies at the lower, B, level are higher than that at the upper, A, level. For instance mean values of radial dominant frequencies are 108Hz and 158Hz at the lower northern and southern levels at building 1 and 72Hz and 36Hz at the upper, A, levels. The closest (06/30/2014) and the furthest (06/02/2014) blasts to the north end of building 1 produced similar dominant frequencies at both B and A levels at the north corner.

4.2 *Natural frequency and damping ratio*

As will be demonstrated later, these urban structures do not respond sufficiently synchronously to allow standard techniques for calculating dynamic response properties of the entire structure. Responses of 17 Hz components were found in several instances, but not those of the building as a whole. Some sense of dynamic structural response properties can be obtained by investigating amplification-deamplification of the excitation motions.

The structure damping ratio was determined using two approaches using the free vibrations part of the transverse velocity time history recorded at the upper northern sensor (parallel to the short axis of the building). As mentioned by Dowding (1985, 2000), the critical damping ratio can be estimated from the decay of the free vibration using:

$$\beta = \frac{1}{2\pi}\left(-\ln\frac{\dot{u}_{n+1}}{\dot{u}_n}\right)$$

Where $\dot{u}_n$ and $\dot{u}_{n+1}$ are successive amplitudes (Thompson, 1981).

As annotated in Figure 9, the blast loading ends around 0.75s and a free vibrations period begins until 1.8s. Two successive peaks were noted:

$$\dot{u}_n = 0.254\text{mm/s and}\,\dot{u}_{n+1} = 0.381.$$

Therefore: $\beta = 66.5\%$

On the other hand, the damped natural period of the first mode of vibration, labeled T can be read on the free vibrations plot: T=59ms

So, the natural frequency is:

$$f_s = 17Hz$$

And the damped circular natural frequency is:

$$p_d = p\sqrt{1-\beta^2} = 2\pi f_s = 106.5rd/s$$

Where p is the undamped circular natural frequency.

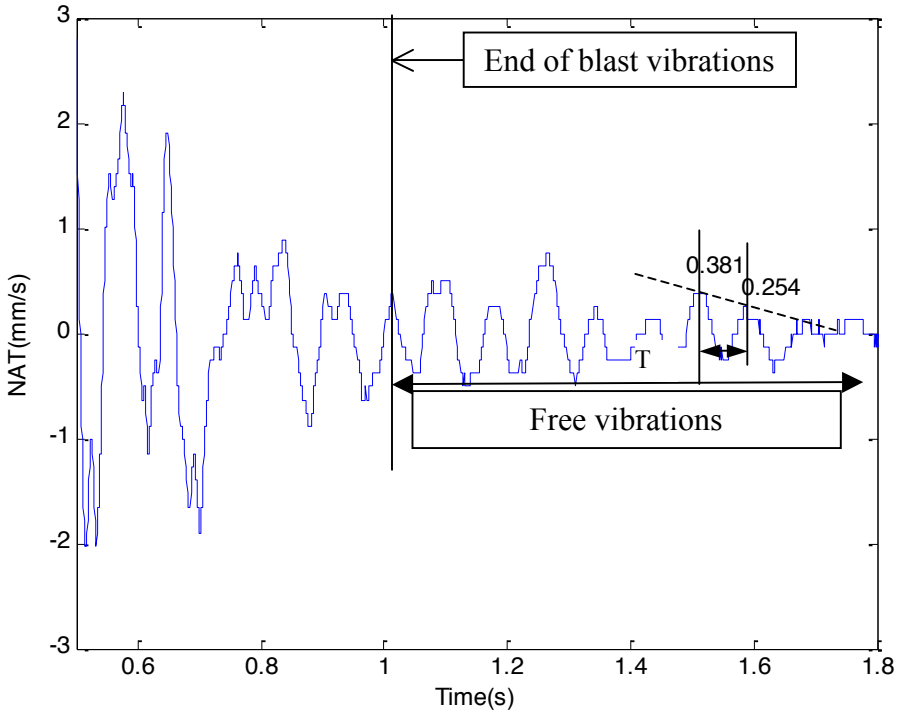

Figure 9. Upper North transverse velocity time history recorded at Building 1 during blast 06/02showing free vibrations of the structure

4.3 *Amplification-deamplification*

A sense of the structural dynamic response properties can be obtained from ratios of response amplification-deamplification. The greater the amplification, the closer is the building's natural frequency to the excitation frequency. These ratios can also be compared to past amplification ratios to determine the degree to which these buildings behave in similar or dissimilar fashion to those studies in the past. The most useful comparison is the amplification values observed by the US Bureau of Mines during their study of cosmetic cracking induced by blasting near residential structures (Siskind et al., 1980). To be compatible with the Siskind study, the ratios were determined from response to the principal (greatest amplitude) pulse of any blast event as illustrated in Figure 10. Given the travel time from bottom to top the response maximum was chosen as the amplitude within 0.01 sec of the principal pulse. This is not the max response; however a study with maximum response, no matter its timing with respect to the principal pulse, returned ratios that were similar.

Three measures of amplification were examined:

- Top (A)/Rock(G): maximum velocity at the upper transducer and that at the rock level.
- Bottom (B)/Rock(G): maximum velocity at the lower transducer and that at the rock level.
- Top(A)/Bottom(B): maximum velocity at the upper transducer and that at the lower.

For each of these amplification factors, the two components (radial and transverse) were considered. Figure 10 presents this procedure for the case of radial lower and radial ground velocities recorded at the northern part of building 1 during the 06/05/2014 blast event. Table 6 presents all amplification factors calculated for the 8 investigated blasts.

4.1 *Mid-wall versus upper structure amplification*

Basement walls are the only freely responding element in direct contact with rock. All other components respond to the attenuated building motions. Thus comparison of basement wall response to that of other elements, lower amplification (Bottom/Rock) and upper amplification (Top/Rock), is of special interest. The response of building 2 during the 08/05/2014 event provides this comparison. Basement deamplification is 0.61, which can be compared to Bottom/Rock amplification of 0.28 and Top/Rock amplification factor 0.51.

4.1 *Comparison with wall and superstructure response measured by USBM*

Figure 11 and Figure 12 compare amplification factors from this case and those reported by Siskind et al. (1980) for one- and two-story residential structures (homes) . Top/rock and top/bottom amplification factors obtained at the corners of the two buildings are found to the extreme right of the superstructure response (Figure 12.a). In no case is there amplification, the largest ratio of 0.92. Wall/rock amplification factor for building 2 during the 08/05 event and bottom/rock amplification factors are again found on the extreme right of the wall response (Figure 12.b) again there is no amplification, even for the basement wall that is in direct contact with the rock. However, even though it sustains high particle velocity, its relative displacement remains low because of the high excitation frequency as discussed below.

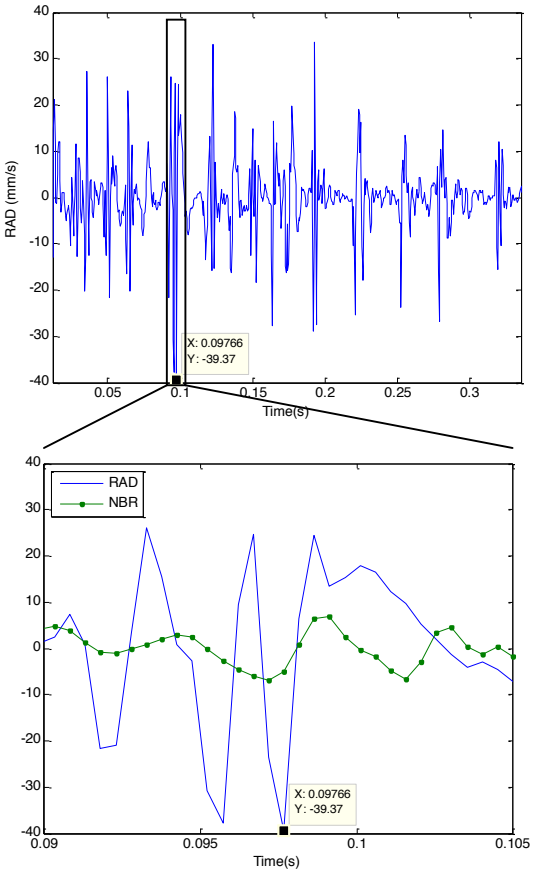

Figure 10. Peak velocities for radial ground motion and north lower radial component during blast 06/05 (duration of the blast equal to 0.33s)

Table 6. Time amplification factors.

		Bottom / Rock amplification				Top / Rock amplification				Top / Bottom amplification			
Building	Blast	NBR/RAD	NBT/TRA	SBR/RAD	SBT/TRA	NAR/RAD	NAT/TRA	SAR/RAD	SAT/TRA	NAR/NBR	NAT/NBT	SAR/SBR	SAT/SBT
Buil1	06/27	-	-	-	-	-	-	-	-	0.39	0.45	0.39	0.50
Buil1	06/30	-	-	-	-	-	-	-	-	0.68	0.92	0.19	0.09
Buil1	07/07	-	-	-	-	-	-	-	-	0.10	0.17	0.21	0.47
Buil1	08/05	-	-	-	-	-	-	-	-	0.26	0.38	0.11	0.36
Buil1	06/05	0.17	0.05	-	-	0.09	0.04	-	-	0.23	0.34	-	-
Buil1	06/09	0.03	0.03	-	-	0.02	0.01	-	-	0.32	0.34	-	-
Buil1	06/02	0.06	0.18	-	-	0.05	0.10	-	-	0.69	0.65	0.17	0.10
Buil1	06/06	0.05	0.007	-	-	0.03	0.09	-	-	0.33	0.24	0.25	0.10
Buil2	08/05	-	-	0.13	0.28	-	-	0.06	0.05	-	-	0.51	0.19

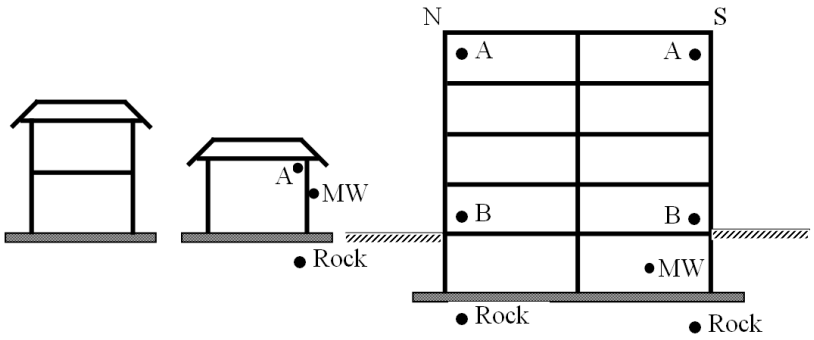

Figure 11. Instrumentation for USBM 1-story, 2-story residential structures and the taller urban structures of this study.

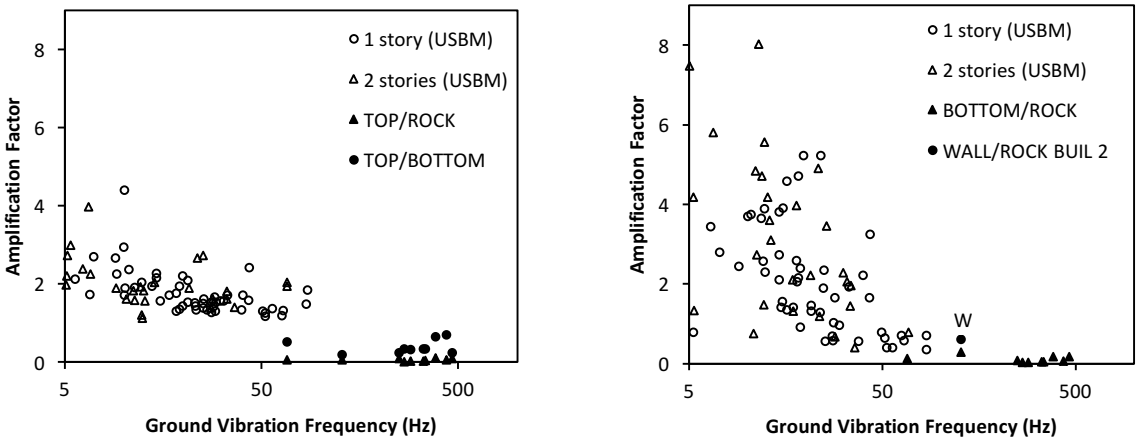

(a) Superstructure (b) Wall

Figure 12. Comparison of ratios of response to excitation observed by Siskind et al. (1980) and those from this study shows that the ultra-high frequency excitation fails to cause amplified response.

5 PSEUDO VELOCITY RESPONSE SPECTRA DEMONSTRATE THE EXPECTAION OF LOW DISTORTION

5.1 *Filtering and SDOF Calculation*

From time to time, a low frequency rider is observed in the velocity time history like that shown in Figure 13 (a-upper). It persists after integration and typical baseline correction in the displacement time history and results in displacement time histories that end with a permanent offset that cannot be true. In addition the rider produces an unusual response spectrum as shown by the thin lined spectrum in Figure 13 (b) In this study, these low frequency riders were filtered with a 200 point window central moving average filter as shown in Figure 13 (a-lower) to return a velocity and displacement time history that oscillates about zero. While many explanations have been advanced for the rider, there is as yet no universally accepted explanation. This particular case is enlightening, as it rules out one possibility, a delayed gas pressure pulse. As shown in Figure 14, the rock motions (G) do not contain this low

frequency motion, while those measured at building's street level, B1 (a) do. Therefore it cannot be a result of a delayed gas pressure pulse, which if it existed, would be evident in the rock motions. The possibility that the rider is the building's fundamental frequency response, is also unlikely as it occurs too early in the time history, was not observed at the south end and there was no free response at this low frequency after excitation ceased.

Pseudo velocity response spectra were calculated with two routines; NUVIB2 and Matlab. NUVIB2 (Chok t al., 2003) is software developed at the Department of Civil Engineering of Northwestern University to process velocity time histories with provisions for filtering, and baseline correction. The Matlab routine was developed by (Papazafeiropoulos, 2014) which is based on the General Single Step Single Solve (GSSSS) family of algorithms published by (Zou and Temma, 2004). These algorithms are employed for direct time integration of the various SDOF oscillators.

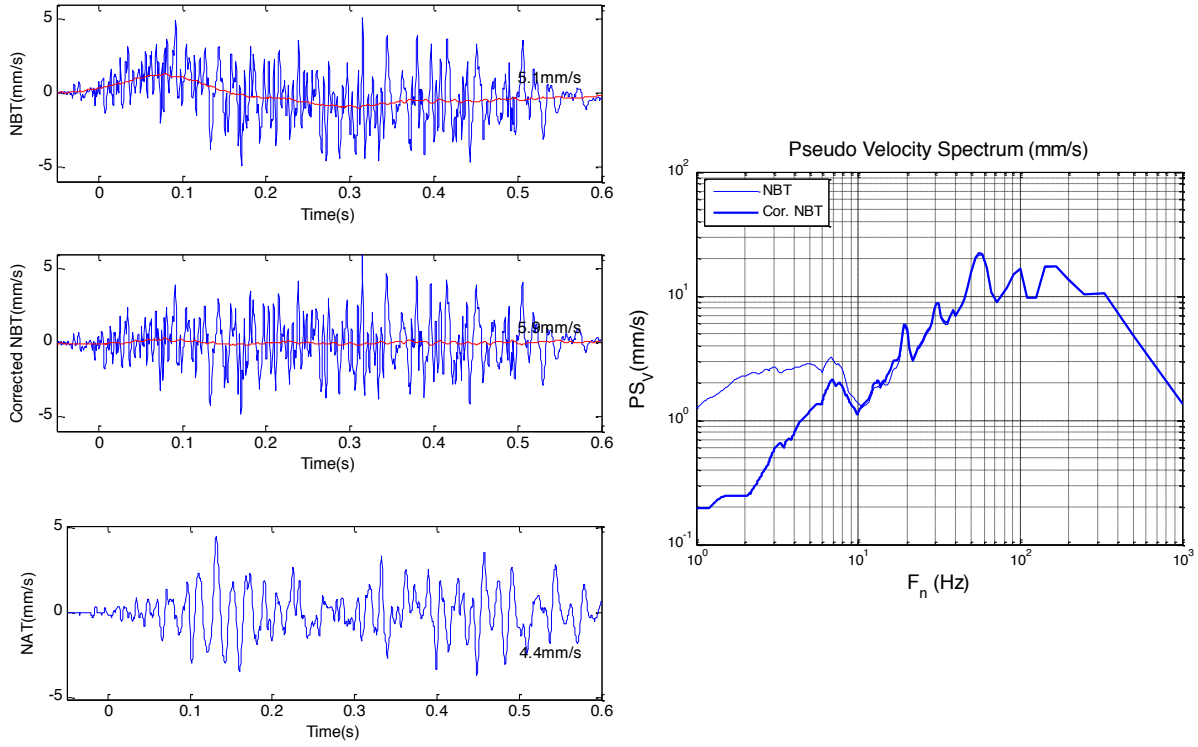

(a) Measured and corrected velocity time histories (b) Measured and corrected response spectra

Figure 13. Drift correction and response spectrum calculation (case of NBT, blast 06/02/2014)

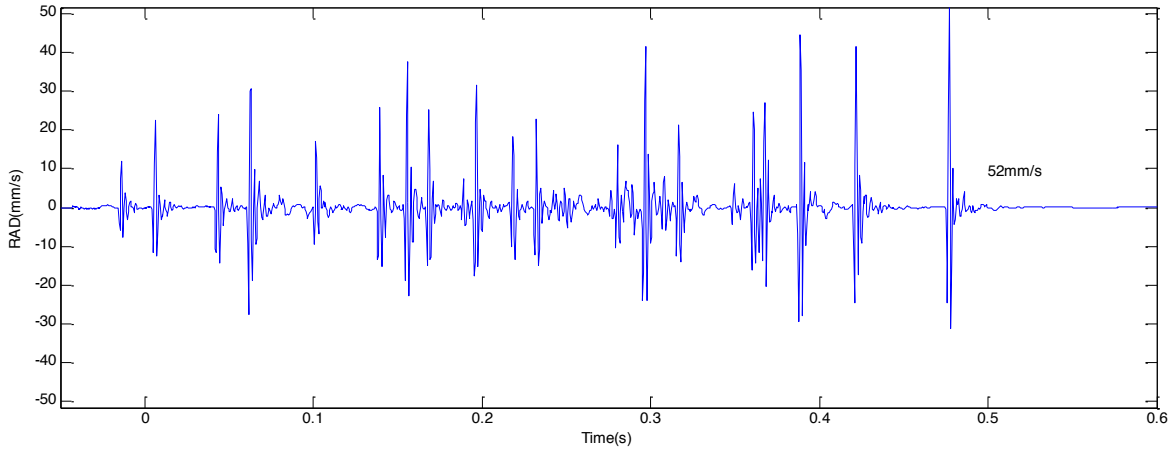

Figure 14. Radial rock motion time history (case of NG, blast 06/02/2014)

5.2 *Comparison with MS Excel 200-central moving average filtering*

The results of such a Matlab procedure was compared to those of performing a simple Central Moving Average of the velocity time history using Excel software. Figure 15 gives the raw measured NBT velocity time history as recorded during 06/02 event and the central moving average using 200 point window. This figure shows the drift phenomenon that should be removed from the raw data. Figure 16 and Figure 17 give the results of data processing using respectively the Excel central average moving filter and the developed Matlab procedure. The Peak Particle Velocities obtained from these two methods are respectively 5.97 mm/s and 5.94 mm/s. This so small difference is due to error in calculations as the Matlab procedure uses integration of raw velocity data (to obtain displacement) and then derivation to recompute the corrected time history velocity.

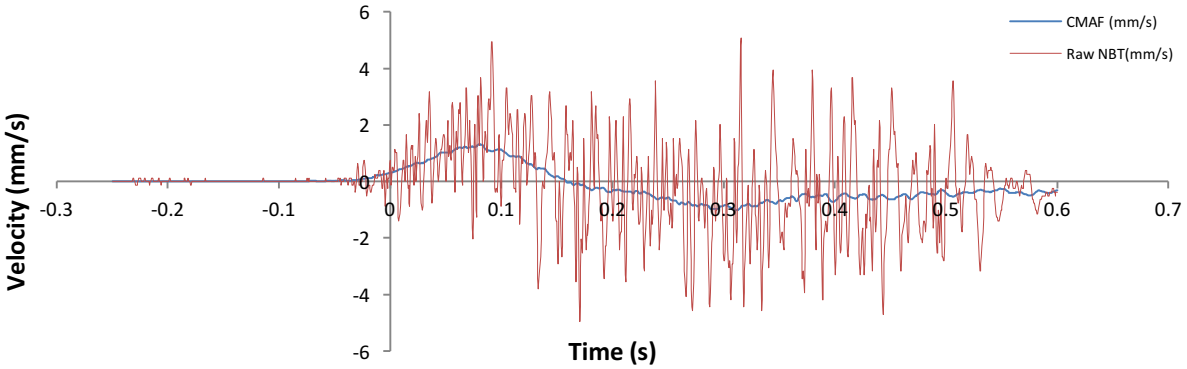

Figure 15. Raw NBT velocity time history as recorded during 06/02 blast event and 200-central moving average.

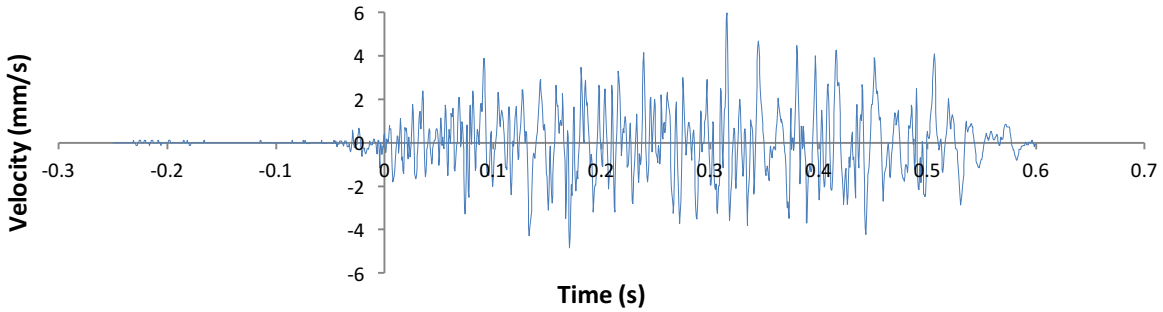

Figure 16. Drift correction using 200-central moving average in MS Excel (case of NBT velocity time history as recorded during 06/02 blast event)

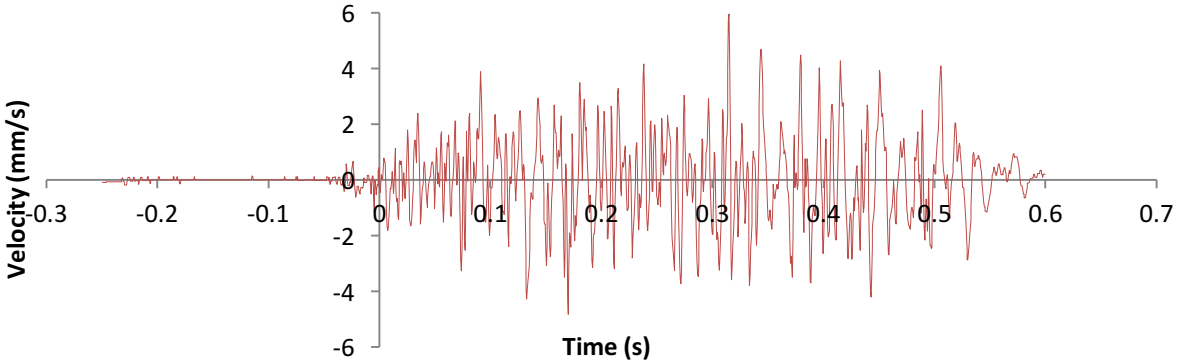

Figure 17. Drift correction using 200-central moving average in Matlab (case of NBT velocity time history as recorded during 06/02 blast event).

5.3 *Comparison with tunnel and quarrying blasts*

Considerations of energy and mass show that response of large, urban structures to ultra-high frequency excitation is likely to be lower than that predicted by standard response spectrum analysis. First consider single degree of freedom (SDOF) pseudo velocity response with 5% damping of the 06/02 event compared to shown with that from a large, distant quarry (B) and close tunnel (A) blast shown in Figure 18. Details of this calculation are described in Appendix B. Spectrum A was developed from ground motions recorded 12m (38ft) away from a 0 to 9 ms delayed tunnel blast with a maximum charge in any single delay of 1.7 kg (3.8lb). Spectrum B was developed from the ground motions recorded 72m (220ft) away from a single 91 kg (200lb) charge detonated in a typical bench blast hole in a limestone quarry. The quarry blast generated a peak radial particle velocity of 43 mm/s (1.7 in/s) and the tunnel blast generated a peak radial particle velocity of 61 mm/s (2.39 in/s) (Dowding, 2000). The 06/02/2014 blast generated a radial peak particle velocity of 51 mm/s in the rock from a 2.4 kg blast some 9+ m distant.

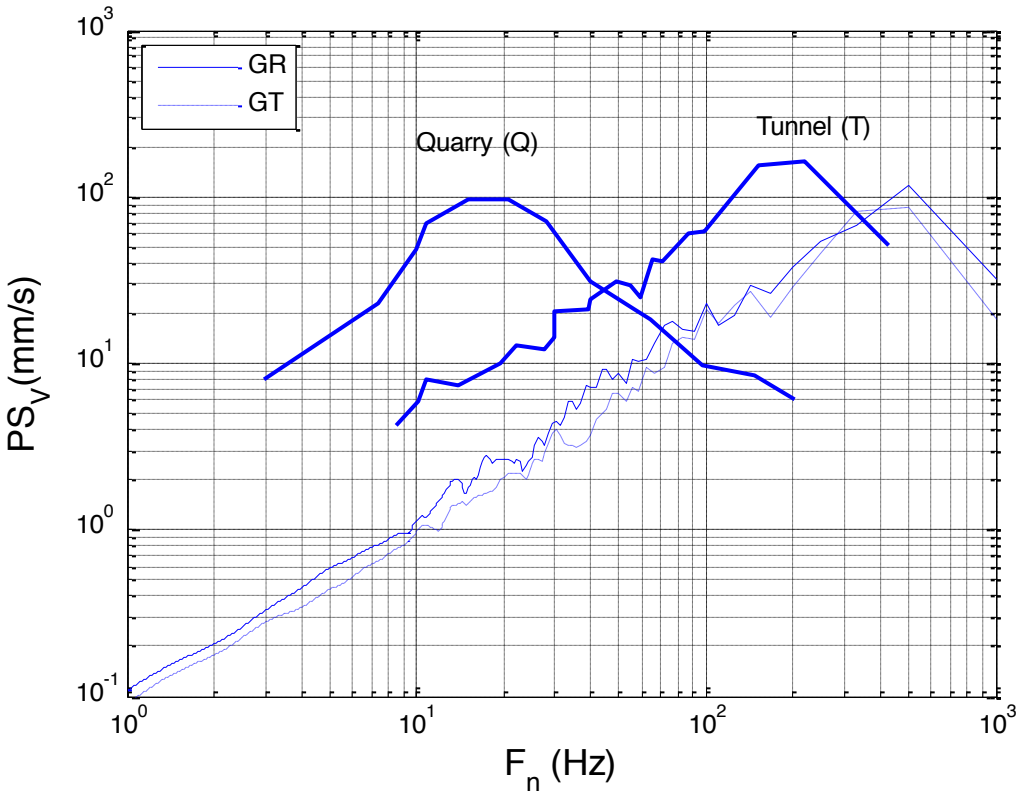

Figure 18. Comparison of response spectra of ground motions from close-in blast event 06/02 and a low frequency quarry blast (Q) and a near-by tunnel blast (T).

Even though the peak particle velocities are similar, standard response spectrum analysis predicts that a single story, 10Hz structure will sustain a response velocity 60 and 6 larger for the quarry and tunnel blasts. Since the pseudo velocity is proportional to relative displacement for structures with the same natural frequency (10 Hz in this case), the 06/02 event would be expected to induce far less relative displacement, strain, and cosmetic cracking to a typical single story residential structure. Now consider that these particular urban structures are far more massive because of their size and masonry construction. Their super structures can be expected to have periods, T, of 1/10 sec per story, where a five story structure would have a

natural frequency (1/T) of 1/ (5*0.1) = 2 Hz. The 2 Hz response to the 06/02 event is 1/5th that of the 10 Hz response and an urban structure would likely sustain 1/5th the relative displacement strain and cosmetic cracking.

Response of the urban structure is likely to be even less than predicted by SDOF analysis. SDOF analysis carries with it an implicit assumption that the entire building is AND can be entirely excited synchronously. First consider synchronous excitation. These urban structures have a larger foot print (65 x 15 m) compared to a residence (8 x 10 m) and are excited by motions with pulses (= ½ a wave length) that are only 10 m (= c/f = 6000 m/s/300 Hz). The distance from the north to the south of building 1 is 3 wave lengths. The same pulse cannot excite the entire structure synchronously. Now consider the mass to energy ratio. A structure with a natural frequency of 2 Hz that is 4 time stiffer than a 10 Hz structure would be some 100 times more massive if its natural frequency could be estimated as the square root of the stiffness divided be the mass. Now consider the energy of the excitation pulses. If it is assumed that the energy of the excitation is proportional to the peak particle velocity divided by peak acceleration (Sucuoglu and Nurtug, 1995) or 1/f of a single principal pulse event with the same displacement, then a 300 Hz excitation is some 100 times less energetic than a 30 Hz event. Thus the energy to mass ratio of the close-in rock blast excitation of an urban structure is 1/10,000 that of a quarry blast excitation of a residential structure. Thus there are two reasons to suspect that close in blast perturbation of a large urban structure will produce less distortion than a SDOF analysis: it is not excited synchronously and the energy to mass ratio is smaller than associated with observations of cosmetic cracking.

6 COMPARISON OF TIME CORRELATED TIME HISTORIES ILLUSTRATES WAVE TRANSMISSION

Time correlated comparison of rock excitation and building response motions demonstrates that the buildings do not respond synchronously as a unit. Table 7 presents maximum velocity amplitudes and arrival times of the blast-induced response at the northern and southern transducer strings of all events. To more clearly illustrate details of building response, velocity time histories from one event are plotted in a common amplitude scale in their relative positions in both time and space in **Error! Reference source not found.**. Differences in times of arrival are illustrated by the arrows. Differences in amplitude are illustrated by differences in size. Arrival times are delayed by some 60 milliseconds (ms). This time difference is large enough to encompass some 3 separate excitation pulses as shown by comparison of differences in arrival times and the excitation motions at the bottom of the figure. Amplitudes and dominant frequencies decline both upward and across (north to south) the structure. Structure response amplitudes and dominant frequencies decline by factors of 5 at the north, which is closest to the blast. Dominant rock excitation frequency is 333 Hz and the dominant response frequency is only 60 Hz. These responses: large deamplification and significant delays in building response are more reflective of wave transmission than synchronous dynamic response.

Table 7. Amplitudes and time arrival at northern upper and southern upper part for the transverse component.

Building	Blast	Symbol	A(NAT) (mm/s)	t(NAT) (ms)	A(SAT) (mm/s)	t(SAT) (ms)	A(S)/A(N) %	Dt (ms)
1	06/27/2014	e	6.1	7.81	0.9	83.98	14.8	76.2
1	06/30/2014	f	19.8	6.34	1.7	58.11	8.6	51.8
1	07/07/2014	g	8.5	12.7	1.1	75.2	12.9	62.5
1	08/05/2014	h	4.1	7.81	1.1	35.63	26.8	27.8
1	06/02/2014	a	4.4	-22.46	1.7	31.74	38.6	54.2
1	06/06/2014	c	10.2	3.42	1	31.25	9.8	27.8
2	08/05/2014	h	8.3	-66.41	2	-40.53	24.1	25.9

Building	Blast	Symbol	A(NBT) (mm/s)	t(NBT) (ms)	A(NAT) (mm/s)	t(NAT) (ms)	A(A)/A(B) %	Dt (ms)
1	06/27/2014	e	10.8	-4.4	6.1	7.81	56.5	12.2
1	06/30/2014	f	17.3	-3.9	19.8	6.34	114.5	10.2
1	07/07/2014	g	22.9	-3.4	8.5	12.7	37.1	16.1
1	08/05/2014	h	6.6	-4.8	4.1	7.81	62.1	12.6
1	06/02/2014	a	5.1	-32.7	4.4	-22.46	86.3	10.2
1	06/06/2014	c	10.8	-5.4	10.2	3.42	94.4	8.8
2	08/05/2014	h	-	-	8.3	-66.41	-	-

7 CONCLUSION

Measurements of multiple positions, time correlated response of two urban buildings to ultra-high frequency excitation allow the following observations to be made. These observations are based upon bidirectional horizontal velocity responses at ten positions during eight blast events, which provided over 70 time histories for analysis.

- Close-in blasting with rock transmission imposes isolated, ultra-high frequency excitation pulses with a short duration.
- First arrival propagation velocities are high as expected for this rock
- Excitation motions attenuate as expected from scaled distance relations
- The structures respond predominantly in a wave transmission mode where there is noticeable difference in time, frequency, and amplitude of motions measured at the extreme top corners of the structure.
- Excitation motions along the base are not the same; they differ significantly in both time, frequency, and amplitude.
- Excitation frequencies are so much larger than the natural frequencies of the structures and components that the excitation motions were deamplified for all events.

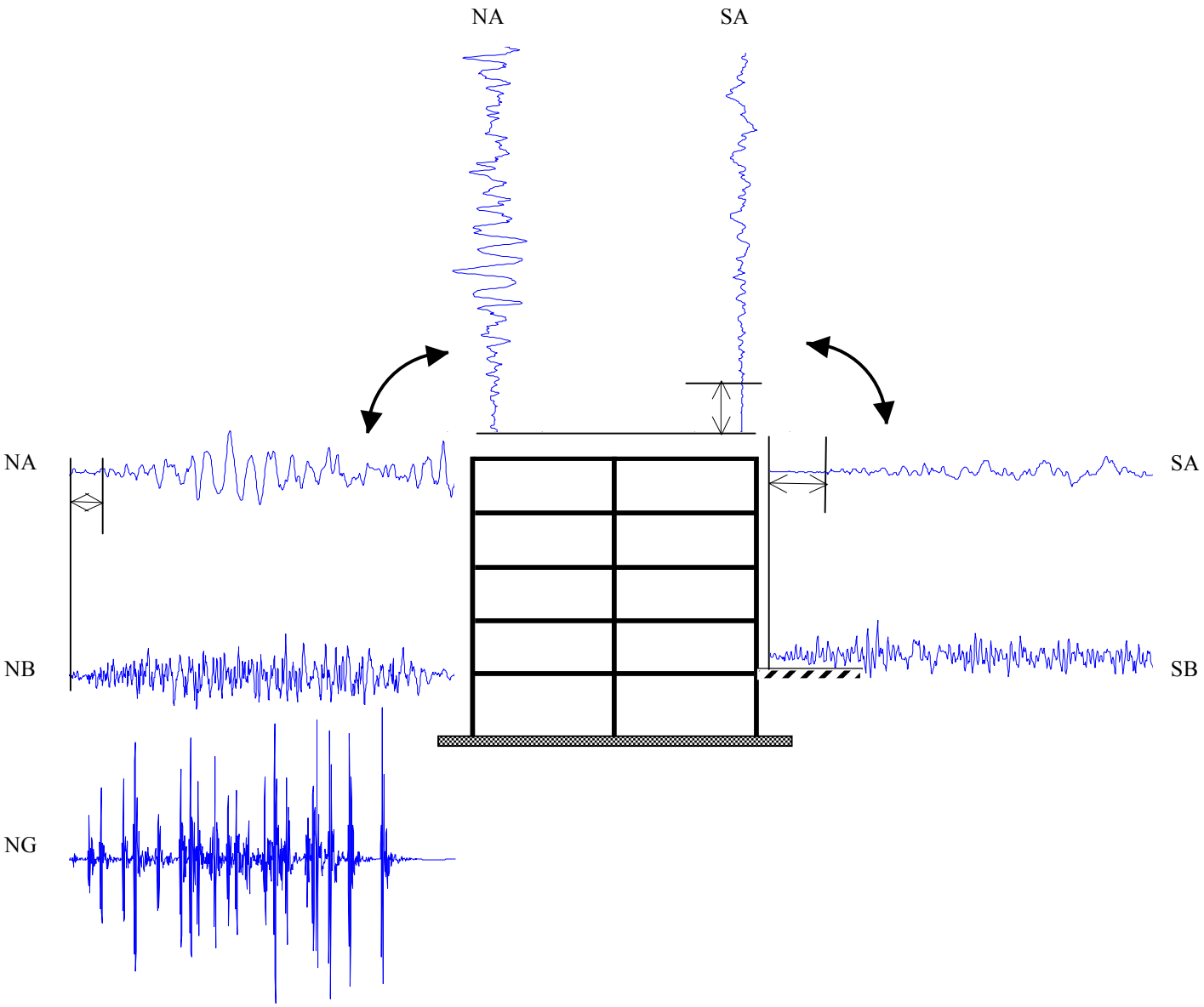

Figure 19. Spatial variation of time correlated transverse building1 velocity during blast 06/02/2014. Shown are differences in 1) times of arrival by arrows 2) amplitude by same scale (except rock motion is at 1/3 scale) 3) dominant frequencies by wave train time histories.

Chapter 3. Close-in blast induced strains

1 GROUND MOTION ENVIRONMENT

Ground motions monitored in this study produced peak particle velocities (PPV's) that attenuate at expected rates when plotted against square root scaled distance. These PPV's and their scaled distances are compared to Oriard's expected values in Figure 7 (Oriard, 1972). Street level (B) PPV's fall between the upper and lower bounds of typical blasts and are well below the upper bound for confined blasts. Rock (G) PPV's occur along Oriard's upper bound. The higher rock motions are likely a result of the unusually small transmission distances and complete rock to rock transmission. These rock to rock motions occur at unusually high frequencies (300 to 500 Hz) and produce unusually low building response as shown by the response spectra of the rock motions in Figure 18. Rock motions are rarely measured in urban blasting because most immediately adjacent urban excavations only allow measurement at the street level, the lower or B level in this study, because rock is inaccessible at the beginning and changes elevation with the adjacent excavation.

There are many possible explanations for the lower PPV's on the building at the street level. Large mismatches between response and excitation frequencies (0.5 and 500 Hz) results in very low velocity response as shown in the response spectrum in Figure 18. The small energy in a 500 Hz pulse is not sufficient to excite these relatively massive (compared to a one story suburban residence) structures. The impulse is so small (due to its infinitesimally small duration) that it imparts little change in the momentum of the structure. High attenuation, and change in phase of excitation motions along the structure creates high damping overall and low response.

1.1 *Integration of velocity time history*

As described in the introduction, strains associated with the fundamental, dominant, or first mode of response can be calculated from time correlated displacements, which were developed by integrating the velocity time histories. Before calculation of strains, the velocity time histories were corrected for baseline irregularities. An example of the four steps in this correction process is shown in Figure 20. First, the velocity time history (Figure 20.a) is baseline corrected. Linear and second order polynomial baseline corrections were tested as shown in Figure 20.b, As can be seen the polynomial correction did not remove the low frequency (~ 2

Hz artifact) that is not in the original velocity time history. It was removed by subtracting the 200 point central-moving–average shown in Figure 20.c to produce the displacement time history that oscillates about 0 as shown in Figure 20.d.

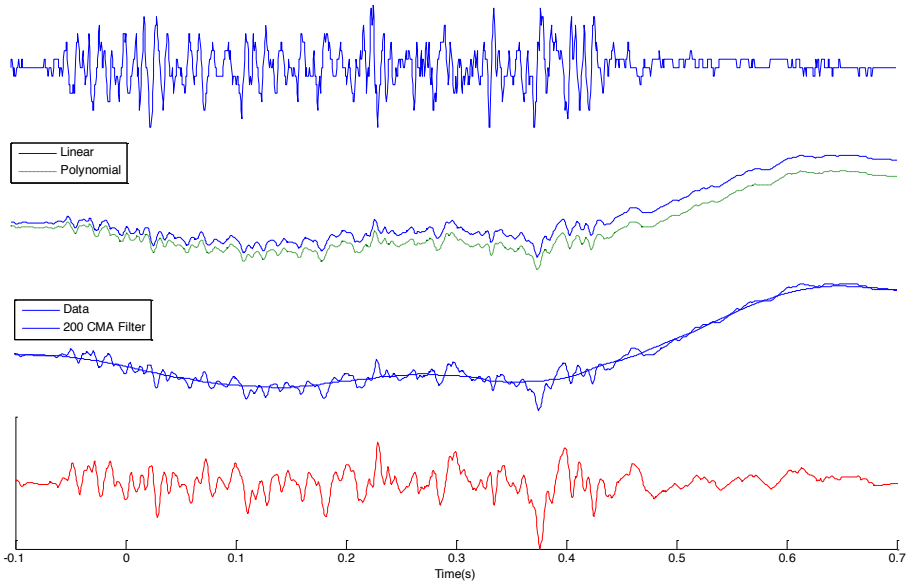

Figure 20. Displacements calculation by drift correction and 200 point central-moving-average filtering (case of SBT recording at Building 2): (a) (top)Velocity recording, (b) Displacement after linear and second order polynomial baseline correction, (c) 200 point central-moving-average filtering of the second order baseline correction displacement, (d) (bottom) Final displacement.

1.2 *Differential displacement calculation*

Prior to the calculation of strains, the differential structure motions were computed from the difference between displacements at the upper, A, and lower, B, transducer positions. Relative displacements, δ, were calculated in both the radial (parallel to the plane of the west wall) and in transverse directions. Differential displacements in these two directions allowed calculation of in-plane shear and tensile strain as well as out-of-plane bending strains. Since the motions were time correlated, the differential displacements are most simply calculated as the difference in displacements at the two transducers at the same time. The high rate of sampling, 2048 samples per second, allows precise time correlation.

Calculation of differential displacement can be subdivided into the following steps that are illustrated in Figure 21 for event 06/06. Velocity time histories are first integrated using the procedure described in the previous section to obtain displacement time histories. Then the differential displacement is found by simple subtraction of the two displacements (at A & B) at the same time. These differential displacements are then searched for the largest. Plots of the transverse velocities recorded at upper and lower transducers of Building 1, as well as corresponding displacements and differential displacements time histories for the 06/06 event are shown in Figure 21.

Table of Appendix A compares the maximum calculated differential displacements between measurement points and PPV's induced by all eight events. The maximum recorded whole or super-structure differential displacement was 334.4μm between the rock (G) and lower (B-street) levels at the north corner of building 1 during the 06/09 event. The maximum calculat-

ed differential displacement between bottom (B) and top (A) was 178.7 μm at the north corner of the building 1 during the 07/07 event.

Appendix B contains all velocity and displacement time histories for all events.

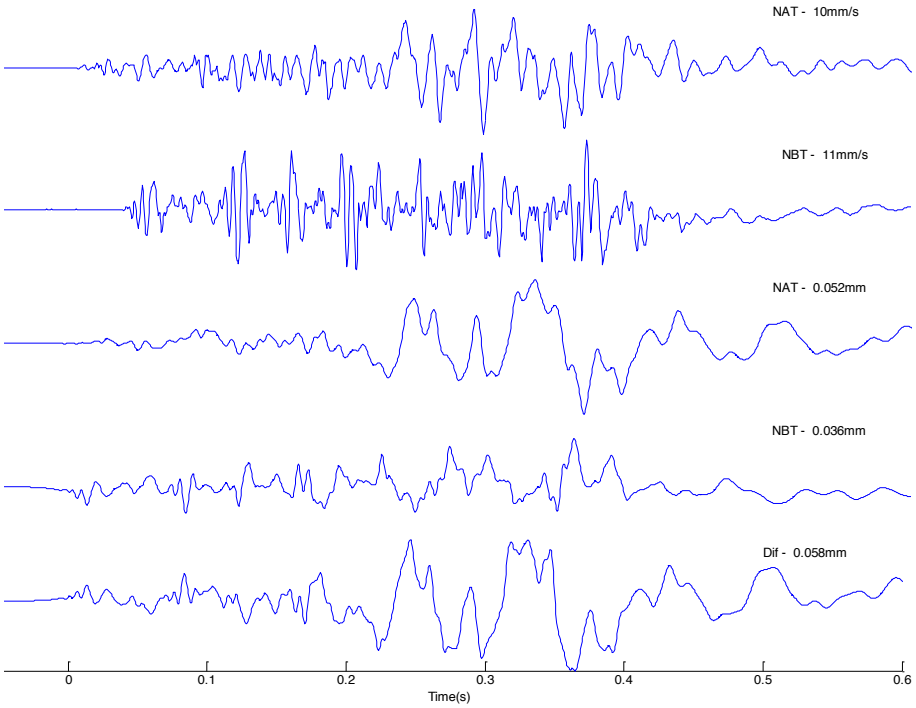

Figure 21. Differential transverse displacements between the top and bottom north corners of building 1 case of the 06/06 event: a) top two time histories–velocities at top (NAT) and bottom (NBT); b) middle two time histories – displacements at top and bottom and c) bottom time history – difference between top and bottom displacements.

2 STRAIN CALCULATIONS

2.1 *Procedure for calculating strains*

Two types of strain can be calculated: a) distortion parallel the plane of the wall and b) distortion perpendicular to the plane of the wall (Dowding, 2000). First consider distortion parallel to the plane of a building wall, which produces shear strains that can be calculated as:

$$\gamma = \frac{\delta}{L} \qquad (1)$$

where L is the wall or building height and δ is the distortion or difference of displacement between the top and bottom of the wall in a direction parallel to the plane of the wall . This shear strain can be translated into tensile strains, ε_t, as follows:

$$\varepsilon_t = \frac{\delta}{L}\sin\varphi\cos\varphi \; ; \; \varphi = \arctan(H/W) \qquad (2)$$

where H is the wall height (or in this case the vertical distance between transducer location) and W is the width (not thickness) of the wall or building face on which the transducers are located. The H and W's employed in these calculations are visible in Figure 2 and are enumerated in a footnote in the Appendix A table.

Now consider distortion in a direction perpendicular to the plane of the wall, which produces bending strains in the wall. A beam deflection model, which assumes a "fixed-fixed" end condition, was used to calculate the strain from the relative displacement δ :

$$\varepsilon = \frac{6\delta c}{L^2} \qquad (3)$$

where *c* is the distance from neutral axis to most extreme fiber, taken here as half the wall thickness and L is the length of the beam or in this case the height of the wall or distance between the two transducers, H. For calculations in this study, the walls were assumed to be 18 mm (7 in) thick. The fixed-fixed condition was assumed as it gives the highest strain calculation (most distorted mode shape)

5.2 *Induced Strains*

Appendix A enumerates and compares all the PPV's and maximum strains induced in the two buildings by the eight blast events. As described above these strains were calculated from the differential displacements that are also compared in this table. Maximum and minimum global (A-B) in plane shear strains were 12.0 and 0.3μ-strains respectively. Corresponding maximum in-plane tensile strain calculated was 4.8μ-strains.

The blast induced strains are low despite high excitation particle velocities. They vary from blast to blast as would be expected. All of the strains are smaller to the south in building 1, which is some 60 m south of the blasts located at the north corner as shown in Figure 1. This consistent difference results (A-B) from the attenuation of the ground motions along the base of the structure. North to south declination on strain ranges from 75% to 97% for the radial strains and from 70% to 96% for the transverse strains.

Basement response is more complex. While shear and tensile strains in the basement can be calculated from the differential displacements, they are not reflective of whole body distortion. They are calculated from differences in displacement time histories which are differences in amplitude of waves propagating through the structure. First consider shear strains. The street level floor is not free to move laterally as the floors above because the basement walls supporting it are restrained from lateral movement by the soil surrounding the basement walls. Thus there can be no free response of the walls or free inter-story "drift" between the basement floor and the street level floor without interaction with the surrounding soil and infrastructure. In other words the basement walls and first story cannot be treated as single degree of freedom systems defined by their mass stiffness and damping.

Calculated basement strains between the rock (G) and lower building transducers (B) tabulated in Appendix A do not reflect the strains that would be calculated from inter-story drift for the freely responding upper floors. Even though they were calculated with equations in Section 5.1, the underlying assumption of synchronous, free inter-story drift, is not valid because of the restraint provided by the surrounding soil. Calculated basement strains are presented only to show the degree to which the differential displacements decline in the above ground section of the building. The ratio between the upper building shear strains (A-B) and the basement shear strains (B-G) strains ranged from 10% to 72% in the transverse direction and 11% to 82% for the radial shear strains. This declination s expected as the lower portion of the building absorbs the vibratory energy first. The greatest declinations of strains above the

basement level occurred with rock motions at the north end of building 1 that exceeded75 mm/s (3 ips). The largest excitation motion was some 200 mm/s (8 ips). These high PPVs occurred at dominant frequencies of greater than 300 Hz.

There is one basement location where there can be response without interaction with the surrounding soil and below-ground infrastructure: out of plane bending of the west basement wall adjacent to the excavation. Response of the basement mid-wall (W) transducer on building 2 to the 08/05 event discussed below demonstrates the extent to which the basement wall responds in this direction

2.3 *Basement Wall response at building 2*

Of special interest is the out plane response of a wall, which cannot be calculated with corner motions. This location is of particular interest as it is the only wall that 1) can respond freely without interaction with the surrounding soil and 2) is distorted directly by rock motions. Walls separating above-ground floors are excited by motions transmitted by the building, which have been shown to decline significantly with distance from the blast location and elevation.

Displacements of the mid wall (W) transducer at building 2 can be employed to calculate tensile bending strains. The out of plane, beam bending model is employed with time correlated displacements measured in the rock (G) and at the street level (B).The L distances needed for this calculation were those shown in Figure 2. For the particular case, three values of the relative transverse displacements, δ , were used: either a) SBT-W, or b) W-GT components, or c) Wall- average SBT and GT as shown in Figure 22. Differential displacements between the transverse rock (GT) and mid-wall (W) motions are shown in Figure 23(a) in relation to the velocity and displacement time histories.

The out of plane response basement wall response is not large. The PPV of the mid-wall was 7.1 with a rock excitation of 5. 2 mm/s at 140 Hz. Calculated tensile bending strains of 0.6 to 1.45 μ-strains are similar to the tensile strains calculated from the in-plane shear strains in walls above the street level. They are small compared to the stains that are necessary to cosmetically crack brick mortar and weak wall covering (300 to 500 μ-strains) (Alan and Adrian, 2002; Dowding, 2000).

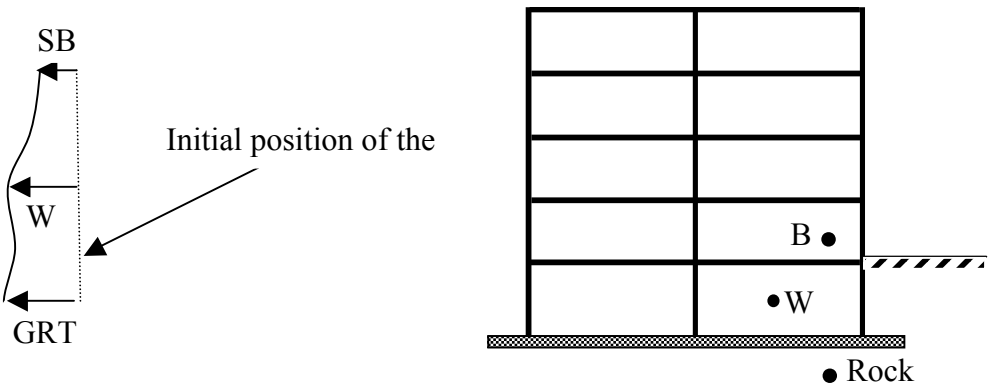

Figure 22. Displacement in the bottom southern part of the wall in Building 2 (W: Mid-wall, SBT: south lower, GRT: transverse ground motion).

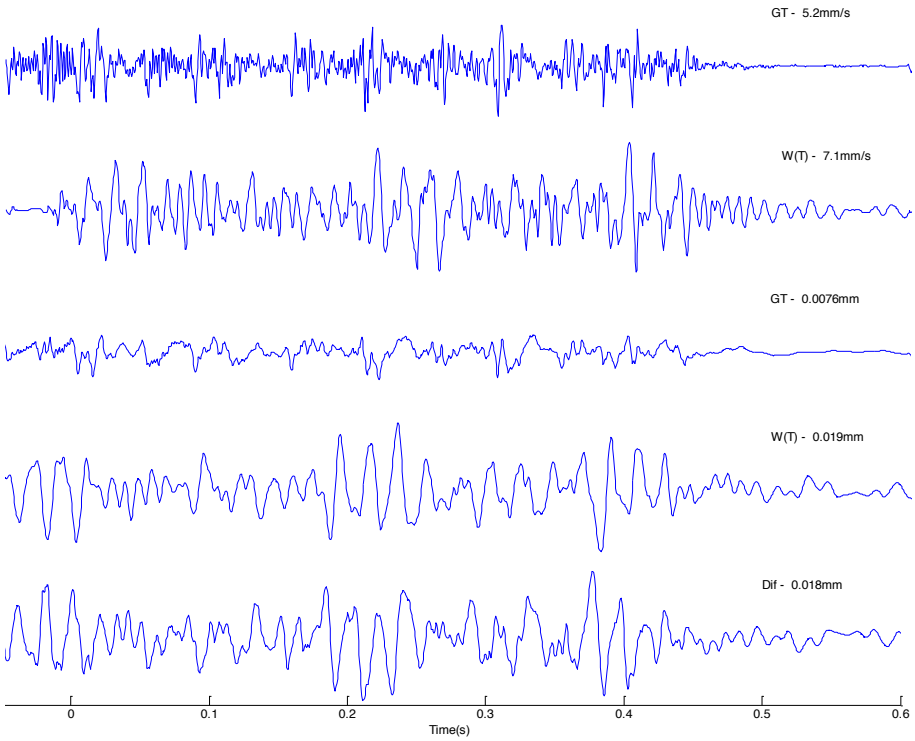

Figure 23. Differential displacements calculation (case of rock and mid-wall recordings at Building 2 during blast 08/05/2014): (a) and (b) Velocity recordings, (c) and (d) Displacements after second order polynomial baseline correction, (e) Final differential displacement.

2.4 *Comparison with ACM surveillance*

Comparison of differential displacements and strains from this case study with those from autonomous crack monitoring (ACM) will allow an assessment of the level of dynamic distortion relative to that induced by weather effects. While this comparison is not as direct as measurement of the weather effects in these urban structures, it does provide a measure of the significance of the differential displacements and strains induced by urban blasting. This comparison is made through use of the Table 2 which presents crack response and strains and differential displacements induced by quarry blasting near suburban, one to two story residential structures as well as strains and differential displacements induced in this study.

Comparisons of the strain columns in Table 2 show that close-in blasting induces less distortion and strain (< 1.5 to 12 μ-strains) in urban structures than does typical quarry blasting near residential structures (0.3 to 280 μ-strains). Furthermore comparison of the blast induced crack response (3rd column from the right) with that induced by weather effects (last two columns on right) shows that these larger blast induced strains in residential structures fail to induce crack response that is greater than that induced by weather effects. Thus by extension, if the urban structures are as responsive to weather effects as the suburban residential structures, than crack responses induced by close-in blasting are small compared to those induced by weather effects.

Further perspective for the significance of strains of less than 12 μ-strains is provided by strains necessary to crack wall covering material such as drywall (plasterboard). Strains nec-

essary for cracking are on the order of 300 to 500(Alan and Adrian, 2002; Dowding, 2000; AS3600, 1998).

Table 8. Differential displacements and strain levels in previous ACM and non ACM studies (d: absolute distance; f:peak frequency; Dif: Maximum differential displacement; τ: Maximum shear strain; σ: Maximum in-plane tensile strain.

Reference	Construction	Blast type	d (m)	Charge (kg)	PPV (mm/s)	f (Hz)	Dif (μm)	H (m)	τ (μstrains)	σ (μstrains)	Crack disp./blast (μm)	Crack disp./daily (μm)	Crack disp./front (μm)
Louis (2000)	Book House	Quarry	-	-	19	-	8.9	2.8	3.2	-	10	6	25
	One-story, concrete masonry	Quarry	-	-	3.3	-	7.0	2.8	2.5	-	43	58	21
McKenna (2002)	Double-wide trailer	Mine	438	277.5	8.1	-	150.2	2.1	71.5	-	0.9	24.4	16.2
	Adobebrick ranch house	Mine	1506	4350	4	-	49.3	4.8	10.2	-	4.2	20.1	9
	Concrete block basement wall	Mine	315	68	5.8	-	19.0	2.4	7.9	-	0.3	12.5	-
	Distressedwood-framed house	Mine	635	476	7.1	-	2.3	6.1	0.3	-	13.6	53	10.9
	Stone-faced, concrete block	Quarry	-	-	4.5	-	11.7	2.9	4	-	5	47	20.7
Alan and Adrian (2002)	Conventional brick veneer	Mine	450	1300	20.8	10	-	-	282.4	47.8	84	2200 (rainfall)	-
	Single and double storey	Mine	700	800	2.37	10	-	-	47.5	6.6	270	-	-
Aimone and Dowding (2005)	Brick structure	Quarry	335	73.4	2.74	8.0	236.2	5	47	21	6.8	38.1	4.5
Aimone and Rosenhaim (2006)	Concrete masonry brick structure	Quarry	825	42.6	1.85	28.4	17.0	2.8	4.6	2.48	2.9	137.8	1386
	Two-structure wood frame	Quarry	825	42.6	1.85	28.4	24.4	2.3	12.4	6.2	7.4	510	30505
Rosenhaim et al. (2005)	Wood frame house - stucco exterior	Pre-split	293	87.9	9.27	5.2	496.1	3.6	135.6	67.4	73.9	300	410
Abeel (2012)	Five-story masonry load bearing	Close-in	-	3.6	62	>150	-	-	12.0	-	-	-	-
Present study	Building 1, d, NT(A-B)	Close-in	6.7	2.41	200.4	500	70	11.6	2.5	-	-	-	-
	Building 1, b, NT(A-B)	Close-in	1.9	2.81	128.8	500	54	11.6	4.7	4.8	-	-	-
	Building 2, h, GT(B-G)	Close-in	24.7	2.96	5.2	143	19.1	15.8	1.4	-	-	-	-

Maximum differential displacements induced in these urban structures by ultra-high frequency ground motion are also compared to those measured in residential structures in Table 2. Responses of the suburban one to two story residential structures were induced by typical quarry blasting during autonomous crack monitoring (ACM) studies (Dowding and McKenna, 2005). The maximum differential displacement observed in that 2005 study was 150 μm for case T. Even in case T the weather induced crack displacements (last two columns in Table 2) were more than 15 times greater than induced by blasting (3rd column from the right)

2.5 *Comparison with previous studies of tall structure response in urban close-in blasting*

Strains measured in this study are lower than those observed in similar tall urban structures by Aimone et al (2014). Figure 24 compares data from this case with that of others by comparing calculated strains with peak ground displacement up to 0.1 mm. Aimone data are presented as the insert to Figure 24, with both the figure and insert possessing the same range of strains (up to 7 μ-strains). While this study included situations with greater peak ground displacement, smaller strains were induced as some of the data fall outside the lower limit curve (A) and upper limit bound (B). The upper bound of all strains vs peak ground displacement as reported by Aimone et al. (2014) is not exceeded.

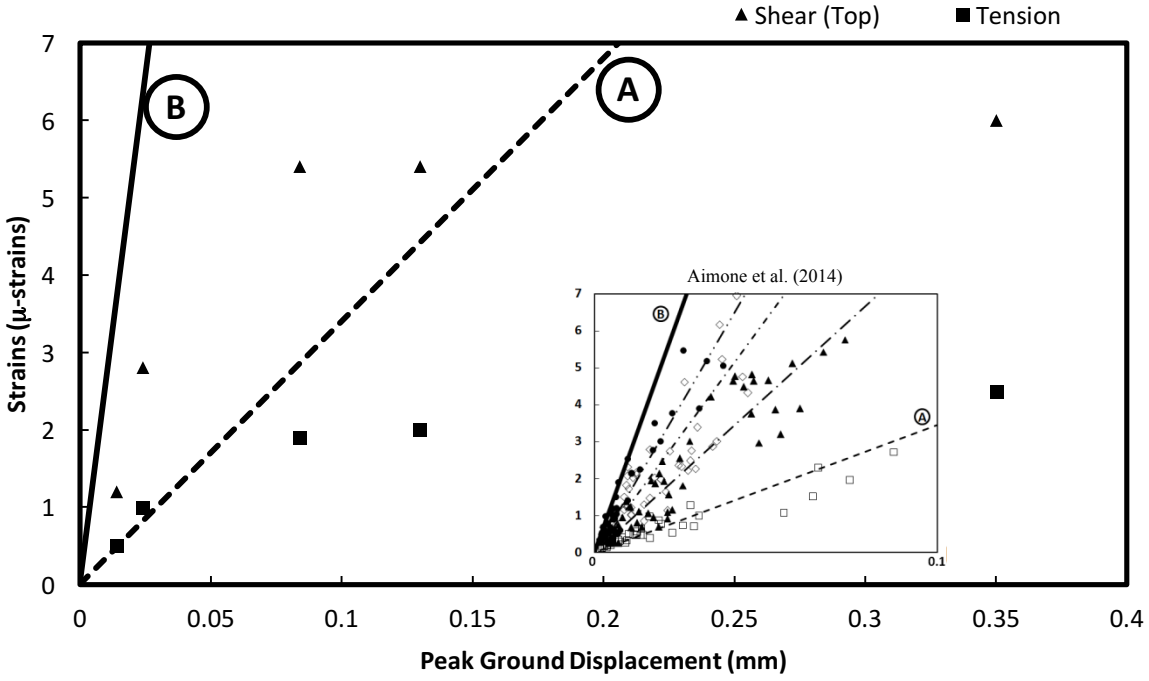

Figure 24. Strains at the top and bottom of buildings versus peak ground displacement. Comparison with Aimone et al. (2014)

3 STRAINS VERSUS PEAK PARTICLE VELOCITIES

Figure 25 to Figure 28 shows the variation of the maximum differential displacement and the resulting shear strains versus the Peak Particle Velocity (PPV) and the ratio PPV over principal pulse frequency. These figures confirm an increasing trend of strains within the structure when the generated PPV or PPV/f ratio increases.

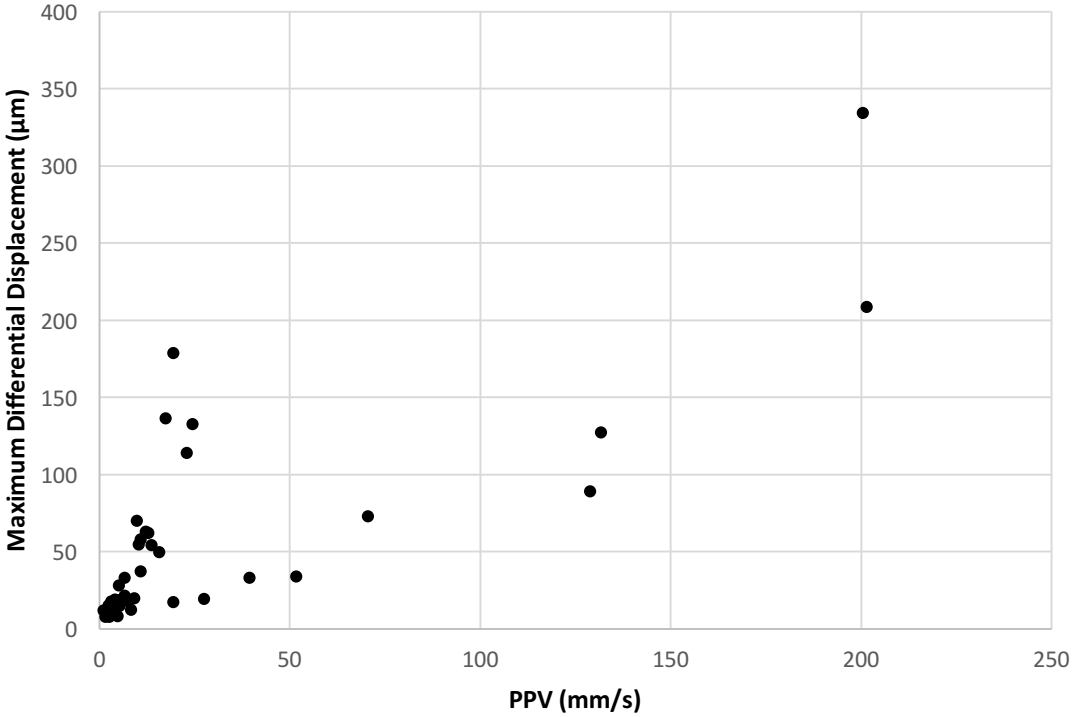

Figure 25. Variation of Maximum Differential Displacement versus the PPV of ground/street level motion.

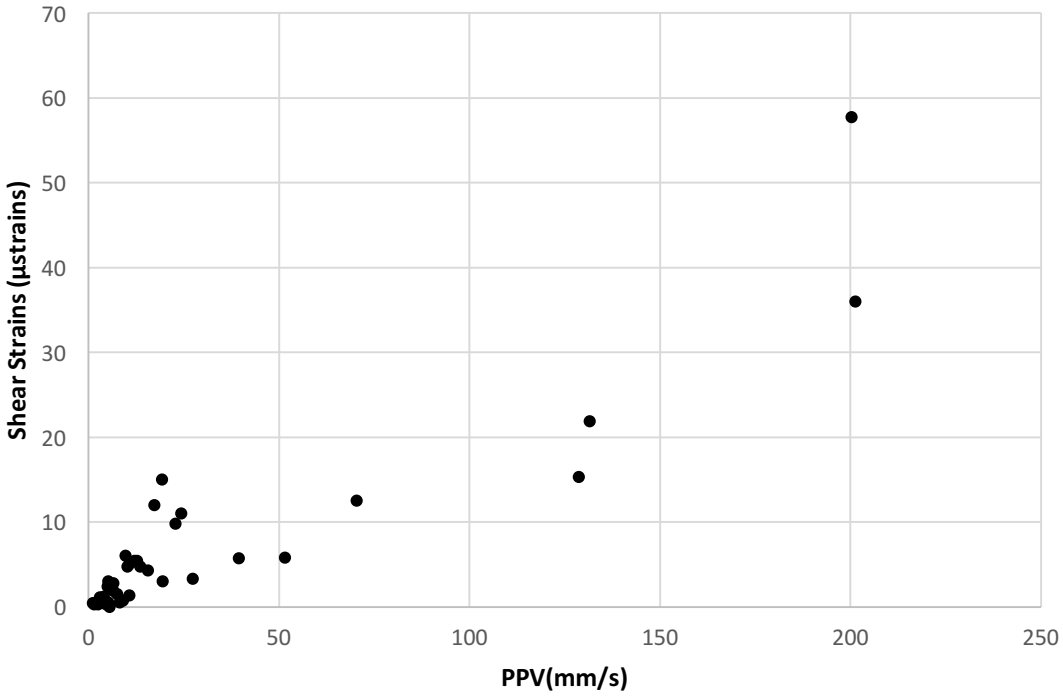

Figure 26. Variation of Shear strains versus the PPV of ground/street level motion.

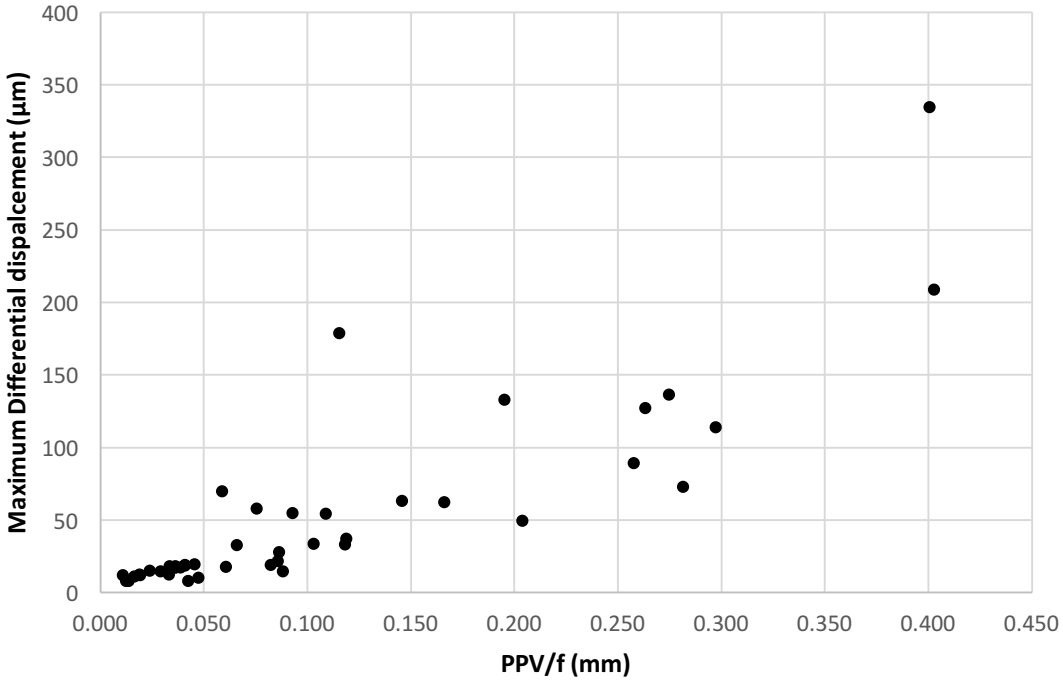

Figure 27. Variation of Maximum Differential Displacement versus the PPV/f of ground/street level motion.

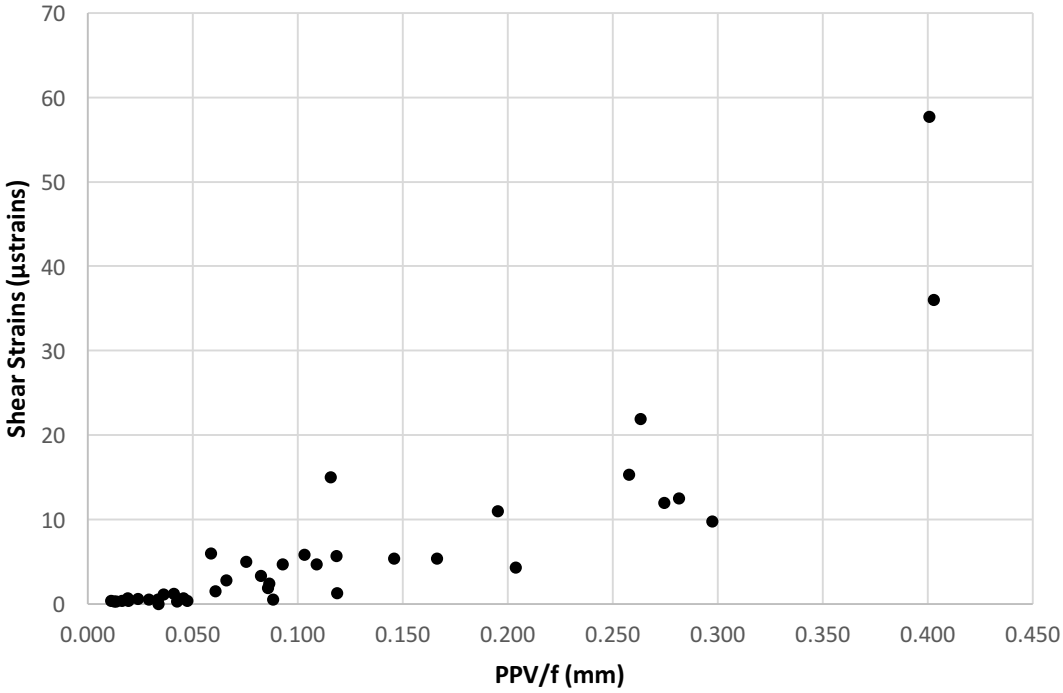

Figure 28. Variation of Shear strains versus the PPV/f of ground/street level motion.

4 SINGLE-DEGREE-OF-FREEDOM RESPONSE SPECTRA

Comparison of the pseudo velocity response spectrum of the 500 Hz dominant frequency rock (G) motions from the 06/02 event is compared with that from a distant quarry (Q) and

close tunnel (T) blast in Figure 18. Spectrum T was developed from ground motions recorded 12m (38ft) away from a 0 to 9 ms delayed tunnel blast with a maximum charge in any single delay of 1.7 kg (3.8lb). Spectrum Q was developed from the ground motions recorded 72m (220ft) away from a single 91 kg (200lb) charge detonated in a typical bench blast hole in a limestone quarry. The quarry blast generated a peak radial particle velocity of 43 mm/s (1.7 in/s) and the tunnel blast generated a peak radial particle velocity of 61 mm/s (2.39 in/s) (Dowding, 2000). The 06/02 blast generated a radial peak particle velocity of 51 mm/s in the rock from a 2.4 kg blast some 9+ m distant.

Even though the peak particle velocities are similar, standard pseudo-velocity response spectrum analysis in Figure 38 predicts that a single story, 10Hz structure or component will sustain a response velocity 60 and 6 times larger for the quarry and tunnel blasts than for the 06/02 event. Since the pseudo velocity is proportional to relative displacement for structures with the same natural frequency (10 Hz in this case), the 06/02 event would be expected to induce far less potential relative displacement, strain, and cosmetic cracking than induced in a typical single story residential structure or 10 Hz component. Furthermore, since the larger urban structures, have lower fundamental frequencies (2 to 3 Hz) expected superstructure relative displacements would be 3 to 5 times lower than 10 Hz structures.

Although the SDOF response spectrum in Figure 38 shows that the relative displacements will be low, additional comparisons show that relative displacements calculated with the SDOF model (SDOF) do not match those calculated from the measured velocity time histories (Diff). For instance, while it is not always true, use of rock motions to calculate SDOF relative displacements will more closely match those measured DIFF relative displacements. Use of street level motions with the SDOF model tended to yield relative displacements that were smaller than measured, Diff. However relative displacements and shear strain calculated with from velocity time histories were still small in absolute sense.

4.1 *Displacement estimated from SDOF response spectrum*

SDOF model response spectrum corresponding to the bottom (rock or street level, B) velocity time histories was used in order to estimate the displacement and compared to the maximum differential displacement computed from integration of the velocity time histories.

The procedure adopted for the estimation of SDOF spectrum based displacement is as follows:

1. For each frequency data between 2.5 Hz and 16Hz, the displacement is computed as:

$$\delta_i = \frac{V_i}{2\pi f_i} \text{ where } V_i \text{ is the Pseudo velocity corresponding to frequency } f_i$$

2. The SDOF based displacement is defined as the average value on all N frequencies of the considered range:

$$\bar{\delta}(SDOF) = \frac{1}{N}\sum_{i=1}^{N}\delta_i$$

For instance, Figure 29 to Figure 32 show the raw velocity time history (a), the corresponding displacement time history (b), the corresponding response spectrum (c) and the SDOF based displacement variation between 2.5 Hz and 16Hz (d) respectively for the NBT and NBR (blast 08/05, building 1) and NBT (blast 07/07 and blast 06/02, building 1).

In the present work, it has been decided to use the average value which is thought to be the most representative value of displacement over the range of frequencies that represent most likely the natural behavior of the building.

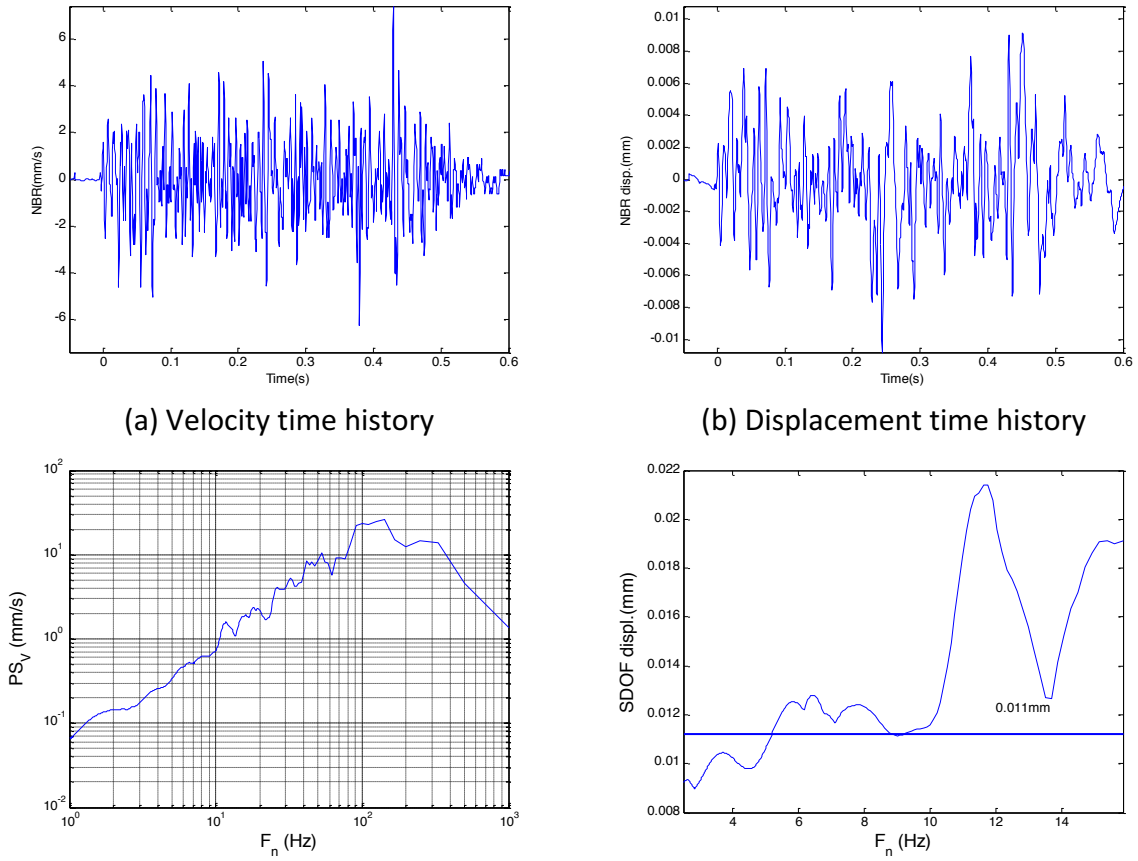

(a) Velocity time history (b) Displacement time history

(c) SDOF spectrum (d) Displacement between 2.5Hz and 16Hz

Figure 29. SDOF displacement calculation for NBR time history recorded during 08/05 event in building 1.

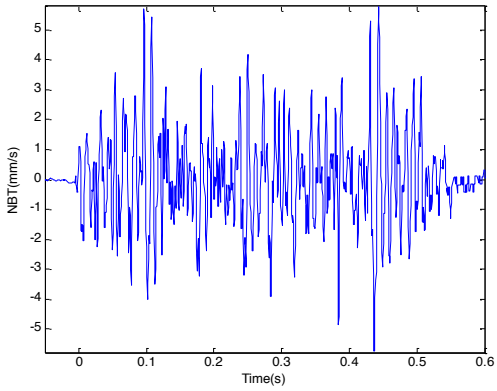

(a) Velocity time history

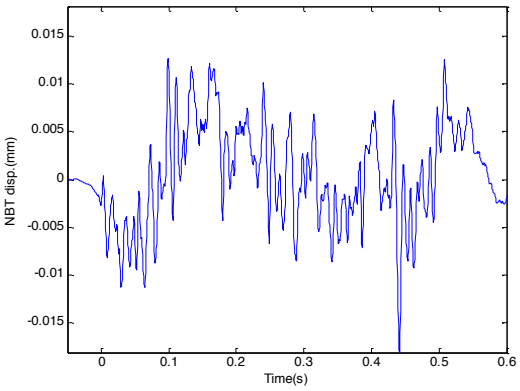

(b) Displacement time history

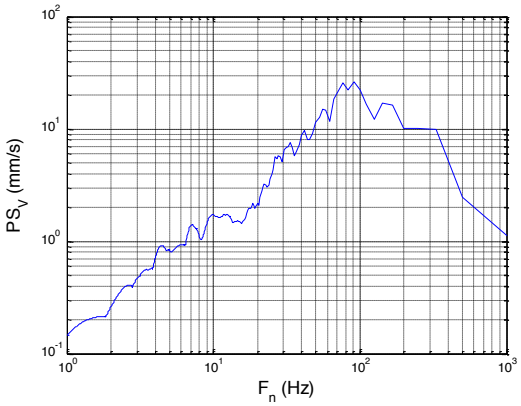

(c) SDOF spectrum

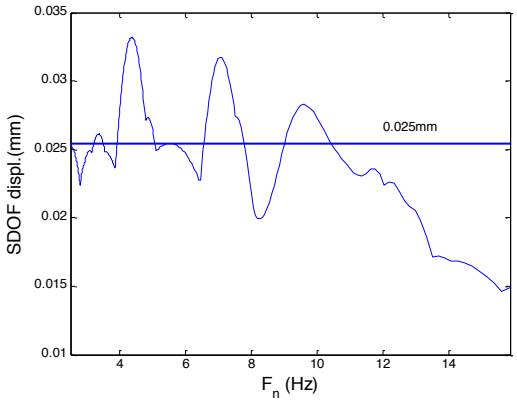

(d) Displacement between 2.5Hz and 16Hz

Figure 30. SDOF displacement calculation for NBT time history recorded during 08/05 event in building 1.

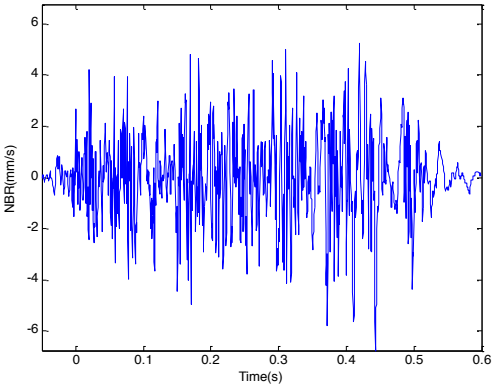

(a) Velocity time history

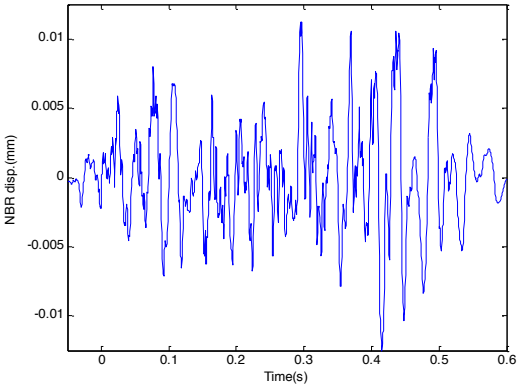

(b) Displacement time history

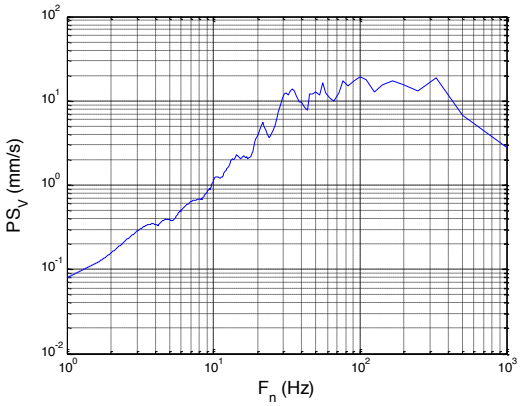

(c) SDOF spectrum

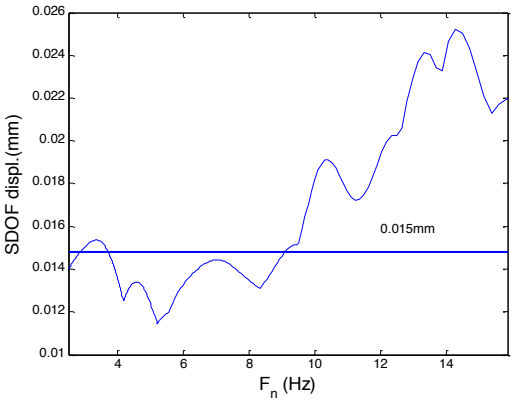

(d) Displacement between 2.5Hz and 16Hz

Figure 31. SDOF displacement calculation for NBR time history recorded during 06/02 event in building 1.

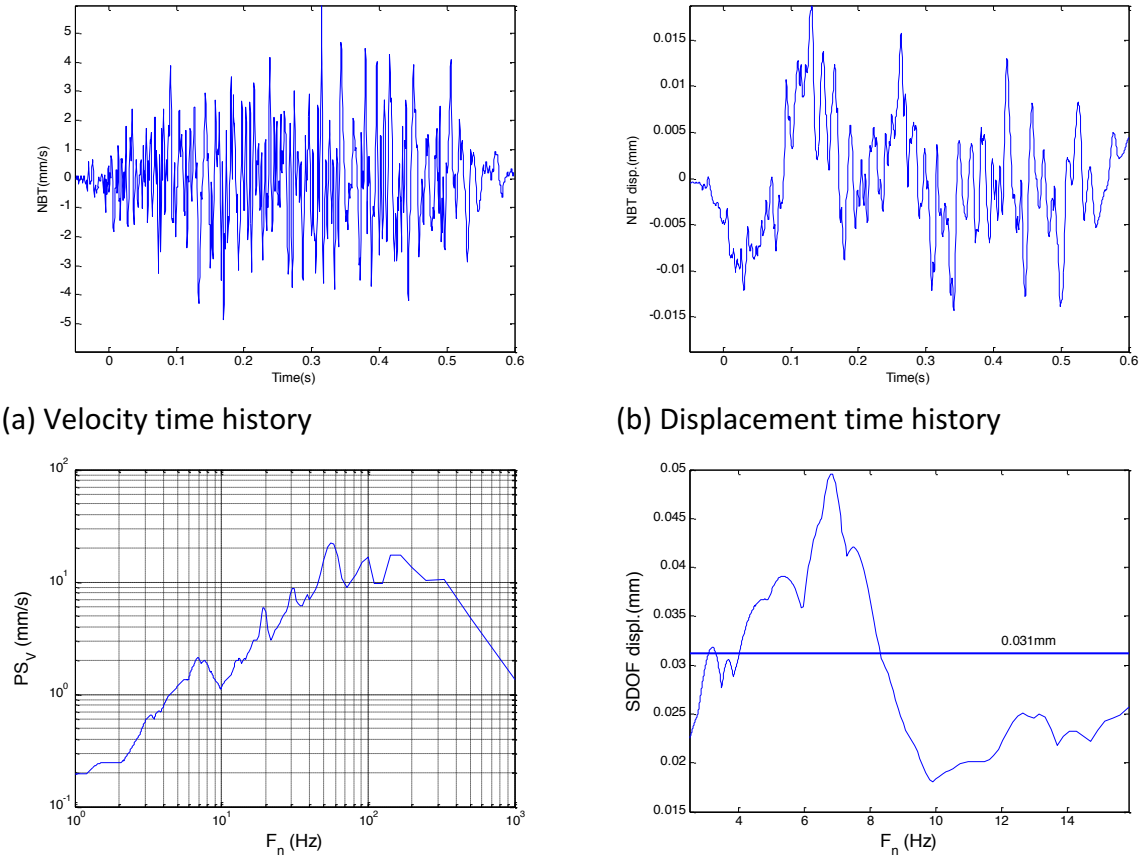

(a) Velocity time history

(b) Displacement time history

(c) SDOF spectrum

(d) Displacement between 2.5Hz and 16Hz

Figure 32. SDOF displacement calculation for NBT time history recorded during 06/02 event in building 1.

4.2 *SDOF displacement versus PPV/freq and PPV*

Figure 33 shows the variation of the so computed SDOF displacement versus the ratio between the PPV and principal pulse frequency of the lower street level velocity time history. Figure 34 draws the variation of the same SDOF displacement versus the PPV of the same lower street level velocity time histories. These two figures prove SDOF displacement, like previously shown for differential displacement between the upper and lower part of the building, increases when the PPV or PPV/f increases.

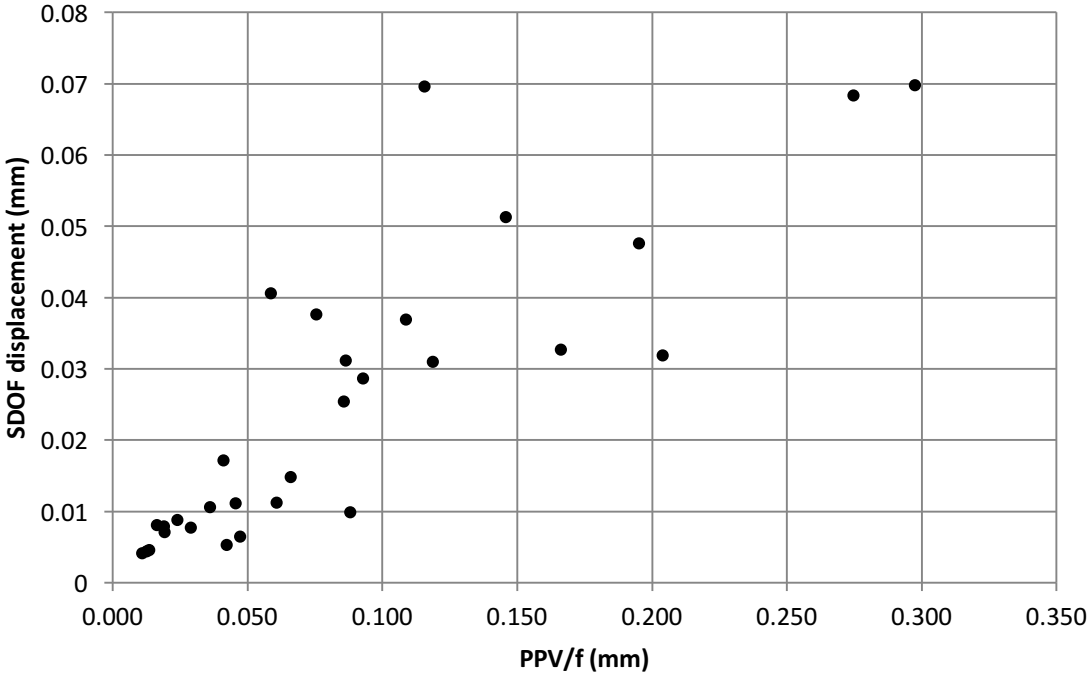

Figure 33. Variation of SDOF displacement versus the PPV/f from lower street level velocity time histories.

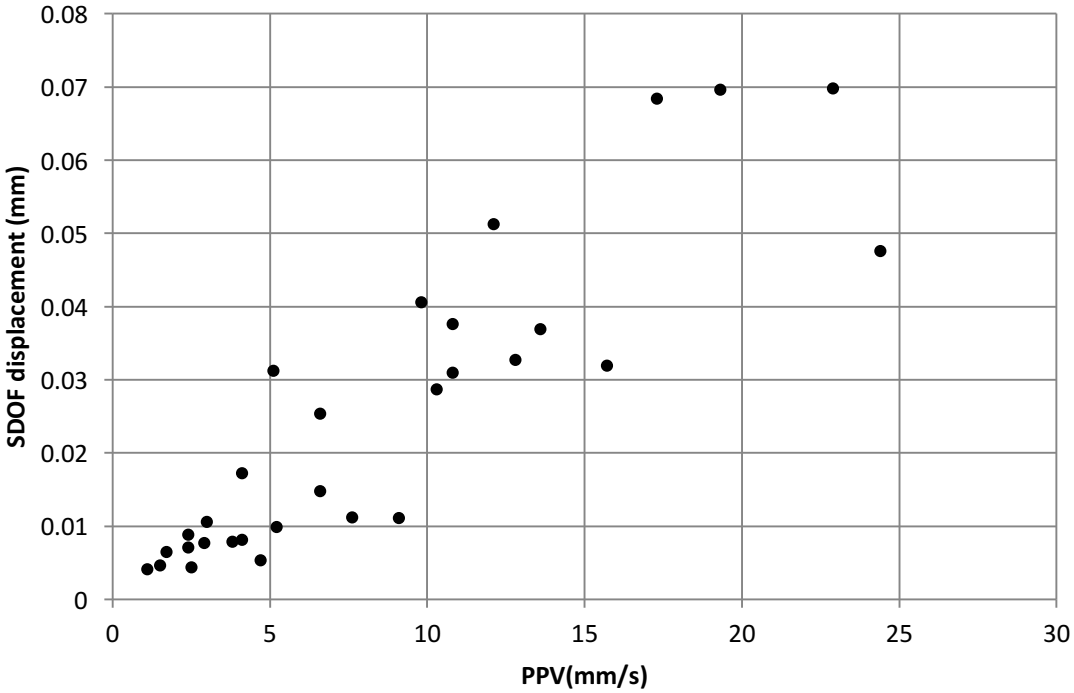

Figure 34. Variation of SDOF displacement versus the PPV from lower street level velocity time histories.

In order to analyze how further the SDOF is based displacement from measured maximum differential displacement in the building between A and B transducer, the ratio SDOF displacement/Differential displacement was plotted in Figure 35 and Figure 36 respectively ver-

sus the principal peak frequency and the ratio PPV/frequency for the rock motion and the street level velocity time histories. These two figures show especially that SDOF model underestimate the real differential displacement if level street velocity time history (B) are considered as input motion (mean value of SDOF displacement/Diff (A-B) is 0.62). On the other side, if the rock motion is considered, the computed SDOF displacement is closer to the measured values (SDOF displacement/Diff (A-B) close to 1).

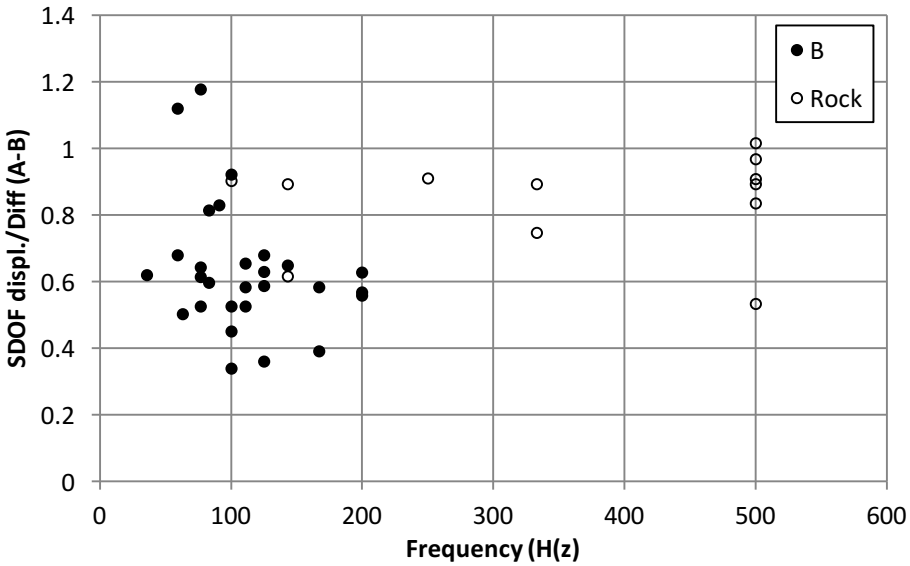

Figure 35. SDOF displacement/maximum differential displacement versus the principal peak frequency from rock motion and lower street level velocity time histories.

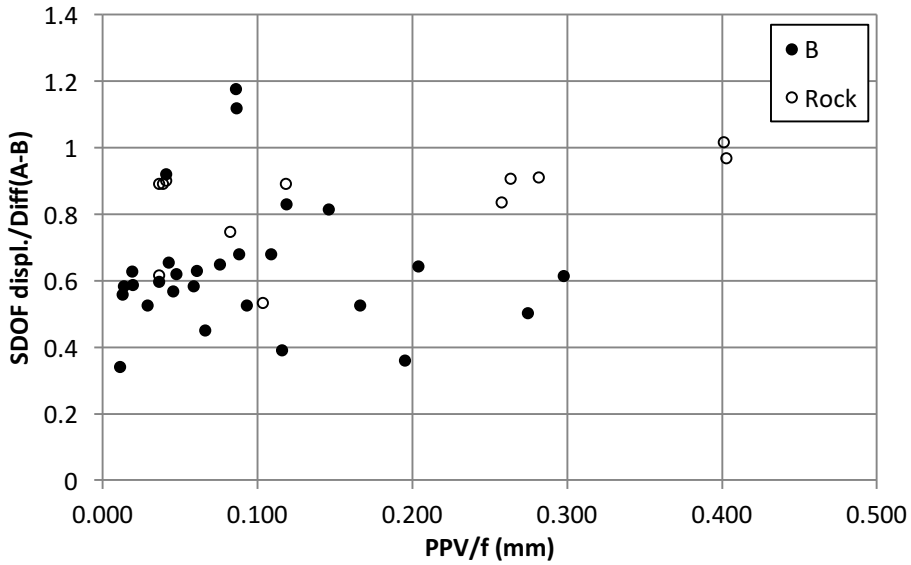

Figure 36. SDOF displacement/maximum differential displacement versus the PPV/f ratio from rock motion and lower street level velocity time histories.

4.1 *Use of SDOF as Control Index*

It is instructive to compare measured relative displacement (or strain) with indices for control of the potential for cosmetic cracking to determine their effectiveness. The most often

employed index is peak particle velocity ground motion (PPV), which is measured immediately adjacent to the structure in the ground. In urban construction often PPVs are measured on the structure at the street level or in the basement of the structures because of the lack of ground between excavation and the structure. Single degree of freedom (SDOF) response can also be employed as an index using ground motion time history. SDOF modeling is advantageous because it takes into account the time history of the excitation motion (dominant excitation frequency) as well as amplitude (PPV). Comparative SDOF modeling is especially applicable since it returns relative displacement which is directly comparable with measured relative displacement. Since displacements are measured in the plane of the wall comparisons are made with excitation velocity time histories measured in a direction parallel to the response motions.

Control indices are compared with measured relative displacements in Figure 37. These data are presented in Table 9Table 9. SDOF displacements model as control indices.. Fidelity of each of these comparisons is assessed with the square of the regression coefficient[1] Maximum measured relative displacements on the X axis for all 9 graphs are compared to three indices or predictors of peak relative displacements (Y axis). These three indices are PPV of the excitation motions (top), SDOF response at 2.5 Hz (Mid) and SDOF response at 16 Hz (Bottom), with 5% damping. There are three columns of these comparisons. The left most is for basement wall relative displacements (B-G) with excitation motions measured in the rock below the structure (G). The middle is for super structure relative displacements (A-B) with excitation motions measured in the rock below the structure (G). And the right most column is for super structure relative displacements (A-B) with excitation motions measured at the street level on the structure (B). The right most column was produced because most often in dense urban settings rock motions are not measured in the rock below the structure but rather on the structure because of access difficulties with immediately adjacent excavation.

Correlation and fidelity of PPV and SODF indices for the measured relative displacement vary with both location of excitation motion, rock-G (two left most columns) and bottom or street level of the building-B (rightmost column). They also vary with the relative displacement being estimated; basement (B-G) on left and super structure (A-B); two columns on the right. Basement relative displacement (or strain) response correlates best with either measure PPV or SDOF calculations with rock excitation motions. No comparisons of basement response with street level motions were made. Super structure relative displacements are less correlated with either PPV or SDOF no matter the location of index motions; rock (G); middle column or building street level (B); right column.

Usefulness of the SDOF model to predict response can be assessed by considering the ratio of model (x) to measured motion (y); or the closeness to the dashed line on the bottom two rows. SDOF prediction of differential displacements in the basement with rock motion excitation with 2.5 or 16 Hz models is nearly 1 to 1 and in the super structure is conservative.

[1] In this paper, the square of the regression coefficient, R^2, was employed to describe the tightness of data to a best-fit trendline. The R^2 value is the square of the Pearson product moment correlation coefficient, which is the proportion of the variance in y, depending on the variance in x. The tightness of fit (of the data to the best-fit trendline) can also be calculated with standard deviations, using the y- distances, as well as the perpendicular distances, of the data points from their respective trendline. Other work [11] has shown that conclusions did not change with varying methods of calculating tightness of data about best-fit trendlines.

SDOF modeling is also acceptable for predicting super structure differential displacement with the 16 Hz systems with excitation motions measured on the structure at the street level, but not with 2.5 Hz systems. One of the possible explanations for this unconservative discrepancy is that time correlated building responses indicate that these large urban structures are do not respond synchronously at their fundamental frequencies to ultra-high (300 to 500 Hz) frequency excitation but in a wave transmission mode ([17], in review). In all instances the measured and SDOF predicted values were small, 30 μ strain for the basement (even with rock PPV's of 200mm/s) and 4 μ strains for the super structure.

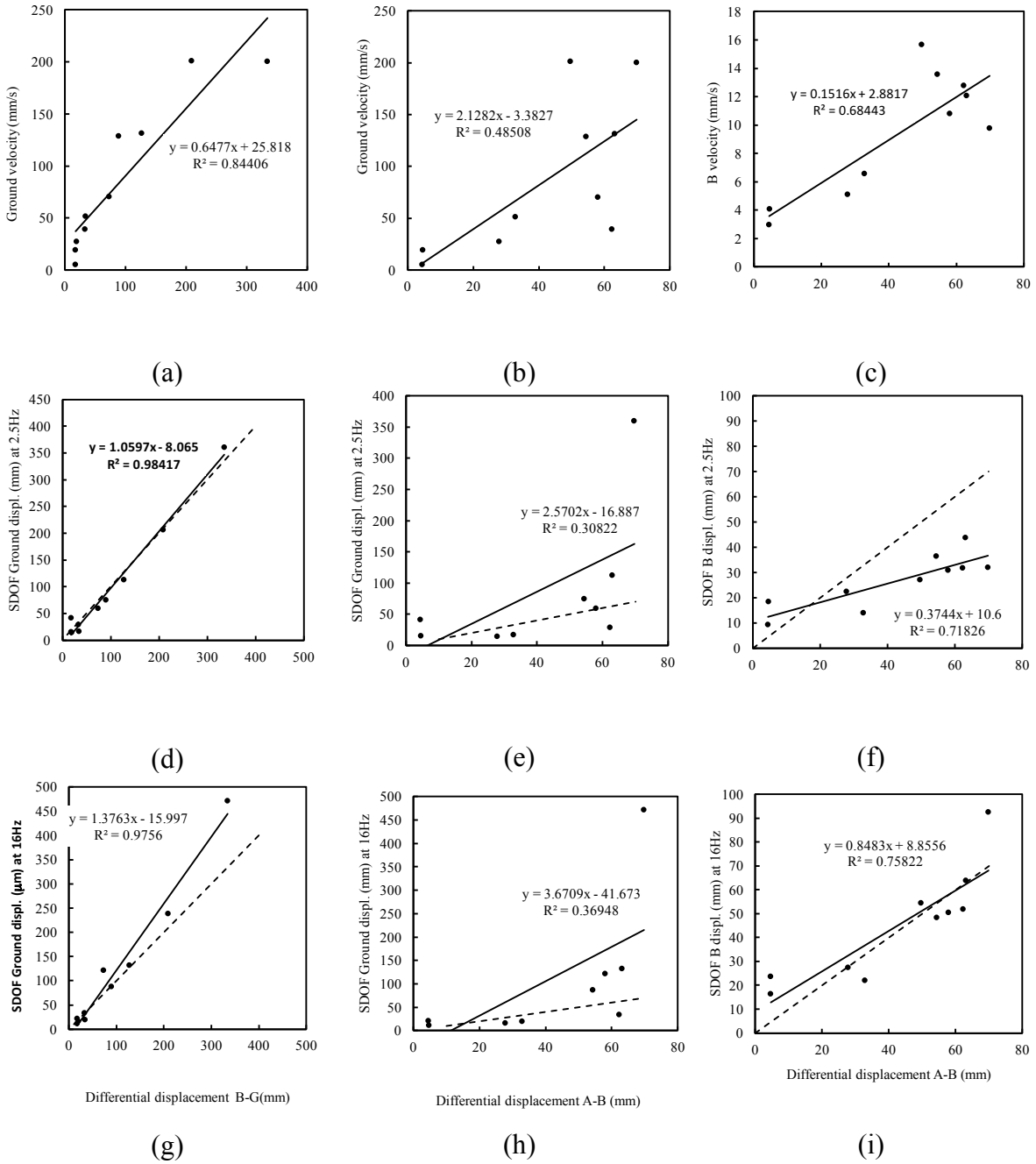

Figure 37. Control indices compared with measured relative displacements: PPV of the excitation motions (top), SDOF response at 2.5 Hz (Mid) and SDOF response at 16 Hz (Bottom), with 5% damping.

Table 9. SDOF displacements model as control indices.

Blast	Symbol	Component	Measured PPV (mm/s)			Ground SDOF displ. (μm)		B SDOF displ. (μm)		Diff. Displ. (μm)	
			Ground	A	B	2.5Hz	16Hz	2.5Hz	16Hz	B-G	A-B
06/05	b	R	39.4	3.6	12.8	28.6	33.4	31.8	51.9	33.1	62.3
		T	128.8	4.1	13.6	74.8	87.3	36.3	48.3	89.1	54.4
06/09	d	R	201.4	7.1	15.7	206.1	238.4	27.0	54.5	208.7	49.7
		T	200.4	10.3	9.8	360.1	471.5	31.9	92.5	334.4	69.8
06/02	a	R	51.6	7.1	6.6	16.8	19.9	14.0	22.0	33.8	32.9
		T	27.4	4.4	5.1	14.5	15.8	22.5	27.4	19.3	27.9
06/06	c	R	131.6	6.6	12.1	112.8	132.2	43.9	63.8	127.1	63.1
		T	70.4	10.2	10.8	59.5	121.1	31.0	50.6	72.9	58.0
08/05	h	R	5.2	4.1	3	41.1	21.3	9.3	16.3	17.4	4.6
		T	19.4	2	4.1	15.3	10.9	18.4	23.7	17.4	4.7

4.2 *Absolute displacement calculations*

SDOF model responses to rock (G) and street level (B) excitation were compared to measured top of building (A) response to assess their applicability. For example Figure 38 presents absolute rock (G) displacements excitation and measured response (top 3 time histories). These measured motions can be compared to the modeled motions in the lower two absolute displacement time histories. Responses of 5% damped SDOF models of 2.5 and 16 Hz systems to 500 Hz rock excitation are shown, with the 16 Hz response on the bottom. The 2.5Hz and 16Hz systems span the range of super structure and wall natural frequencies for these urban buildings. The 2.5 Hz system response is essentially zero, while the 16 system response, more closely matches the frequency content of the upper story response, but with 1/3 measured amplitude.

While street level motions are not true excitation motions, it is of interest to compare the top (A) response with SDOF model response to street level (B) motions. Figure 39 compares measured A & B displacement responses (top two time histories), to SDOF absolute displacement response of 2.5 and 16 Hz systems. While use of the street level motions as excitation motions returns response amplitudes (0.034 and 0.057 mm) that are closer to the measured 0.041 mm at A, the 16 Hz system more closely matches the frequency content but not time history. This consistent closer match of the 16 Hz models indicates that the measured response is most likely that of a component rather than the super structure.

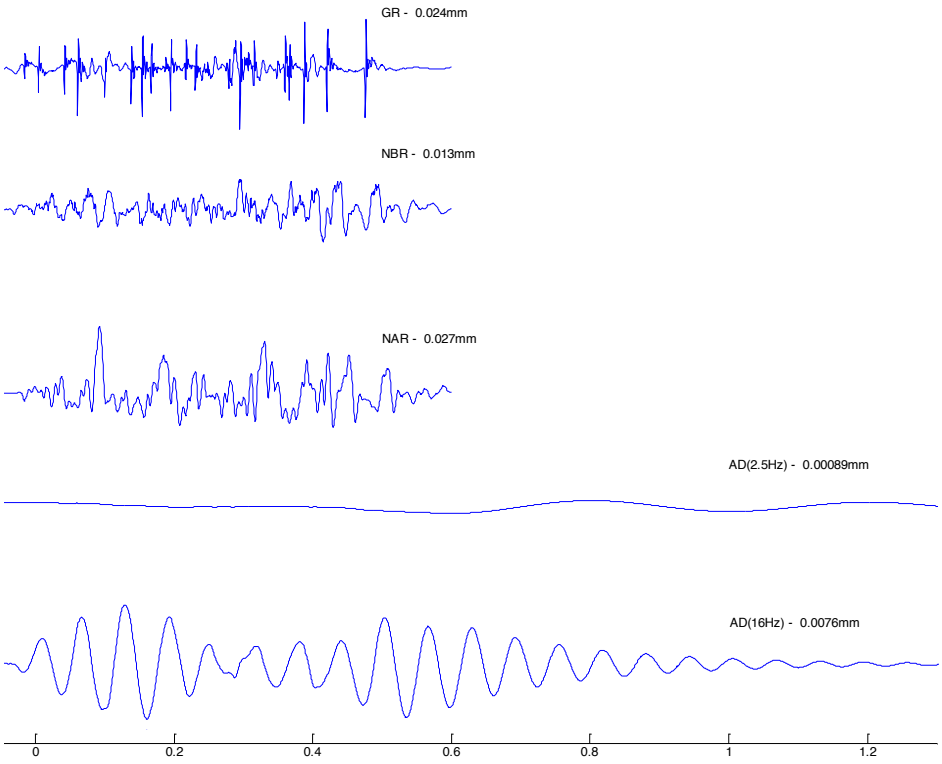

Figure 38. SDOF based prediction of absolute displacements at 2.5Hz and 16Hz case of radial rock motion input excitation as recorded during blast 06/02/2014 at building 1, comparison with measured NAR and NBR displacement time histories (scale for absolute displacement corresponding to 2.5Hz is multiplied by 3).

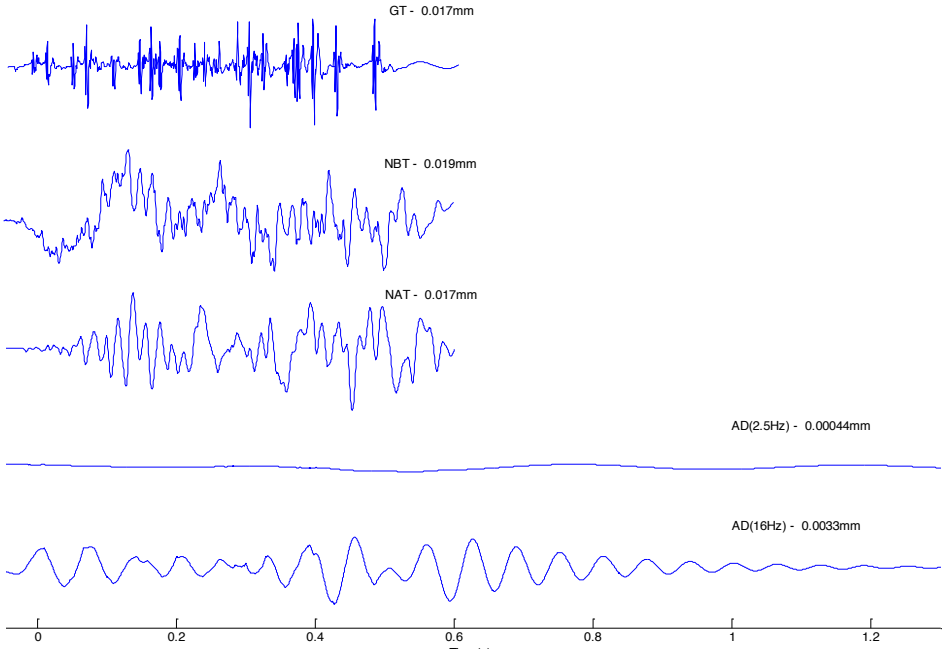

Figure 39. SDOF based prediction of absolute displacements at 2.5Hz and 16Hz case of GT input excitation as recorded during blast 06/02/2014 at building 1, comparison with measured NAT and NBT displacement time histories (scale for absolute displacement corresponding to 2.5Hz is multiplied by 3).

8 COMPARISON WITH USBM SAFE BLASITNG CRITERIA FOR RESIDENTIAL STRUCUTRES

Impact of ultra-high frequency excitation ground motions can be assessed by comparing them to the USBM "Z" curve criteria (Siskind et al. 1980) and European, DIN 4150 (1999) standards. Time histories of the motions of the eight events were converted to a PPVs- dominant frequency format and potted with the Z curve in Figure 40. The second, right hand step in Figure 40 represents a typical 100 mm/s control limit for blasting adjacent to urban structures with slot separation of the fragmented volume from the rock beneath the adjacent structure. Rock ground motions solid dots are identified by letters defining events plotted in Figure 1 and tabulated in Appendix A. Dominant frequency was determined by calculating the zero crossing times for the pulse with the greatest amplitude. Particle velocities measured at street level (NB & SB) are also plotted as these are often assumed to be the default motions because of the inaccessibility of the rock surface.

Generally speaking, the rock motion has the highest frequencies and highest PPVs. Lower north and south transducers (NB & SB) recorded PPV's that do not exceed regulatory limits. For those velocities, the frequencies ranged from 36 Hz to 250Hz. As discussed earlier, even the events with the high rock PPVs produce only small building differential and strain response.

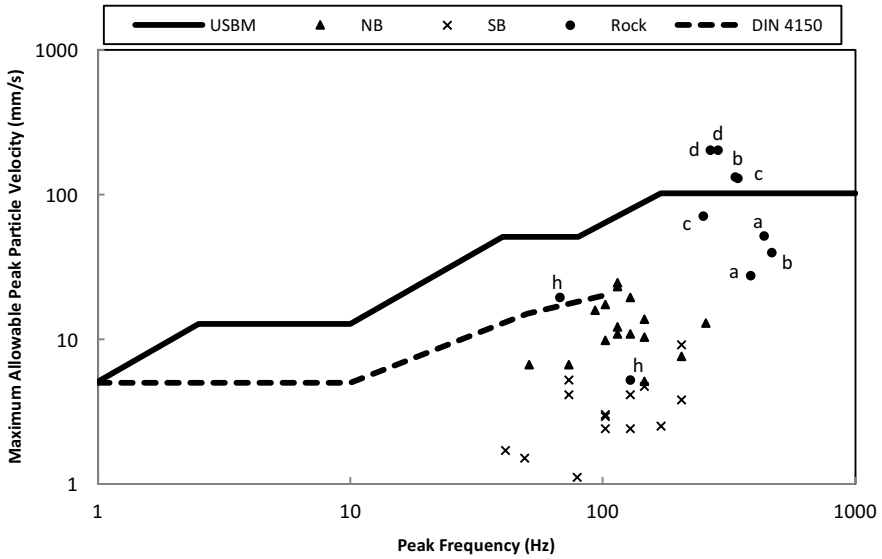

Figure 40. Frequency and Maximum Peak Velocity compared to the safety USBM and DIN 4150 criteria.

5 CONCLUSIONS

Time correlated velocity response to ultra-high frequency blast vibration excitation was measured at multiple positions in two urban buildings allow the following observations regarding blast induced strains. These observations are based upon tangential and radial velocity responses at ten positions during eight blast events, which provided over 70 time histories for analysis. Strains in these multiple story, urban structures are compared to those measured

in one to two stories, residential structures, whose response serves as the basis of many current blasting regulations:

- Close-in blasting practice with overlapping line-drilled slots combined to produce ultra-high frequency excitation motions.
- Despite high peak particle excitation velocities, differential displacements (and thus strains) along a structure are similar to and often less than those measured in residential structures with lower peak particle velocity excitation.
- These measured strains are lower than those necessary to crack masonry structures and weak wall covering materials.
- Since blast induced differential displacements are similar to those in residential structures, which induce less crack response than changes in the weather, it is expected that blast induced crack response of urban structures will also be less than that induced by weather effects (changes in temperature and humidity).
- Measurement techniques presented herein demonstrate how strain calculated from differential displacement can be employed to control blasting activities.
- Displacement response calculated with damped single degree of freedom models of the structures shows that differential displacements should be low.

References

Abeel P.A. 2012. Building and Crack Response to Blasting, Construction Vibrations and Weather Effects. Northwestern University Master of science thesis. 114p.

Aimone-Martin C. and Dowding C. (2005)"Blast- Induced Structural and Crack Response of a Brick Residential Structure Near an Aggregate Quarry" Proceedings of 31st Conference on explosives and Blasting Technique, International Society of Explosive Engineers, Cleveland, OH, USA.

Aimone-Martin C., Rosenhaim V. 2006. Structure response of two structures near the Sibley limestone quarry, Trenton, MI 38p

Aimone-Martin C., Meins B., Lauer J., Brent R (2014). Tall structure response to close-in urban blasting in New York City. The Journal of Explosives Engineers, 16p.

Ambraseys NR, Hendron AJ. Dynamic behaviour of rock masses: rock mechanics in engineering practices. London: Wiley; 1968.

Alan B. R. and Adrian J. M. 2002. Structure Response to Blast Vibration. Report C9040. 83p.

Australian Standard AS3600 – 1998: Masonry Structures.

Blair D.P. (2008) Non-linear superposition models of blast vibration. International Journal of Rock Mechanics & Mining Sciences 45 235–247

Blair DP. (1987) The measurement, modelling and control of ground vibrations due to blasting. In: Second international symposium rock fragmentation by blasting, Keystone, Colorado;, pp. 88–101

Bureau of Indian Standard. (1973) Criteria for safety and design of structures subjected to underground blast. ISI Bull IS-6922.

Chok, K., Huang, F. & Dowding, C. H. (2003). "NUVIB2 Northwestern University Vibration Analysis Program User's Manual, Version 1.01." Northwestern University, Evanston, IL.

DIN 4150, 1999. Part 3, Structural vibration - Effects of vibration on structures.

Dowding C.H. (1971), Response of Buildings to Ground Vibrations Resulting from Construction Blasting", Ph.D. thesis, Department of Civil Engineering, University of Illinois, Urbana, IL.

Dowding, C.H. (2000) Construction Vibrations, Available through Amazon. 1996 version: Prentice Hall, NJ, USA, 620 pages

Dowding, C.H. and McKenna, L. (2005) "Crack Response to Long-Term Environmental and Blast Vibration Effects", Journal of Geotechnical and Geoenvironmental Engineering, ASCE, Vol. 131. No. 9, pp 1151-1161.

Duvall WI, Petkof B. (1959) Spherical propagation of explosion generated strain pulses in rock. USBM Report of Investigation 5483;. p. 21

Ghosh A, Daemen JK. (1983) A simple new blast vibration predictor. In: Proceedings of the 24th US symposium on rock mechanics, College Station, Texas. p. 151–61.

Hinzen, K. G., (1988), Modelling of blast vibrations, Int. J. Rock Mech. Min. Sci. Vol. 25, N°. 6 pp. 439-445, 1988

Hudaverdi, T. (2012) Application of multivariate analysis for prediction of blast-induced ground vibrations. Soil Dynamics and Earthquake Engineering 43 (2012) 300–308

Khandelwal M, Singh TN. (2006), Prediction of blast induced ground vibrations and frequency in opencast mine—a neural network approach. J Sound Vib; 289:711–25.

Khandelwal M, Singh TN. (2007) Evaluation of blast induced ground vibration predictors. Soil Dyn Earthquake Eng 27:116–25

Khandelwal M, Singh T.N. (2009) Prediction of blast-induced ground vibration using artificial neural network. International Journal of Rock Mechanics & Mining Sciences 46 1214–1222

Langefors U, Kihlstrom B. (1963) *The modern technique of rock blasting*. New York: Wiley;

Louis M. 2000. Autonomous Crack Comparometer Phase II. M.S. Thesis , Northwestern University, 115p.

McKenna, L. 2002. Velocity Response of Atypical Residential Structure and Autonomous Crack Monitoring, M.S. thesis , Northwestern University.

Meirovitch, L. (1975) *Elements of Vibration Analysis*, McGraw-Hill Book Company, New York.

Mohamed MT. (2009) Artificial neural network for prediction and control of blasting vibrations in Assiut (Egypt) limestone quarry. Int J Rock Mech Min Sci; 46:426–31

Newmark, N.M., and Hall, W.J. (1982), Earthquake Spectra and Design, Earthquake Engineering Research Institute, Berkeley, CA, 103 pp.

Oriard, L. L. (1972) “Blasting Effects and Their Control in Open Pit Mine” Proceedings of Second International Conference on Stability in Open Pit Mining, C.O. Brawner and V. Milligan, editors, ASME-AIME, Littleton, CO,pp 197-222.

Papazafeiropoulos G. 2014. General Single Step Single Solve integration algorithm. Direct linear or nonlinear explicit or implicit time integration of structural dynamics problems Web: http://www.mathworks.com/matlabcentral/fileexchange/44649-general-single-step-single-solve-integration-algorithm

Panish, P.T. (1992) The Mt. Prospect region of western Connecticut; mafic plutonism in Iapetus-sequence strata and thrust emplacement onto the North American margin, IN Robinson, Peter, and Brady, J.B., eds., Guidebook for field trips in the Connecticut Valley region of Massachusetts and adjacent states; Volume 2: University of Massachusetts, Geology Department Contribution, no. 66, New England Intercollegiate Geological Conference, 84th Annual Meeting, Amherst, MA, October, 9-11, 1992, p. 398-423.

Richart, F.E., Hall, J.R. and Woods, R.C. (1970), *Vibrations of Soil and Foundations*, Prentice Hall, Englewood Cliffs, NJ.

Rosenhaim V.L., Dowding C. H., Aimone-Martin C. T. (2005)“Structure Response to Trench and Road Blasting,” Proceedings of the 3rd World Conference on Explosives and Blasting, European Federation of Explosive Engineers, Brighton, England. GB.

Singh TN, Dontha LK, Bhardwaj V. (2008) Study into blast vibration and frequency using ANFIS and MVRA. Mining Technology 117(3):116–21.

Siskind, D.E., Stagg, M.S., Kopp, J.W., Dowding, C.H. (1980) “Structure Response and Damage Produced by Ground Vibrations from Surface Blasting”, Report of Investigations 8507, U.S. Bureau of Mines, Washington D.C.

Snider M.L. (2003) Crack Response to Weather Effects, Blasting, and Construction Vibrations M.S. Thesis,

Sucuoglu, H. and Nurtug, A (1995) “Earthquake Ground Motion Characteristics and Seismic Energy Dissipation” Earthquake Engineering and Structural Dynamics, Vol. 24, pgs 1195-1213.

Thompson, W.T.(1965), *Vibration Theory and Applications*, Prentice Hall, Englewood Cliffs, NJ.

Veletsos, A.S. and Newmark, N.M. (1964), *Design Procedures for Shock Isolation Systems of Underground Protective Structures*, Vol III, *Response Spectra of Single Degree-of-Freedom Elastic and Inelastic Systems*, Technical Documentary Report RTD TDR-6363096 AD44989, Volume 111, Air Force Weapons Laboratory, Kirkland, AFB.

Woods, R. & Jedele, J. (1985) “Energy-Attenuation Relationships from Construction Vibrations,” in Vibration Problems in Geotechnical Engineering (G Gazetas and E.T. Selig, Eds.), Special Technical Publication, ASCE, New York, pp. 187-202.

Zhou, X. and Tamma, (2004) “Design, Analysis, and Synthesis of Generalized Single Step Single Solve and Optimal Algorithms for Structural Dynamics,” International Journal for Numerical Methods in Engineering, Vol. 59, pp. 597-668.

Appendix A

Table A1. Frequency analysis of the different recorded particle velocity time histories (Max: velocity amplitude; fg: pseudo-velocity spectrum peak frequency).

Building	Set	Blast	Symbol	Position	Max (mm/s)	fg (Hz)
Building 1	Set 1	06/27/2014	e	NBR	10.3	111
				NBT	10.8	91
				NAR	6.6	91
				NAT	6.1	36
				SBR	2.5	200
				SBT	1.5	111
				SAR	1.5	34
				SAT	0.9	16
		06/30/2014	f	NBR	24.4	125
				NBT	17.3	63
				NAR	16.8	63
				NAT	19.8	63
				SBR	5.2	59
				SBT	2.9	100
				SAR	2.5	34
				SAT	1.7	17
		07/07/2014	g	NBR	19.3	167
				NBT	22.9	77
				NAR	21.3	77
				NAT	8.5	67
				SBR	2.4	125
				SBT	1.7	36
				SAR	2.0	36
				SAT	1.1	18
		08/05/2014	h	NBR	7.6	125
				NBT	6.6	77
				NAR	3.6	59
				NAT	4.1	63
				SBR	4.7	111
				SBT	1.1	100
				SAR	1.0	42
				SAT	1.1	15
	Set 2	06/05/2014	b	NBR	12.8	77
				NBT	13.6	125
				NAR	6.1	71
				NAT	8.0	29
				rad	39.4	333
				tra	128.8	500
		06/09/2014	d	NBR	15.7	77
				NBT	9.8	167
				NAR	7.1	71
				NAT	10.3	59
				rad	201.4	500
				tra	200.4	500
	Set 3	06/02/2014	a	NBR	6.6	100
				NBT	5.1	59
				NAR	7.1	100
				NAT	4.4	53
				SBR	9.1	200
				SBT	3.8	200
				SAR	1.5	42
				SAT	1.7	17
				rad	51.6	500
				tra	27.4	333
		06/06/2014	c	NBR	12.1	83
				NBT	10.8	143
				NAR	6.6	45
				NAT	10.2	71
				SBR	4.1	250
				SBT	2.4	100
				SAR	2.0	31
				SAT	1.0	15
				rad	131.6	500
				tra	70.4	250
Building 2		08/05/2014	h	NAR	5.6	167
				NAT	8.3	250
				SBR	3.0	83
				SBT	4.1	100
				SAR	4.1	83
				SAT	2.0	71
				rad	19.4	500
				tra	5.2	143
				wall	7.1	50

Table A1. Strain level estimation in the different parts of the two investigated buildings.

Building	Set	Blast	Symbol	Position	Differential displacement (μm)	Shear strain (μstrains)		Tensile strain (μstrains)
Building 1	set 1	06/27/2014	e	NR(A-B)	54.8	4.7		0.9
				NT(A-B)	37.4	1.3		0.5
				SR(A-B)	7.9	0.3		0.1
				ST(A-B)	7.9	0.3		0.1
		06/30/2014	f	NR(A-B)	132.8	11.0		2.0
				NT(A-B)	136.5	12.0		4.9
				SR(A-B)	14.6	0.5		0.2
				ST(A-B)	14.7	0.5		0.2
		07/07/2014	g	NR(A-B)	178.7	15.0		2.8
				NT(A-B)	113.9	9.8		4.0
				SR(A-B)	12.1	0.4		0.1
				ST(A-B)	10.5	0.4		0.2
		08/05/2014	h	NR(A-B)	17.8	1.5		0.3
				NT(A-B)	21.6	1.9		0.8
				SR(A-B)	8.1	0.3		0.1
				ST(A-B)	12.1	0.4		0.2
	Set 2	06/05/2014	b	NR(A-B)	62.3	5.4		1.0
				NT(A-B)	54.4	4.7		1.9
				GR(B-G)	33.1	5.7		0.5
				GT(B-G)	89.1	15.3		3.7
		06/09/2014	d	NR(A-B)	49.7	4.3		0.8
				NT(A-B)	69.8	6.0		2.5
				GR(B-G)	208.7	36.0		3.4
				GT(B-G)	334.4	57.7		14.1
	Set 3	06/02/2014	a	NR(A-B)	32.9	2.8		0.5
				NT(A-B)	27.9	2.4		1.0
				GR(B-G)	33.8	5.8		0.5
				SR(A-B)	19.6	0.7		0.3
				ST(A-B)	12.6	0.7		0.3
				GT(B-G)	19.3	3.3		0.8
		06/06/2014	c	NR(A-B)	63.1	5.4		1.0
				NT(A-B)	58.0	5.0		2.0
				GR(B-G)	127.1	21.9		2.1
				SR(A-B)	11.2	0.4		0.1
				ST(A-B)	15.1	0.6		0.3
				GT(B-G)	72.9	12.5		3.0
Building 2		08/05/2014	h	SR(A-B)	17.8	1.1		0.5
				ST(A-B)	18.7	1.2		0.5
				WT(B-W)	19.1	-	2.0*	-
				WT(G-W)	18.4	-	0.8*	-
				WT(W-Avg(SBT,GT))	17.5	-	1.9*	-
				Roof radial (SR-NR)	18.2	-		0.7
				Roof transverse (ST-NT)	12.5	0.5		0.1

* Bending strains

Distances used for the strain computation:

- H=11.6m and W=22.2m for the North transverse components and H=11.6m and W=61m for the north radial components for the Building 1;
- H=27.4m and W=22.2m for the South transverse components and H=27.4 and W=61m for the south radial components for the Building 1.
- H=5.8m and W=22.2m for the North rock to bottom transverse components and H=5.8m and W=61m for the north rock to bottom radial components for the Building 1.
- H=15.8m and W=7.6m for the transverse components and H=15.8m and W=26.2m for the radial components for the Building 2;
- H=3.5m and W=7.6m for the rock to mid-wall transverse components and H=3.5m and W=26.2m for the rock to mid-wall radial components for the Building 2;
- H=2.2m and W=7.6m for the mid-wall to bottom transverse components and H=2.2m and W=26.2m for the mid-wall to bottom radial components for the Building 2;

Appendix B

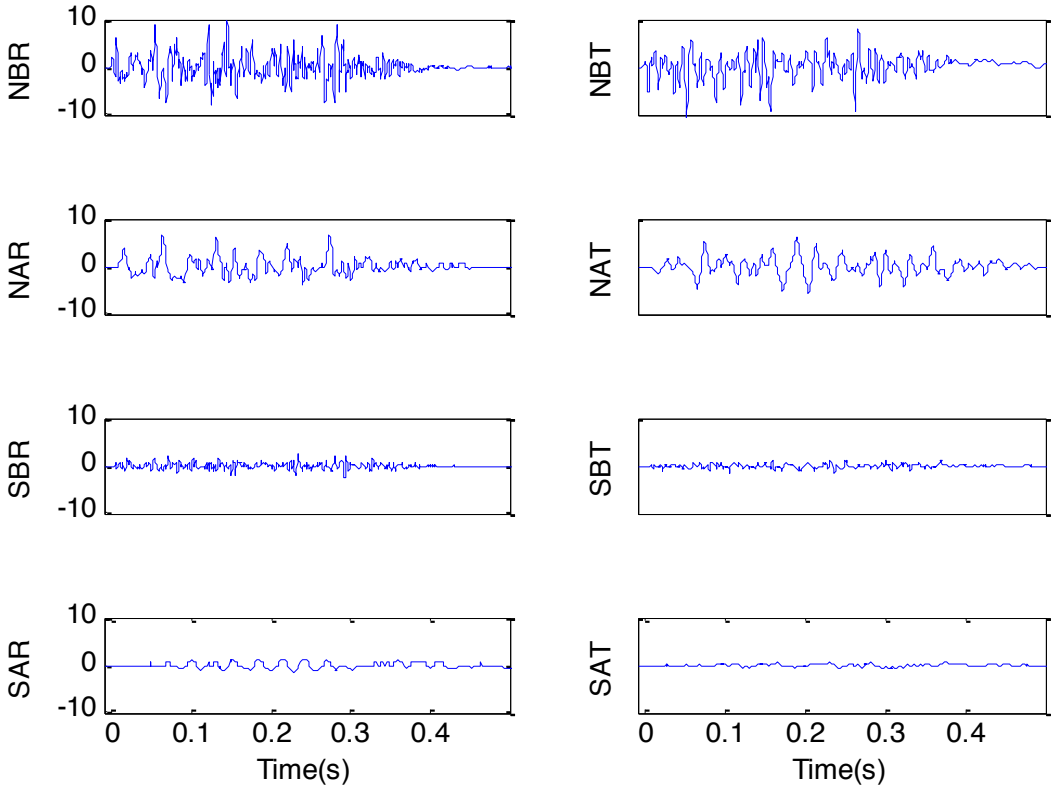

Figure B.1. Recorded velocity time histories for blast 06/27/2014.

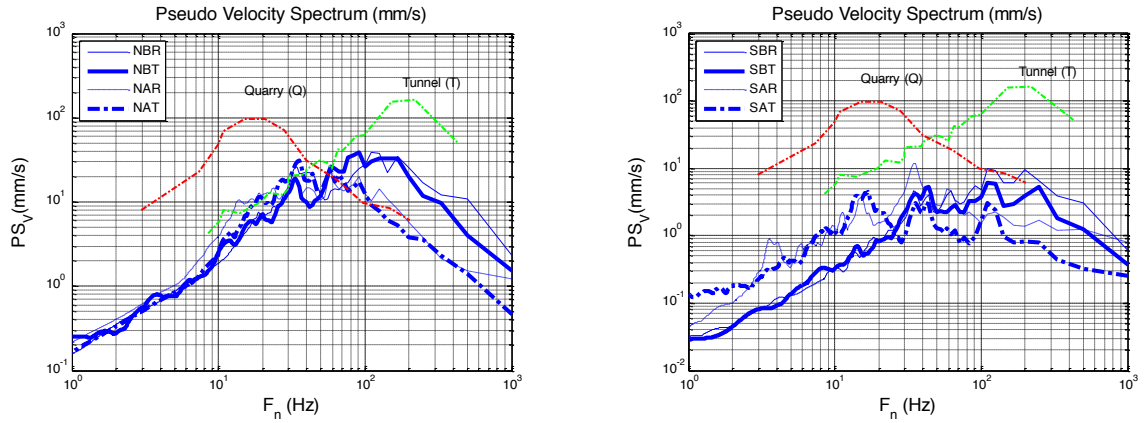

(a) North part (b) South part

Figure B.2. Response spectra for blast 06/27/2014.

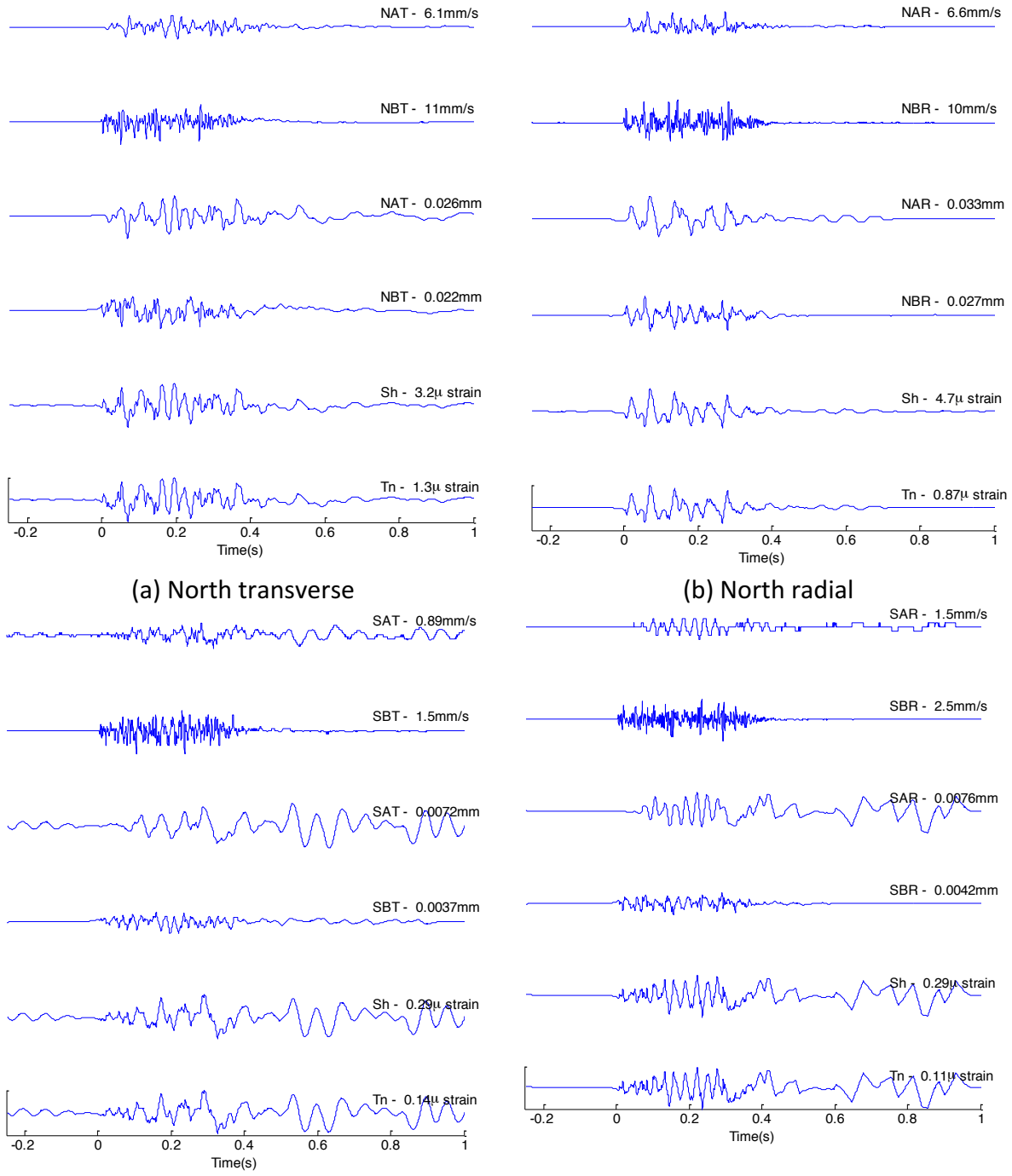

Figure B.3. Strain level calculations for blast 06/27/2014.

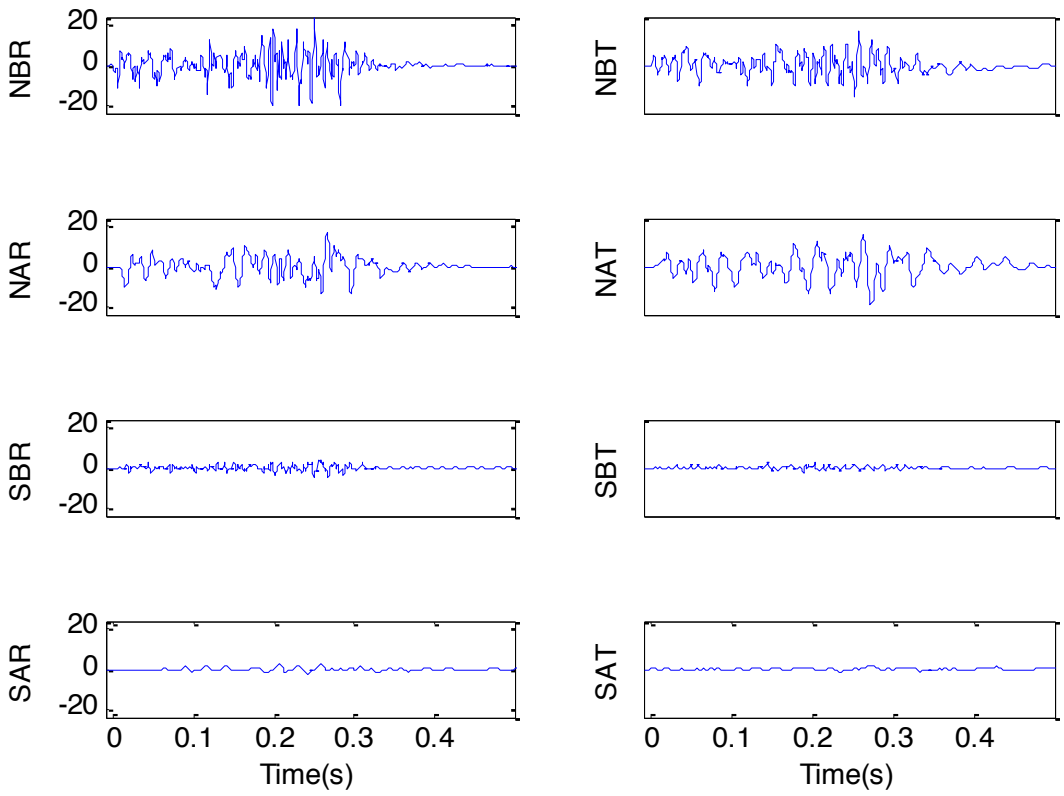

Figure B.4. Recorded velocity time histories for blast 06/30/2014.

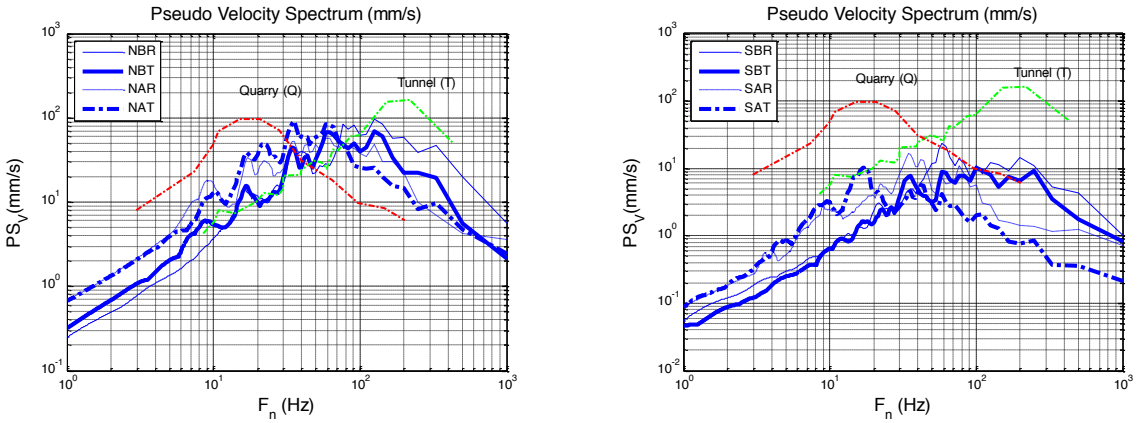

(a) North part (b) South part

Figure B.5. Response spectra for blast 06/30/2014.

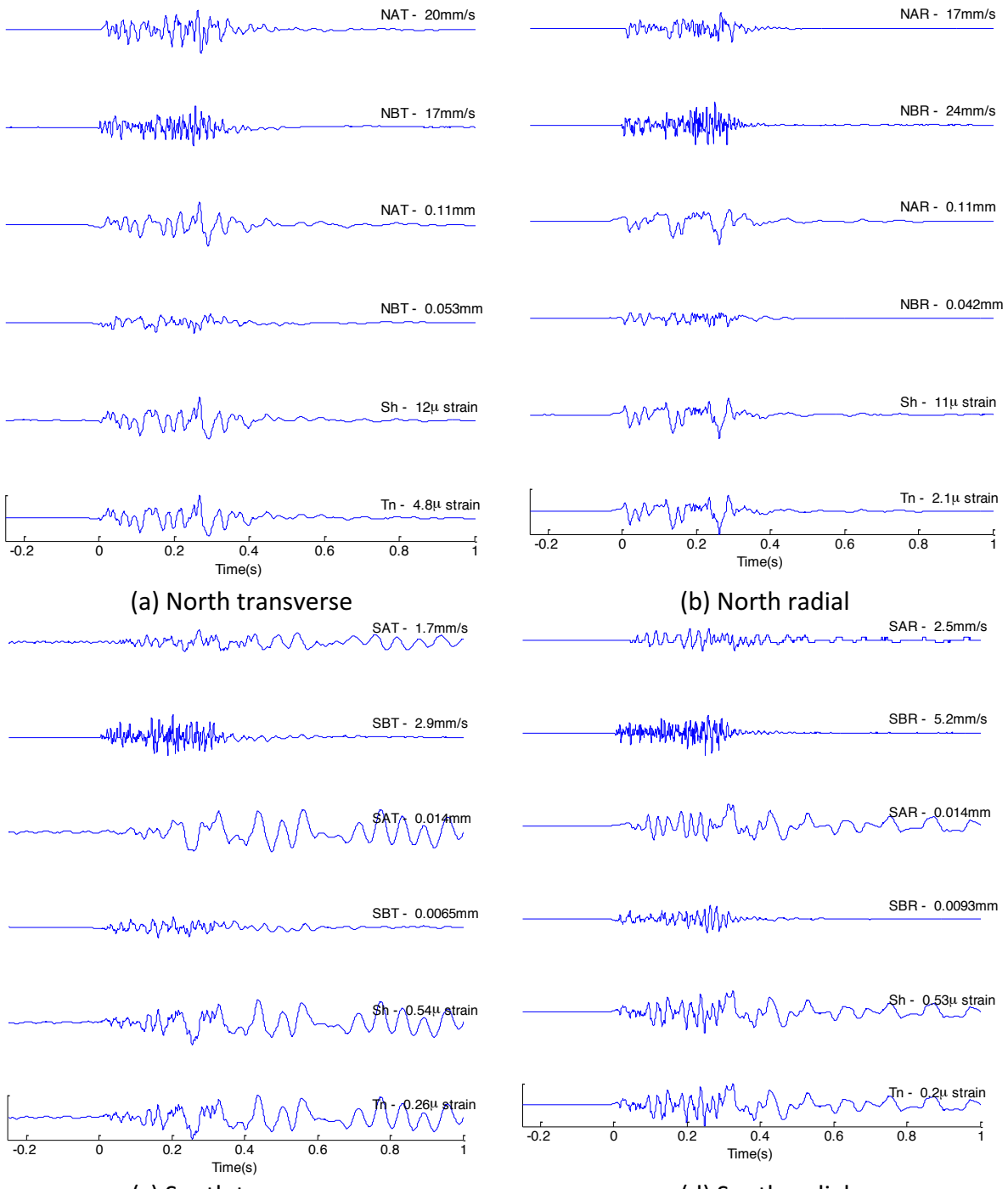

Figure B.6. Strain level calculations for blast 06/30/2014.

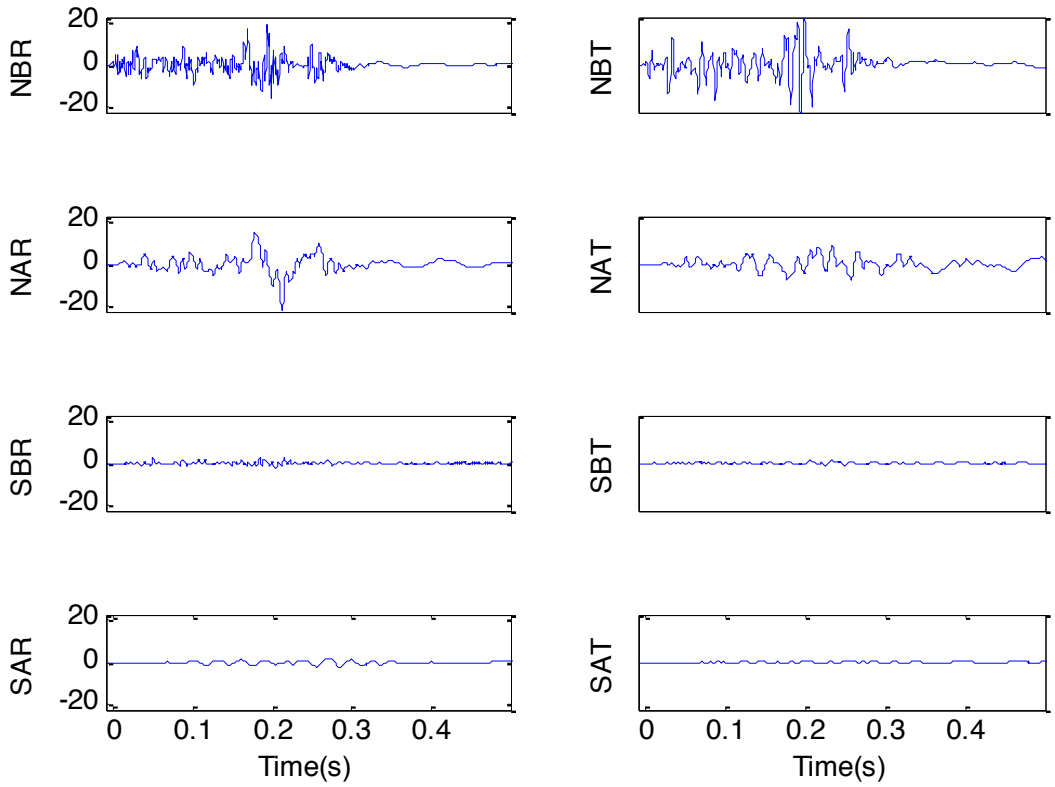

Figure A.7. Recorded velocity time histories for blast 07/07/2014.

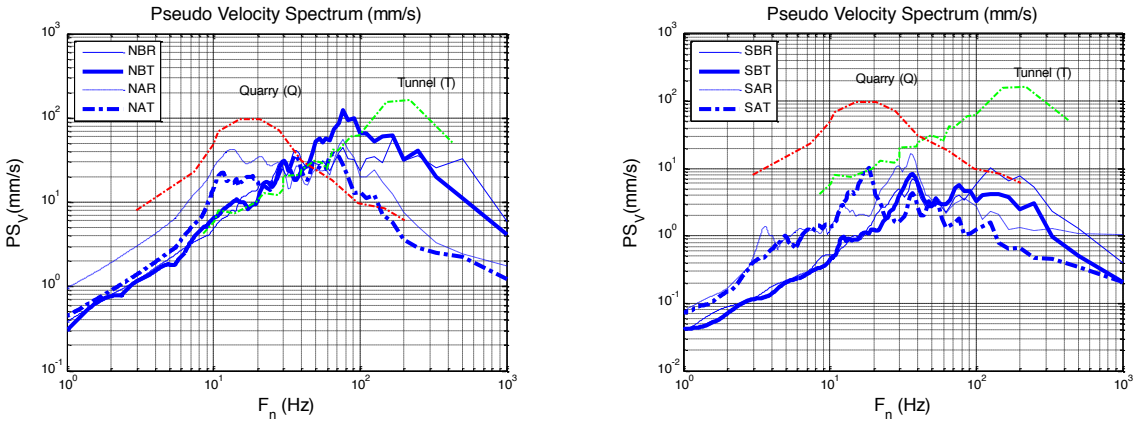

(a) North part (b) South part

Figure B.8. Response spectra for blast 07/07/2014.

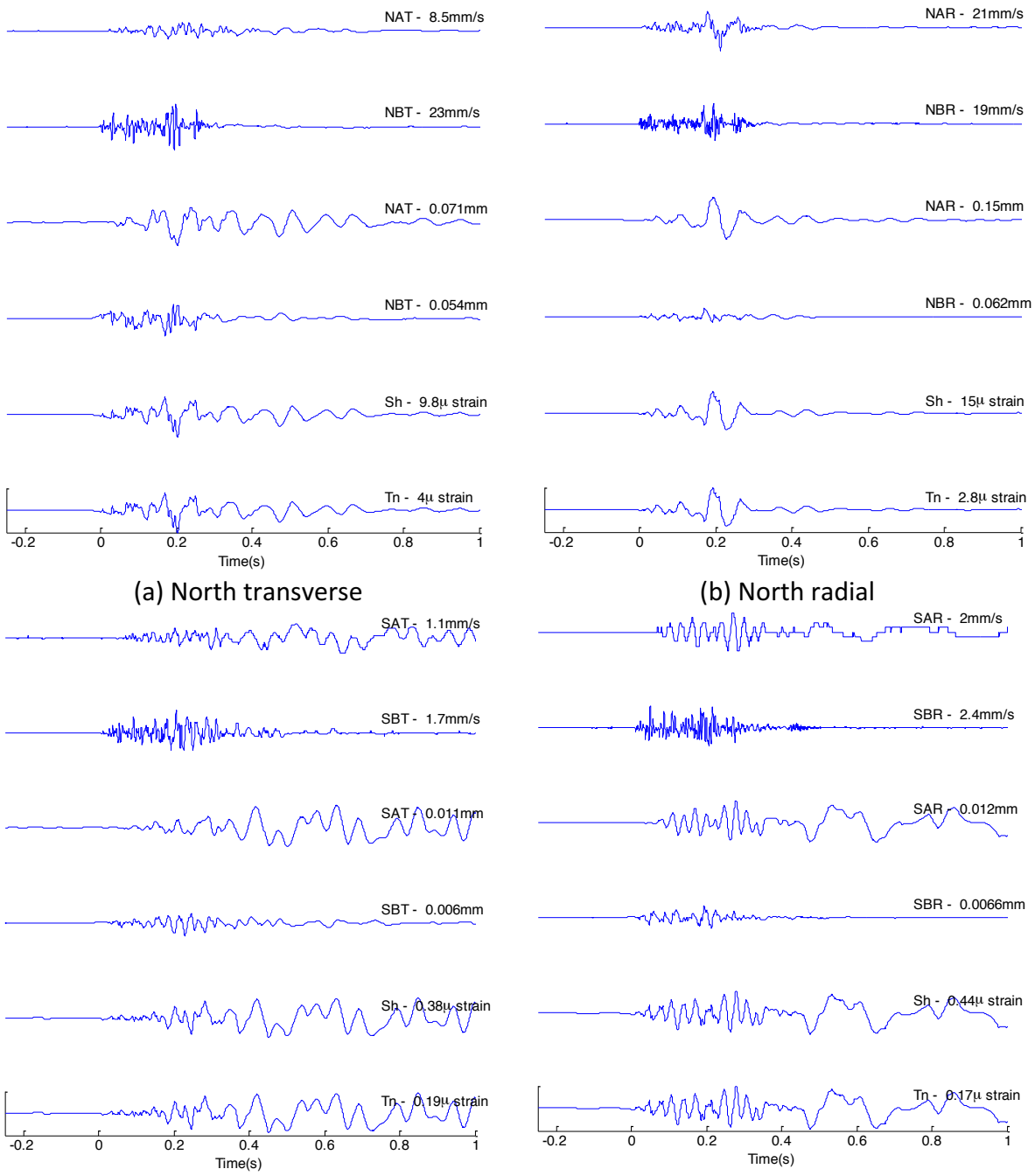

Figure B.9. Strain level calculations for blast 07/07/2014.

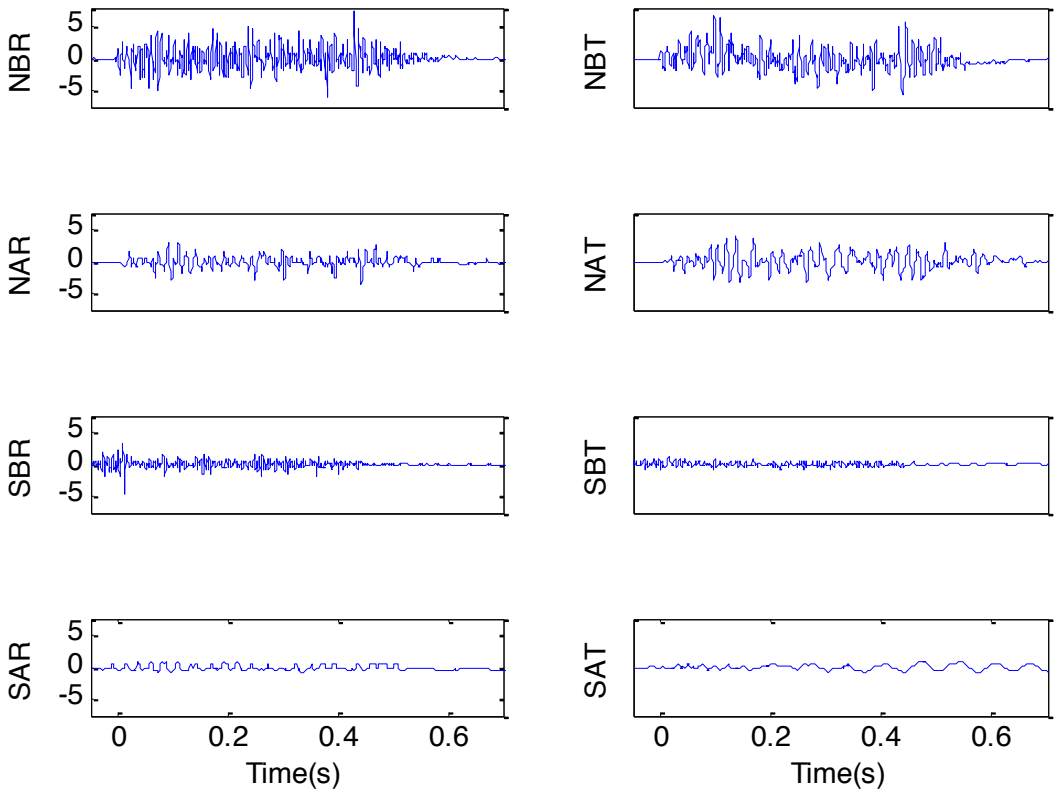

Figure A.10. Recorded velocity time histories for blast 08/05/2014.

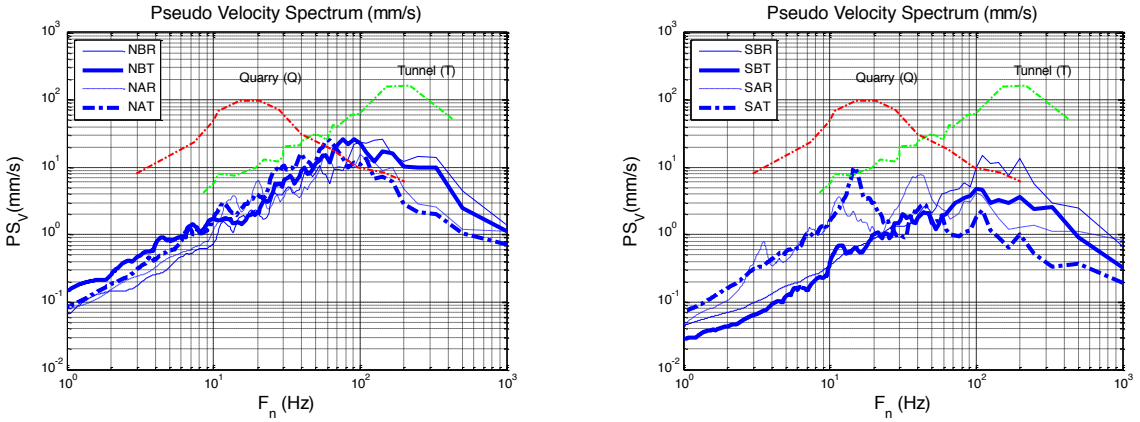

(a) North part (b) South part

Figure B.11. Response spectra for blast 08/05/2014.

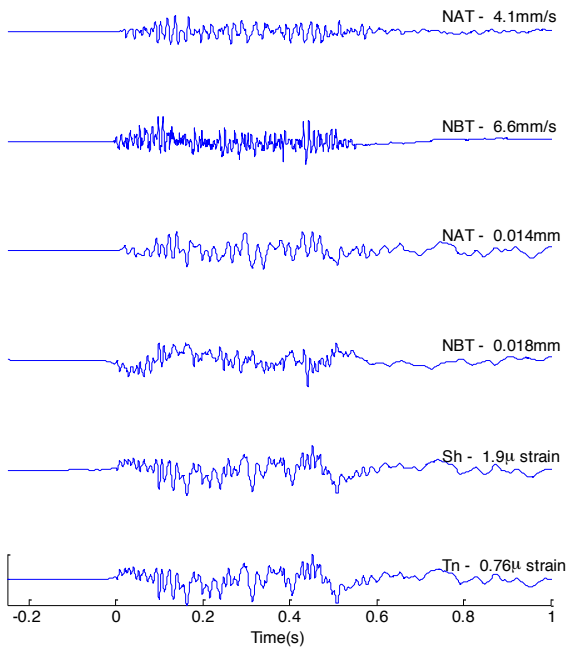

(a) North transverse

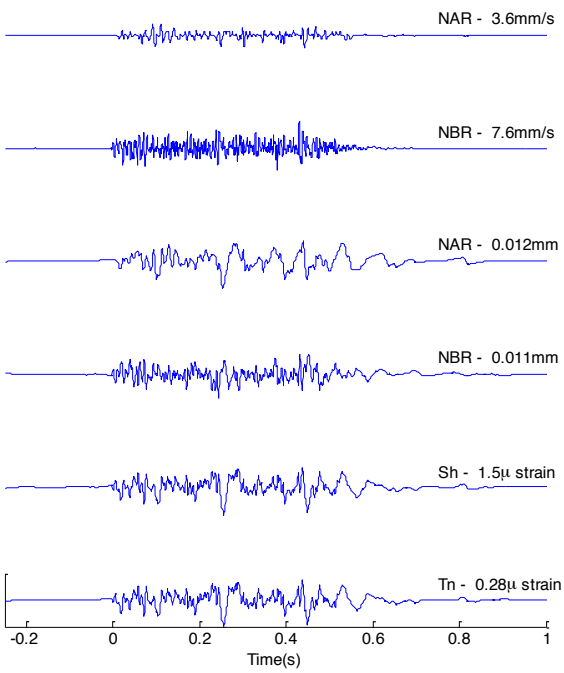

(b) North radial

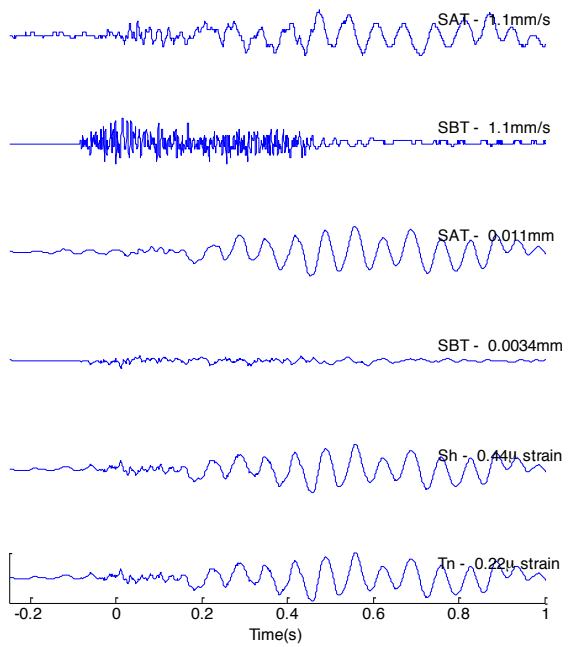

(c) South transverse

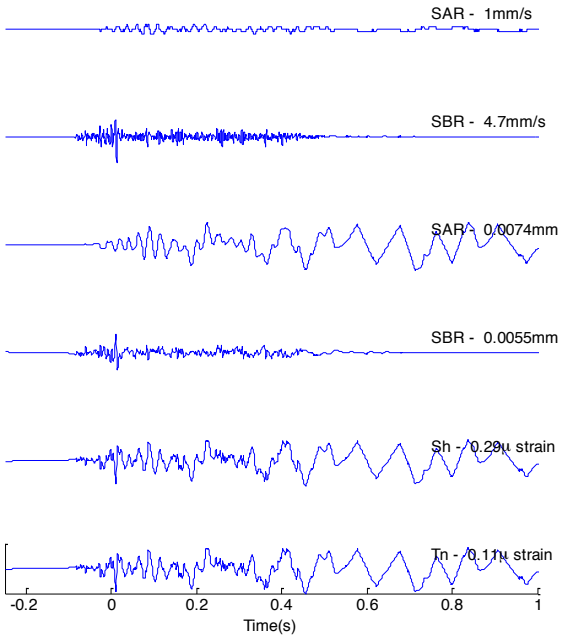

(d) South radial

Figure B.12. Strain level calculations for blast 08/05/2014.

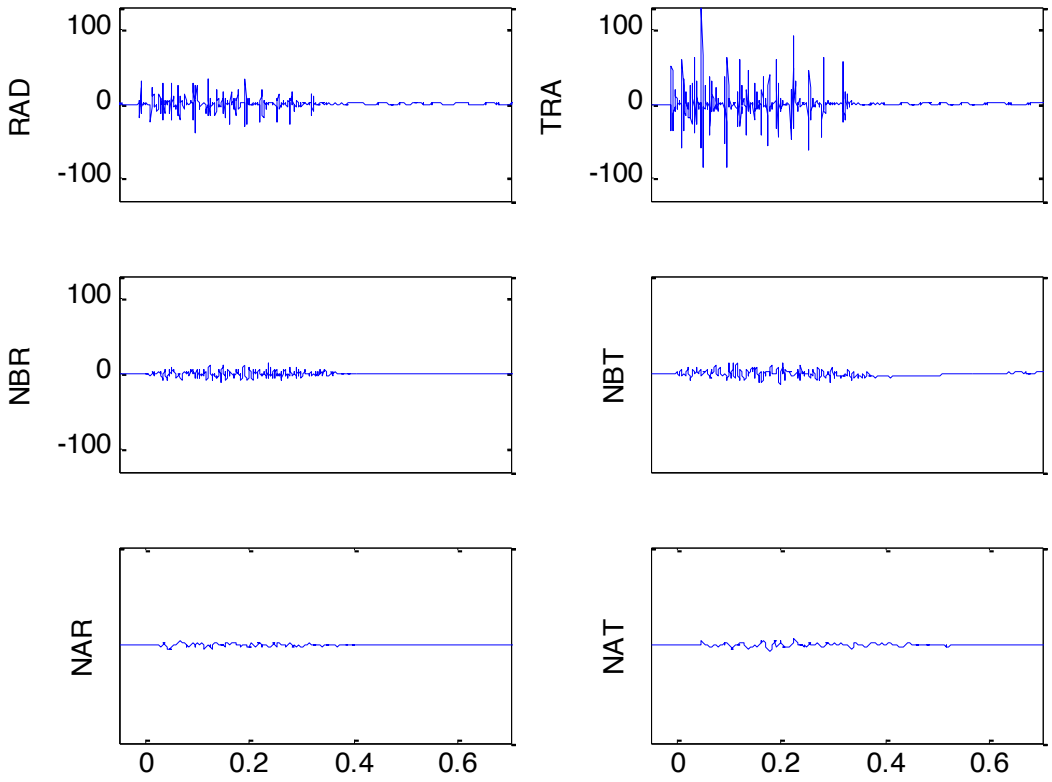

Figure B.13. Recorded velocity time histories for blast 06/05/2014.

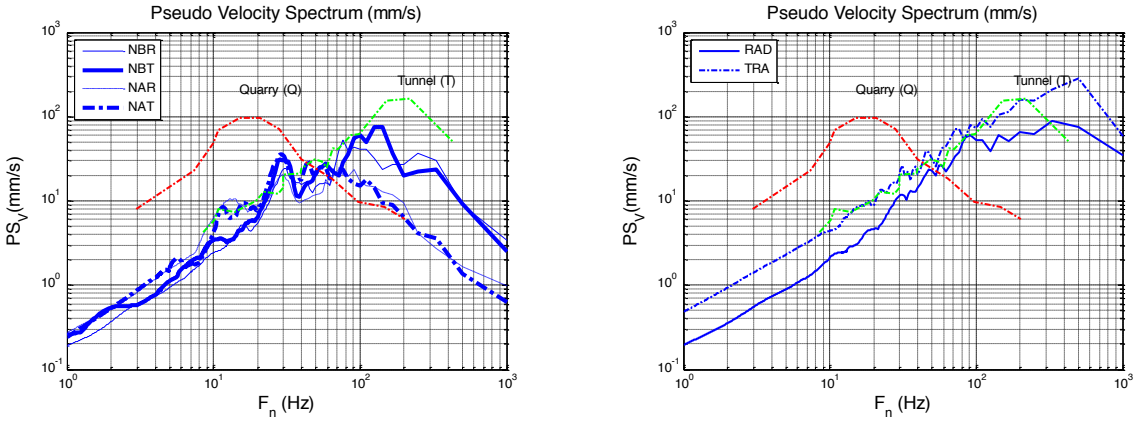

(a) North part (b) Ground motion

Figure B.14. Response spectra for blast 06/05/2014.

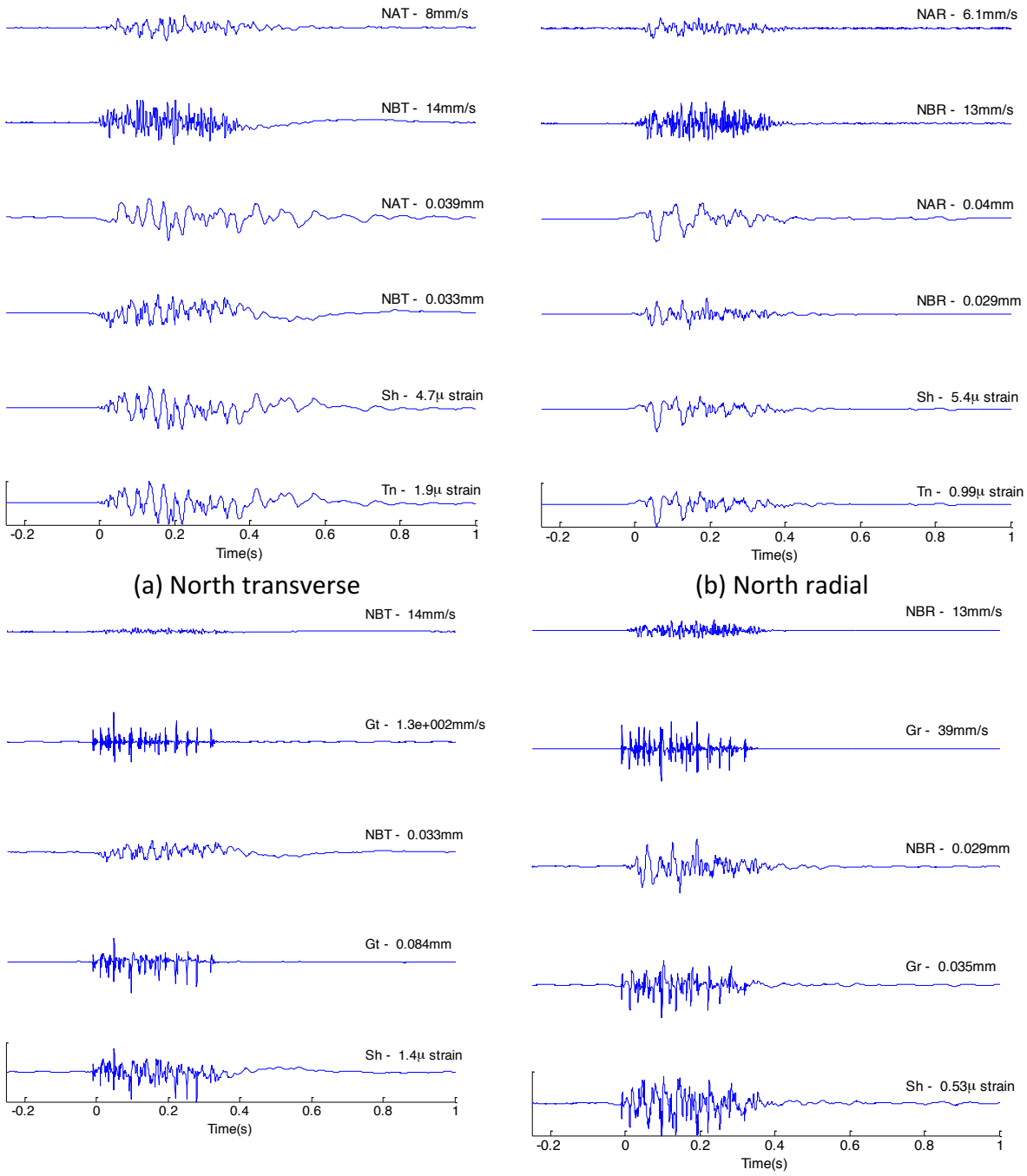

Figure B.15. Strain level calculations for blast 06/05/2014.

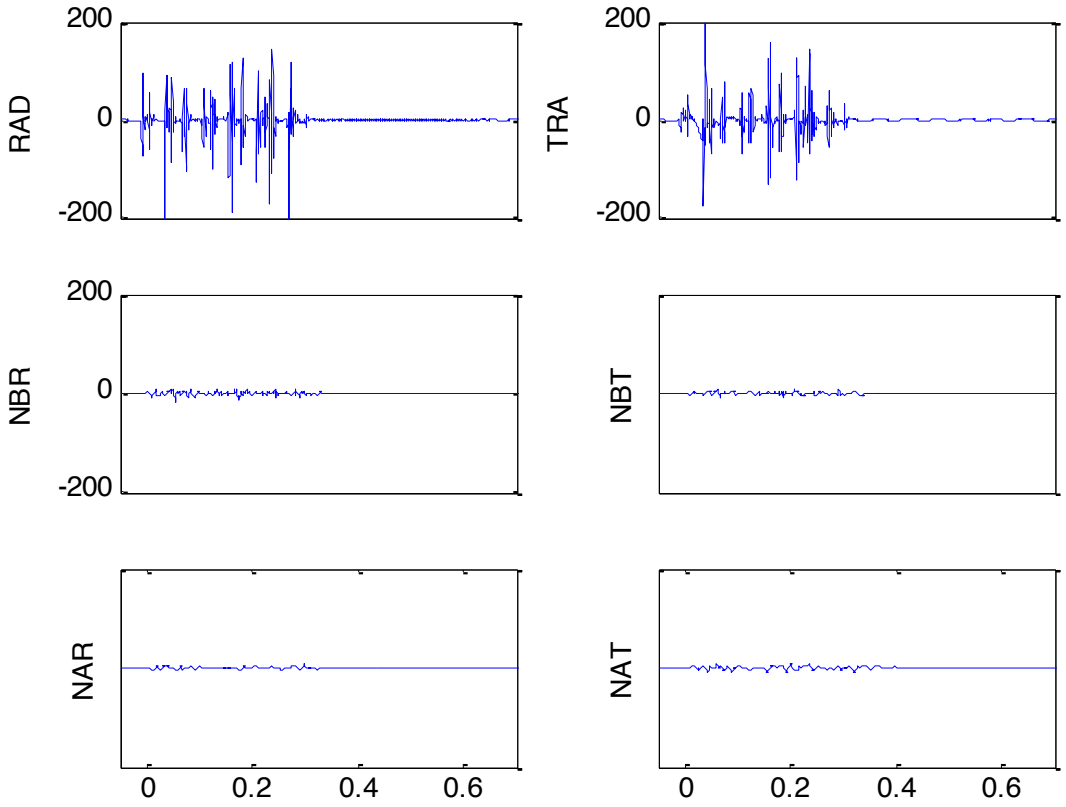

Figure B.16. Recorded velocity time histories for blast 06/09/2014.

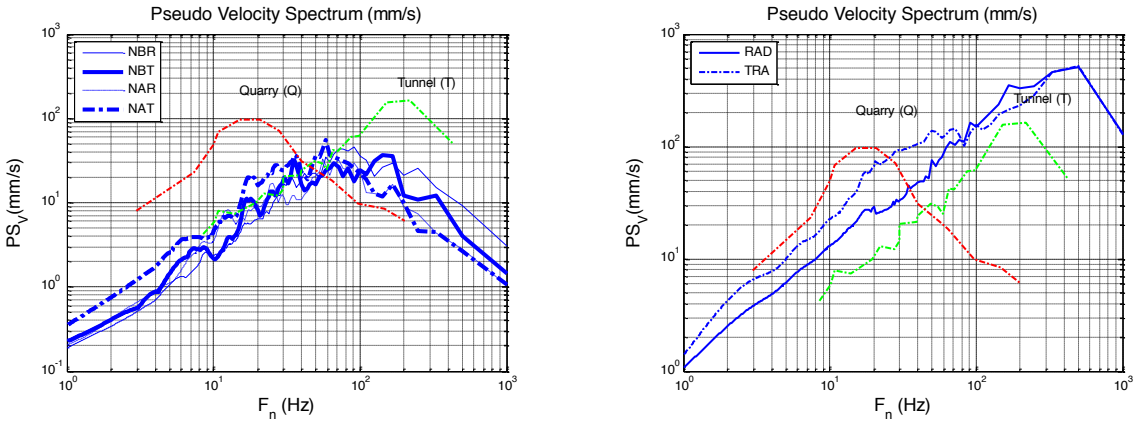

(a) North part (b) Ground motion

Figure B.17. Response spectra for blast 06/09/2014.

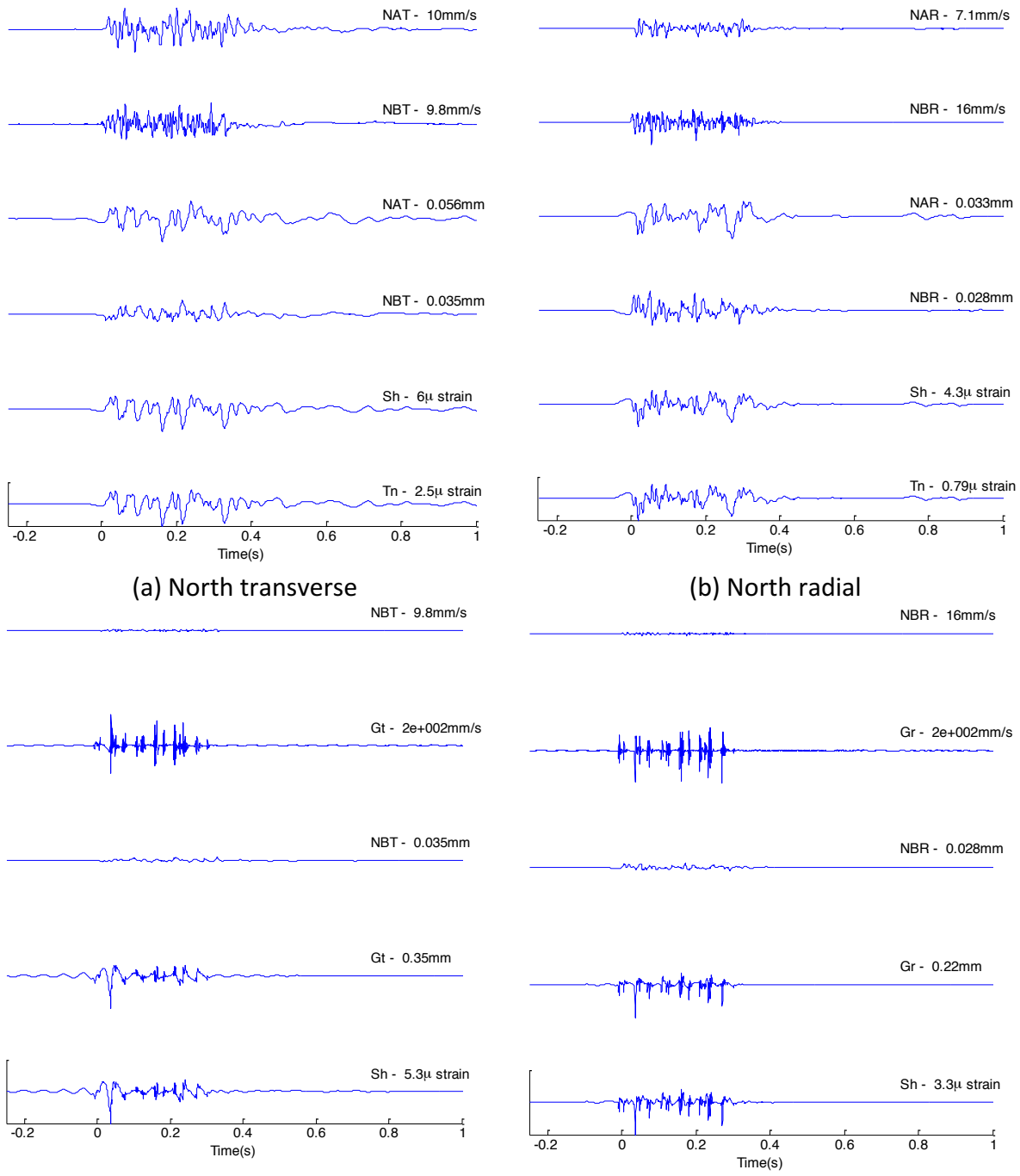

Figure B.18. Strain level calculations for blast 06/09/2014.

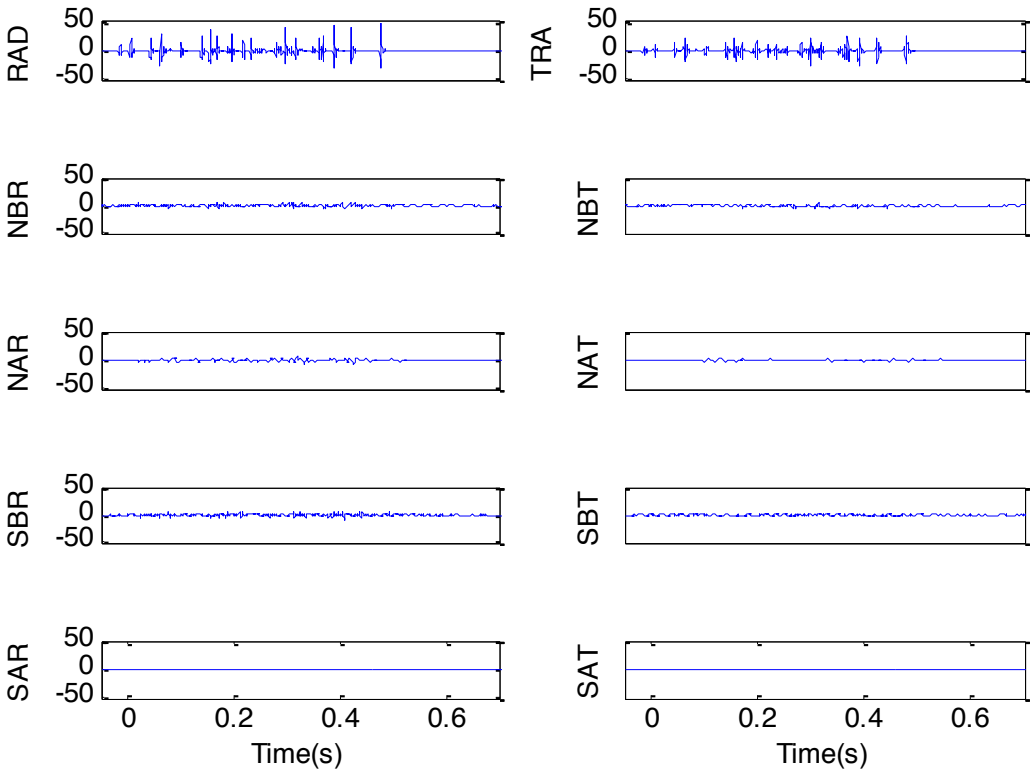

Figure B.19. Recorded velocity time histories for blast 06/02/2014.

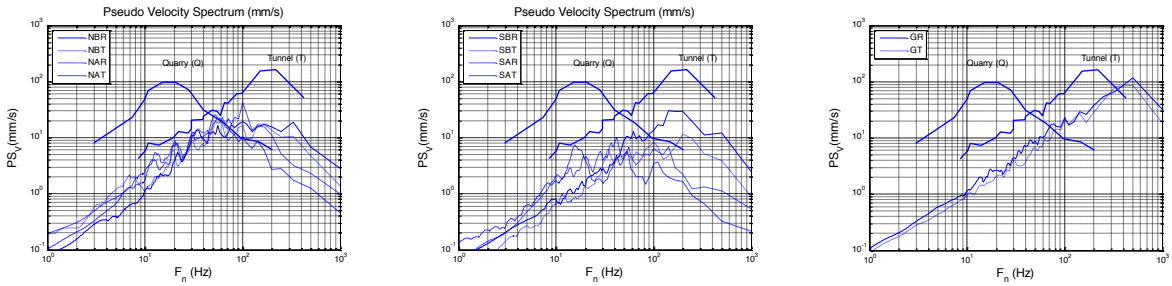

(a) North part (b) South part (c) Ground motion

Figure B.20. Response spectra for blast 06/02/2014.

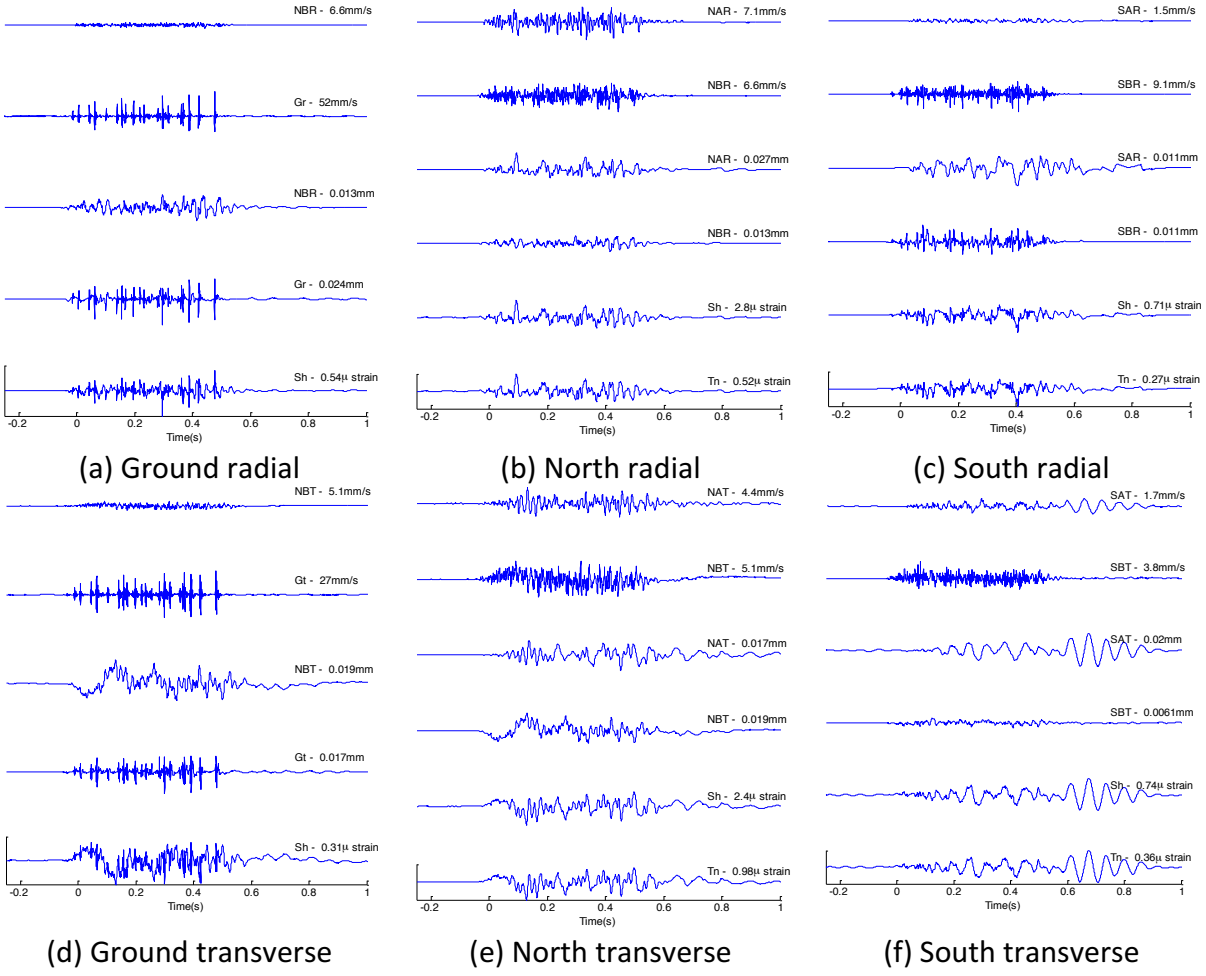

(a) Ground radial (b) North radial (c) South radial

(d) Ground transverse (e) North transverse (f) South transverse

Figure B.21. Strain level calculations for blast 06/02/2014.

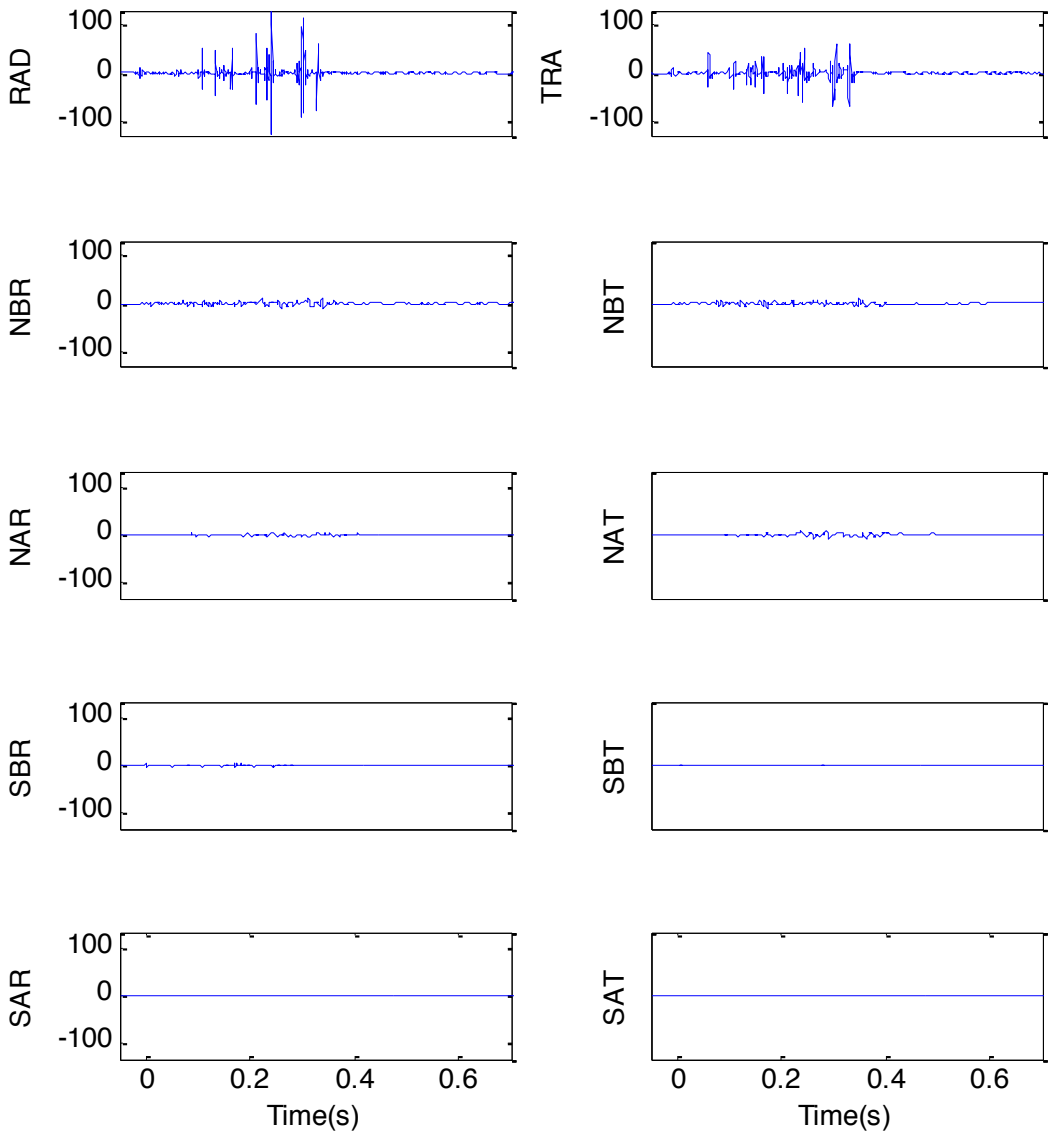

Figure B.22. Recorded velocity time histories for blast 06/06/2014.

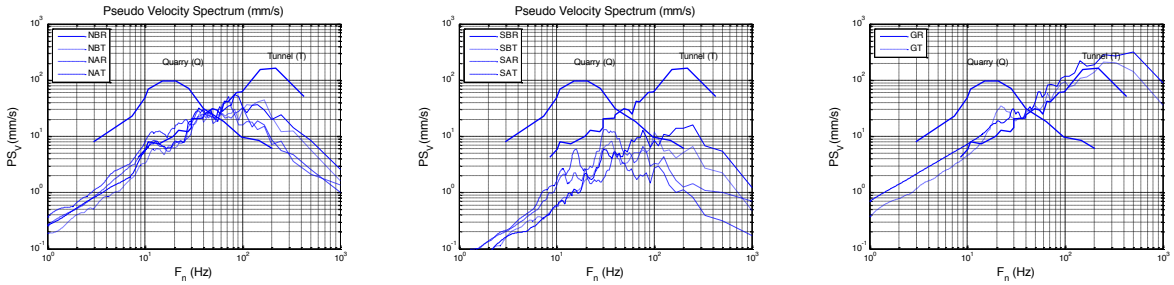

(a) North part (b) South part (c) Ground motion

Figure B.23. Response spectra for blast 06/06/2014.

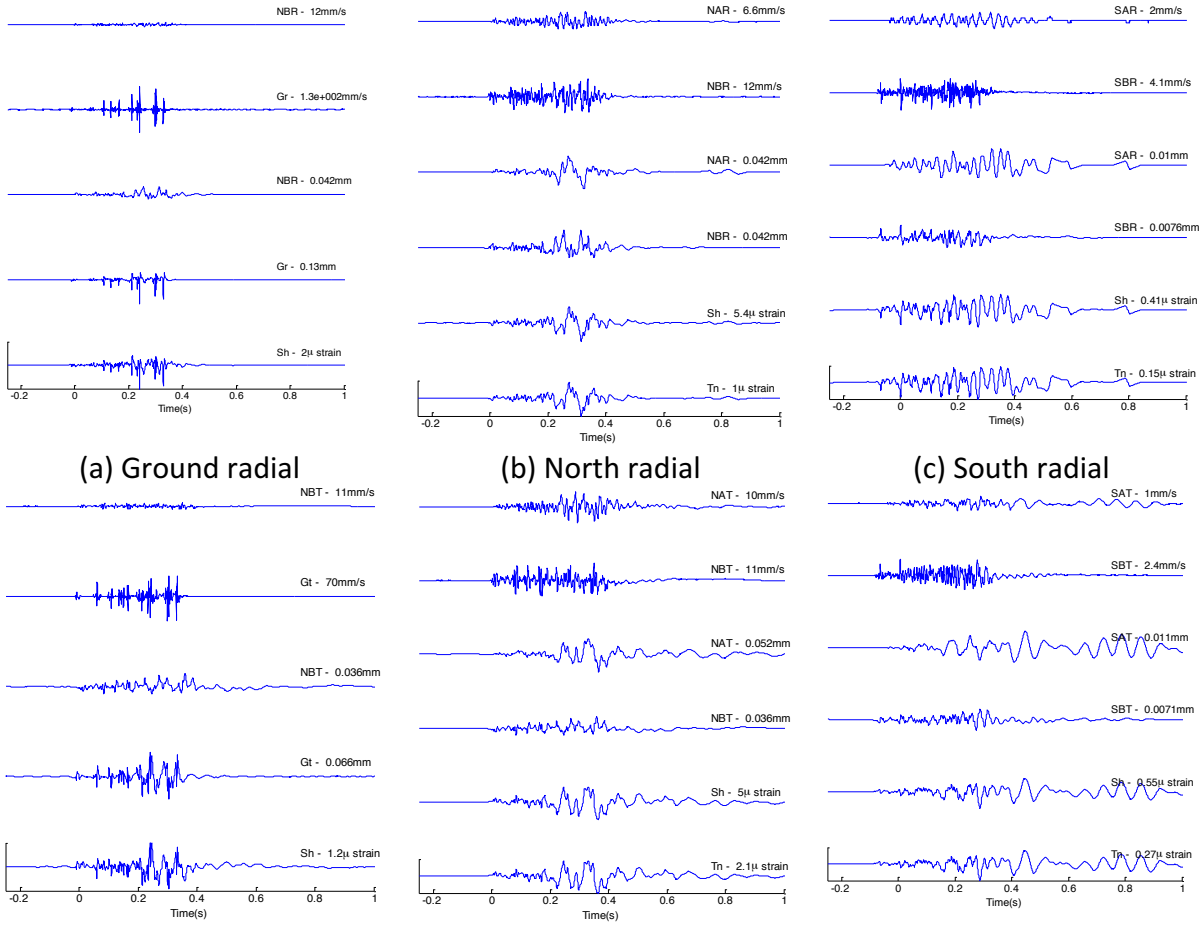

(a) Ground radial (b) North radial (c) South radial

(d) Ground transverse (e) North transverse (f) South transverse

Figure B.24. Strain level calculations for blast 06/06/2014.

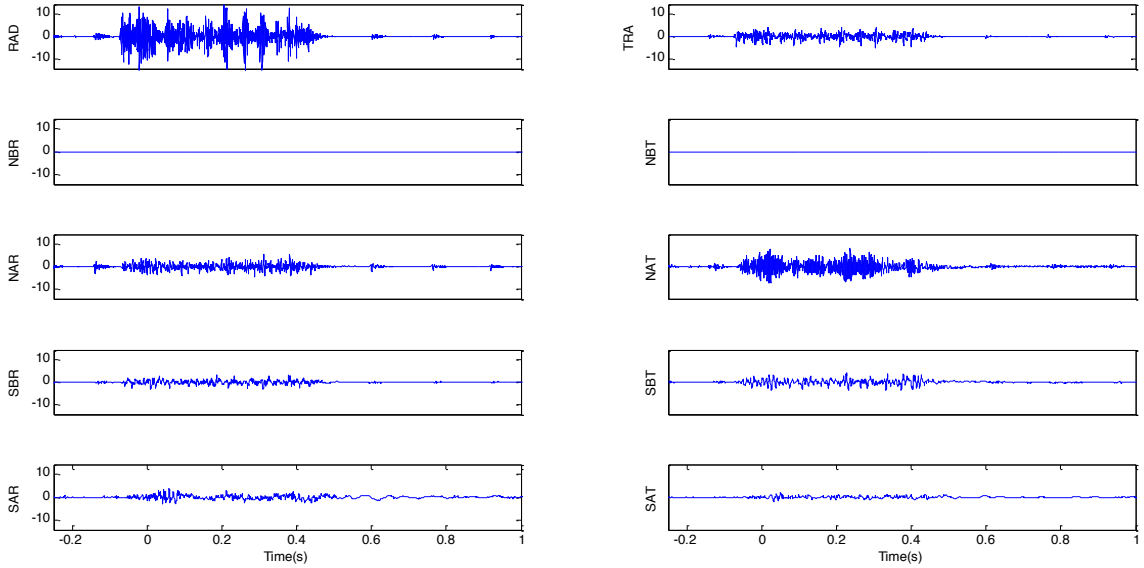

Figure B.25. Recorded velocity time histories for blast 08/05/2014 (building 2).

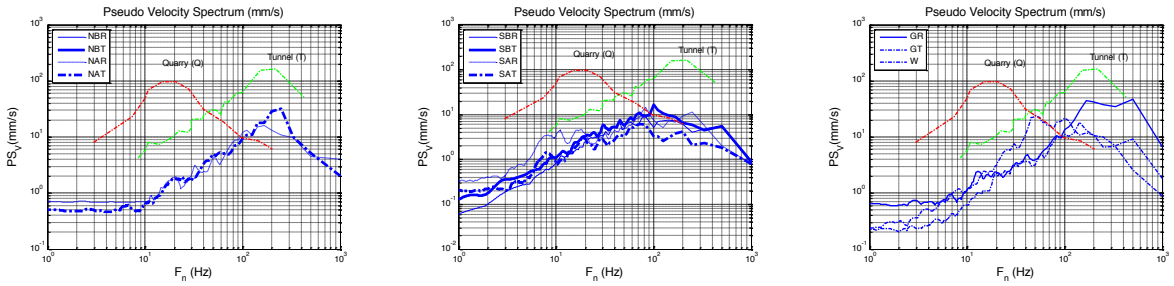

(a) North part (b) South part (c) Ground motion

Figure B.26. Response spectra for blast 08/05/2014 (building 2).

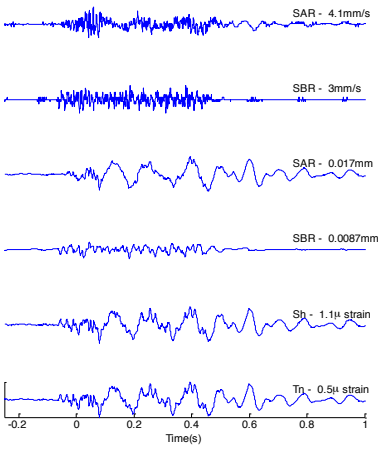

(a) South radial

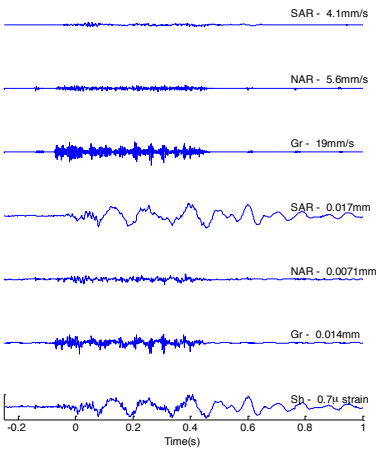

(b) Roof radial

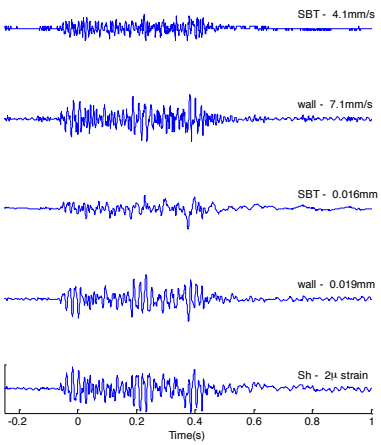

(c) Wall/SB transverse

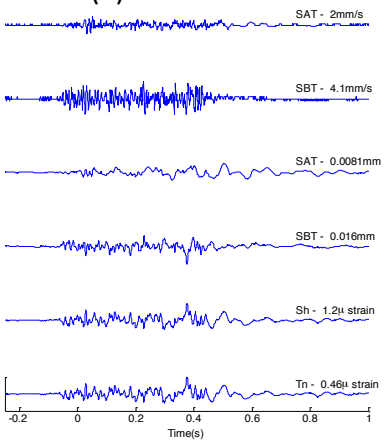

(d) South transverse

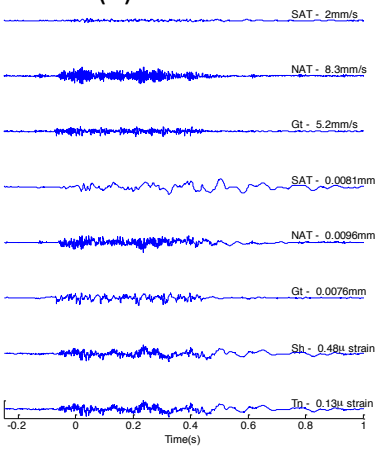

(e) Roof transverse

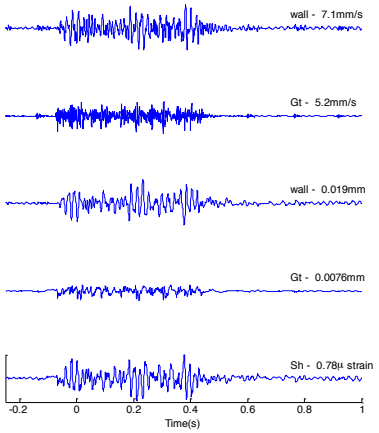

(f) Wall/Ground transverse

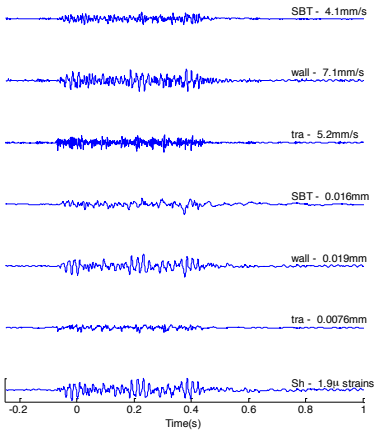

(g) Wall/Average (SB transverse,Ground transverse)

Figure B27. Strain level calculations for blast 08/05/2014 (building 2).

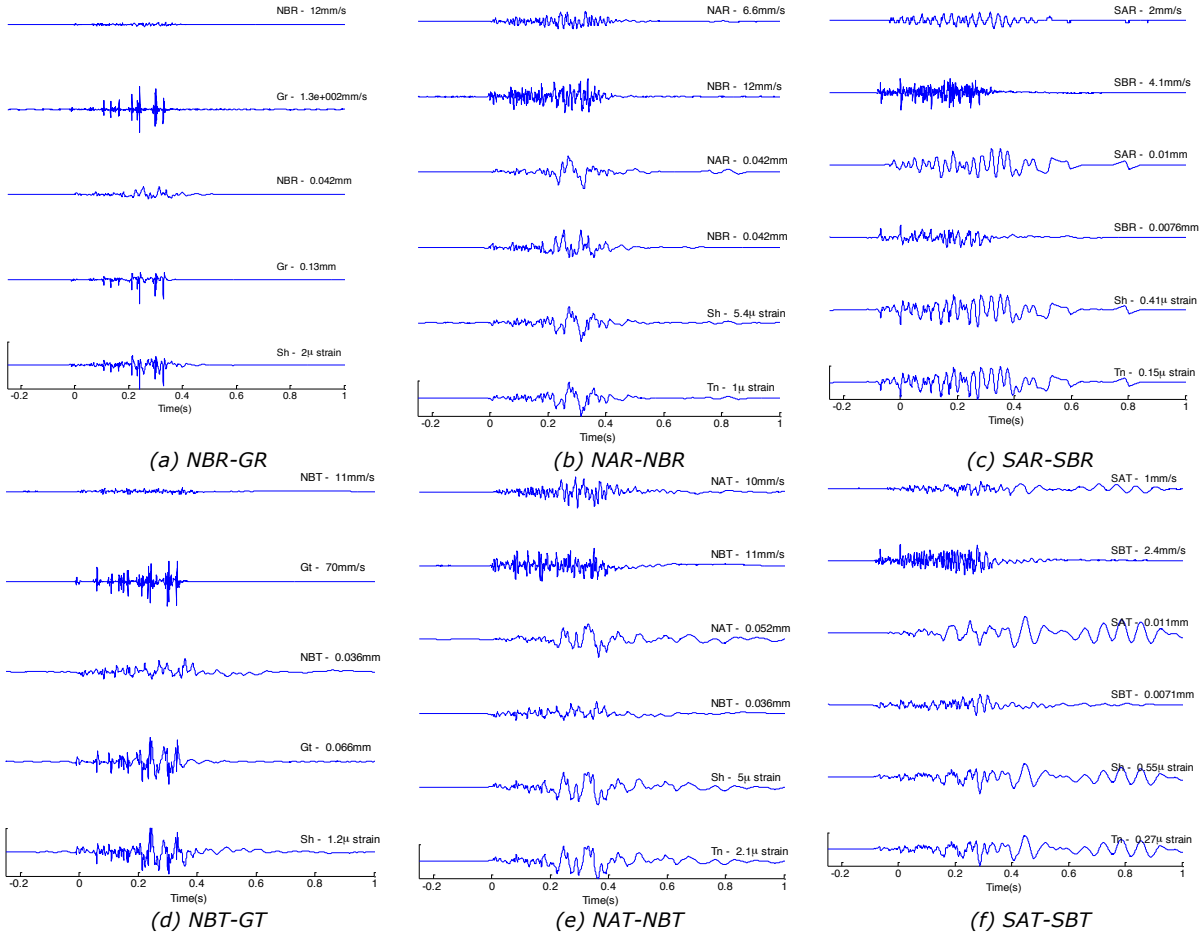

Figure B.28. Strain level calculations for blast 06/06.

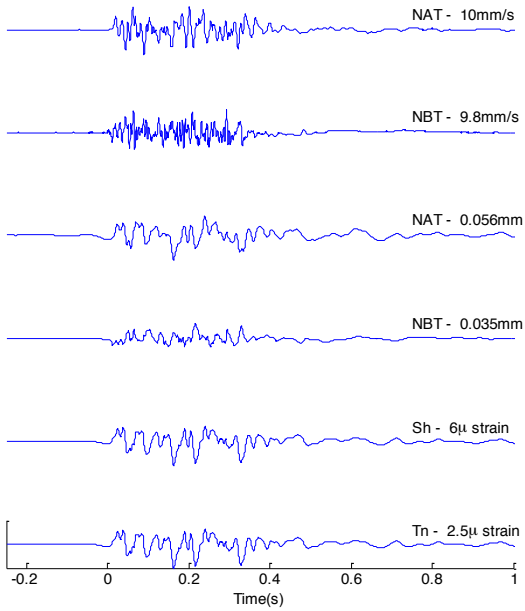

(a) NAT-NBT

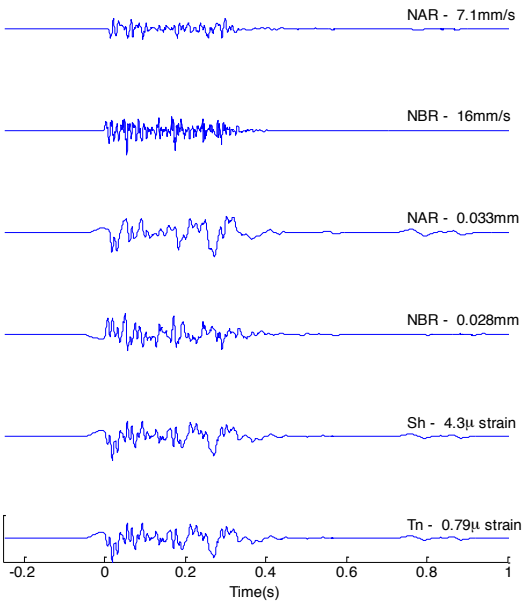

(b) NAR-NBR

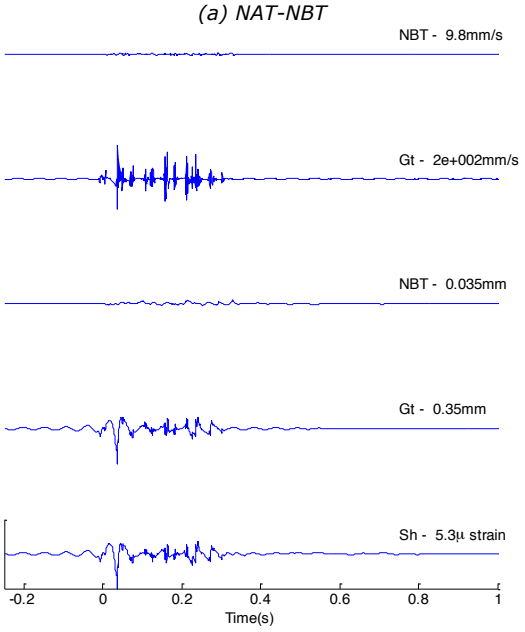

(c) NBT-GT

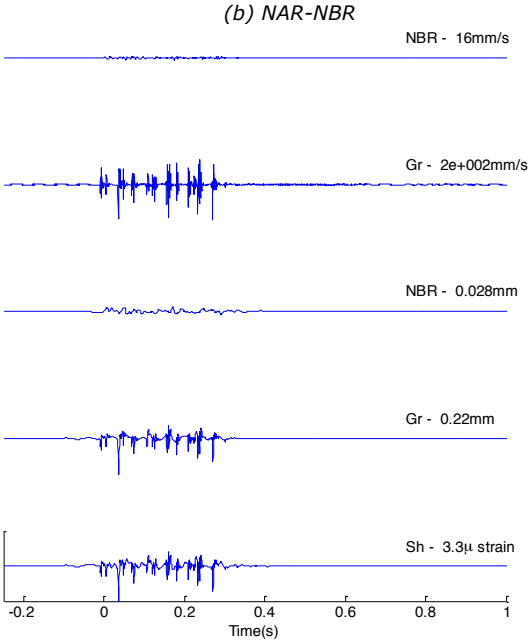

(d) NBR-GR

Figure B.29. Strain level calculations for blast 06/09.